Engineering

RR

Journal of Research

of the

National Bureau of Standards

JULY 1984

VOLUME 89 NUMBER 1

U. S. DEPARTMENT OF COMMERCE
Sinclair Weeks, Secretary
NATIONAL BUREAU OF STANDARDS
A. V. Astin, Director

JULY • 1954
VOLUME • 53
NUMBER • 1

JOURNAL OF RESEARCH

of the

NATIONAL BUREAU OF STANDARDS

PERIODICALS OF THE NATIONAL BUREAU OF STANDARDS

The National Bureau of Standards is engaged in fundamental and applied research in physics, chemistry, mathematics, and engineering. Projects are conducted in thirteen fields: electricity, optics and metrology, heat and power, atomic and radiation physics, chemistry, mechanics, organic and fibrous materials, metallurgy, mineral products, building technology, applied mathematics, electronics, and radio propagation. The Bureau has custody of the national standards of measurement and conducts research leading to the improvement of scientific and engineering standards and of techniques and methods of measurement. Testing methods and instruments are developed; physical constants and properties of materials are determined; and technical processes are investigated.

JOURNAL OF RESEARCH

The Journal presents research papers by authorities in the specialized fields of physics, mathematics, chemistry, and engineering. Complete details of the work are presented, including laboratory data, experimental procedures, and theoretical and mathematical analyses. Annual subscription: domestic, $5.50; foreign, $6.75.

TECHNICAL NEWS BULLETIN

Summaries of current research at the National Bureau of Standards are published each month in the Technical News Bulletin. The articles are brief, with emphasis on the results of research, chosen on the basis of their scientific or technologic importance. Lists of all Bureau publications during the preceding month are given, including Research Papers, Handbooks, Applied Mathematics Series, Building Materials and Structures Reports, Miscellaneous Publications, and Circulars. Each issue contains 12 or more two-column pages; illustrated. Annual subscription: domestic, $1.00; foreign, $1.25.

BASIC RADIO PROPAGATION PREDICTIONS

The Predictions provide the information necessary for calculating the best frequencies for communication between any two points in the world at any time during the given month. The data are important to all users of long-range radio communications and navigation, including broadcasting, airline, steamship, and wireless services, as well as to investigators of radio propagation and ionosphere. Each issue, covering a period of one month, is released three months in advance and contains 16 large pages, including pertinent charts, drawings, and tables. Annual subscription: domestic, $1.00; foreign, $1.25.

Order all publications from the Superintendent of Documents
U. S. Government Printing Office, Washington 25, D. C.

The printing of this publication has been approved by the Director of the Bureau of the Budget, May 12, 1953.

Journal of Research of the National Bureau of Standards Vol. 53, No. 1, July 1954 Research Paper 2510

Correlation of Polarized Light Phenomena With the Orientation of Some Metal Crystals

C. J. Newton and H. C. Vacher

A photometric study was made of the reflection of plane polarized light normally incident in a metallographic microscope upon specimens of tin, aluminum, and monel, with various surface treatments. A high degree of correlation was found in most cases between the extinction position and the projection of the optic axis or of the cubic axis making the greatest angle with the surface normal. Moreover, a fourth power sine relationship was observed between the change of intensity and the angle between the surface normal and the optic axis in tin. The intensity correlation in the case of the cubic metals was not so clear, but a slight indication of position dependence was observed for aluminum. The results indicate that the optically anisotropic effects observed with cubic metals can be caused both by anisotropic films and by oriented surface contours, but that the latter is the source of those effects that are correlated with the crystallographic orientation of the grain.

1. Introduction

In continuation of an investigation [*1*, *2*][1] of the utility of plane polarized light in metallography, a study has been made of tin and aluminum crystals, and additional data have been obtained from monel, a 70 nickel–30 copper alloy. The previous work at the National Bureau of Standards by D. H. Woodard [*1*] showed a nonuniformity of intensity of polarized light reflected from plastically deformed metal grains, suggesting an observable correlation between such intensity and crystallographic orientation. The specific problem of such correlation was pursued in a study by H. C. Vacher [*2*], who showed a correlation between extinction positions and the projection azimuth of a cubic axis.

In the present study the relative maximum and minimum intensities of the reflected light were measured photometrically and correlated with crystal orientation. Woodrow, Mott, and Haines [*3*] used a photometric method but gave no data correlating intensities with orientation. Supplementary experiments were made to provide information concerning the cause of the observed optical anisotropy, which has been the subject of some uncertainty [*4*].

2. Theoretical Aspects

The theory of the reflection of plane polarized light from metallic specimens is one of considerable complexity [*5*]. This discussion will be limited to a qualitative description of the special case of a plane polarized beam incident normally upon the reflecting surface [*6*], which is very nearly the case when the metallographic microscope is used with low-powered objectives.

For isotropic metals (cubic structure), normally incident plane polarized light is reflected inherently with neither rotation of the plane of polarization nor introduction of elliptical polarization; therefore, examination by rotation of the stage of the microscope with crossed nicols exhibits continuous extinction. A like situation exists when the optic axis of the crystal is perpendicular to the surface of a crystal belonging to the uniaxial classification, which includes the tetrogonal, hexagonal, and trigonal systems. If the optic axis and the surface normal do not coincide, it is necessary to consider the orientation of the plane they determine. The intersection of this plane with the surface determines a line called the principal direction, and the incident light vector can be resolved into components parallel to and perpendicular to this direction. Reflectivities and phase changes upon reflection differ for these two components. The reflected light is, in general, elliptically polarized, and the field observed through the crossed analyzer of the microscope is bright. There are, however, four special positions in a complete revolution of the stage where the plane of vibration of the normally incident beam is parallel to or perpendicular to the principal direction in the specimen surface. At these special positions of the stage, the reflected light remains plane polarized in the original plane and is extinguished by the analyzer.

The theory of reflection from orthorhombic, monoclinic, and triclinic materials is of great complexity and will not be discussed here. Fortunately these cases of lower symmetry rarely arise in metallurgical problems.

The above discussion has been confined to the effect on polarized light of the intrinsic optical characteristics of a single flat surface. In view of the possibility, however, that the optical anisotropy of metallographic specimens may be caused by surface contours, the process of multiple reflection of plane polarized light must be considered. To this end, experiments were conducted as will be described later with models made with one, two, or three perpendicular front-surfaced aluminized mirrors.

The polarization figure [*7*] is another phenomenon that can sometimes be observed with the polarizing microscope and, if distinct, can be used in crystal orientation problems. It resembles the interference

[1] Italic figures in brackets indicate the literature references at the end of this paper.

301746—54——1

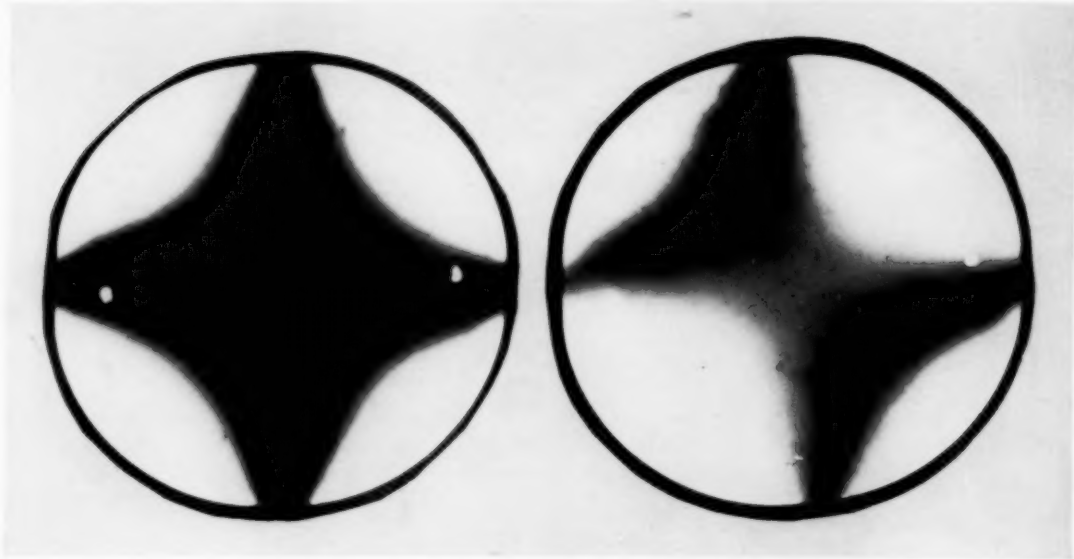

FIGURE 1. *Polarization figures formed by reflection from monel.*
Monel contrast solution, 41× objective, and short focal length telescope as an ocular.

figure [8] observed with convergent plane polarized light passing through transparent anisotropic materials. Instead of arising from path differences caused by birefringence, the polarization figure, according to Cameron and Green [9], results from the rotation and ellipticity introduced in reflected polarized light when the incident beam is not normal to the reflecting surface. The procedure for observing the figures is given in section 3.3. When this procedure is followed, a bright field containing two dark lines, called the isogyres, will be observed. These arise from reflections at those special angles from the surface where, because of particular relations of the planes of the polarizer and analyzer, the angle and plane of incidence of the convergent beam and the optical characteristics of the surface itself, there is a cancelling out of the various factors that disturb the plane polarization in the reflected beam. From those special angles alone, therefore, is the reflected light extinguished by the analyzer. As illustrated in figure 1, the isogyres generally appear as two branches of a hyperbola in the field, but a cruciform figure is formed at four special positions. These are the same positions that give extinctions when the incident light is quasi-normal as is the case with a low-powered objective. The details, even if only qualitative, of the cause of this phenomenon are rather involved. For a reasonably elementary explanation, the reader is referred to an article by E. N. Cameron and L. H. Green [9], who have studied these figures as they relate to the optical properties of ore minerals.

3. Materials and Procedures

3.1. Materials

The greatest experimental difficulty encountered in this study was the securing of suitable metallographic specimens with large grains and with surfaces as free as possible from imperfections such as fine scratches, irregular pits or nonuniform films, which would mask the pertinent polarized-light phenomena. In order to avoid errors arising from differences in surface preparation, polycrystalline specimens were used. Many specimens were examined, but the data presented in this report were obtained from four: One each of tin and aluminum and two of monel. The purity of the tin was 99.96 percent and that of the aluminum, 99.99 percent. The monel was commercial grade, which had been heat treated to grow large crystals [2]. The preparation of each specimen is described in section 4.

3.2. Determination of Crystal Orientation

A major preliminary activity was the determination of the crystallographic orientation of each grain used in each specimen. This orientation was defined with respect to the normal to the surface of the specimen and a reference mark on the surface defining zero azimuth.

In the case of monel, these determinations were made by means of angular measurements of the

traces of twinning planes in two mutually perpendicular surfaces [10]. Monel is a face-centered cubic metal, and the twinning planes are (111) planes. With this information, and with the aid of stereographic plots and standard projections, it was possible to establish the orientations of groups of twinned crystals near the edges of the specimens.

Specimens of aluminum and tin were obtained with grains large enough for the determination of orientations by X-ray diffraction, using the back-reflection Laue method with a Greninger net [11, 12]. This method was very simple to employ in the case of the cubic aluminum, but considerable difficulty was encountered with the tetragonal tin. In practice, one pattern alone was not sufficient with the latter to allow the assignment of an unquestioned orientation to a grain. It was necessary to make one or more check patterns with the X-ray-beam incident at an angle to the specimen surface so as to be parallel to some low-index crystallographic direction, according to the tentative interpretation of the first exposure. If the resulting pattern agreed with the proper standard pattern made previously from another grain whose orientation was known with assurance, the orientation of the new grain was considered determined.

3.3. Measurement of Reflected Polarized Light

The microscope used in this study uses a Foster prism [13] as the polarizing-analyzing element. The objectives were nominally strain-free. This prism acts as permanently crossed nicols; hence, no effect of slightly uncrossing the analyzer was investigated. The prepared specimen was placed on the rotating stage of this polarizing microscope and set in the zero azimuth position with reference to an edge, grain boundary, or scratch on the surface. A 5.6x objective lens and a 5x ocular were used. By means of stage adjusting screws, a particular grain was centered under the cross lines on the ground glass of the microscope camera. After satisfactory centering and magnification, the bellows was adjusted until the grain under study would cover the photocell aperture. The ground glass was removed and a slide bearing the photomultiplier tube, centered and limited by a $\frac{3}{32}$-in.-diameter aperture, was put in its place. The light flux passing into the sensitive tube caused a proportional deflection of the needle on the dial of a commercial electronic photometer. As the specimen was rotated, the intensity of the reflected light would rise and fall in an approximately sinusoidal pattern. The usual procedure was to make three complete revolutions of the stage while recordings were taken of the angular settings of the stage and the photometer current proportional to the light intensity at each of the four maxima and each of the four minima.

It was observed for any one surface that the minimum intensities from all grains were nearly the same, arising from the scattered light from surface imperfections and from the microscope elements. All of the maximum intensities from a grain were averaged together, and the difference taken between that average and the average minimum intensity readings from the grain. This intensity difference, ΔI, is the quantity used in the reported results. Other intensity functions, such as the ratios of various intensities, were examined but were found to be less satisfactory. The angular settings for maximum intensity and minimum intensity (extinctions) were also averaged in a manner to allow for their distribution throughout the complete circle, yielding a grand average value of the first quadrant extinction angle, which was based upon all 24 angular readings. Through the use of results based on averages of large numbers of readings, personal errors were minimized. The extinction angle is defined as the angle from the fiducial line to the position of minimum reflection. If, moreover, polarization figures could be observed (as they readily were with the monel specimens), their crossing positions were also averaged into the value of the extinction angle for each grain. To make these figures visible, the incident light was made highly convergent by the use of a high-powered objective, such as 41x. Moreover, as the figure was formed at the back focal plane of the objective, the method of observation was modified by the removal of the eyepiece. Usually the figure could then be seen directly or through a pinhole eyepiece; viewing was often improved by a lens system, such as a short-focus telescope, which allowed focusing in the proper plane.

4. Results

4.1. Tin

The tin specimen was prepared by melting the tin in a $\frac{3}{4}$-in. quartz ring resitng on a piece of polished graphite. It was then air-cooled. Approximately 15 specimens were made, resulting in only one instance of a specimen (1144, fig. 2) whose surface contained numerous grains large enough (about 1 mm in smallest dimension) for convenient determination of orientation by X-ray diffraction.

Considerable difficulty was encountered in preparing the surface of this soft metal. It was never ground on papers but polished with only a diamond abrasive, 0 to 2 microns, on microcloth that has been boiled for 2 hours before being used. Then the specimen was etched in acidified ferric chloride reagent [14]. Figures 3, a and b, show the same surface lightly and heavily etched.

On the surface of the specimen there were 29 grains large enough to give usable back-reflection Laue patterns. The crystallographic orientation of the surface normal for each grain is shown in the stereographic triangle in figure 4. The stereographic angular coordinates of the optic axis (the c-axis, or [001] axis), the azimuth referred to a fiducial line in the surface and the colatitude, or zenith distance relative to the surface normal, are given in table 1.

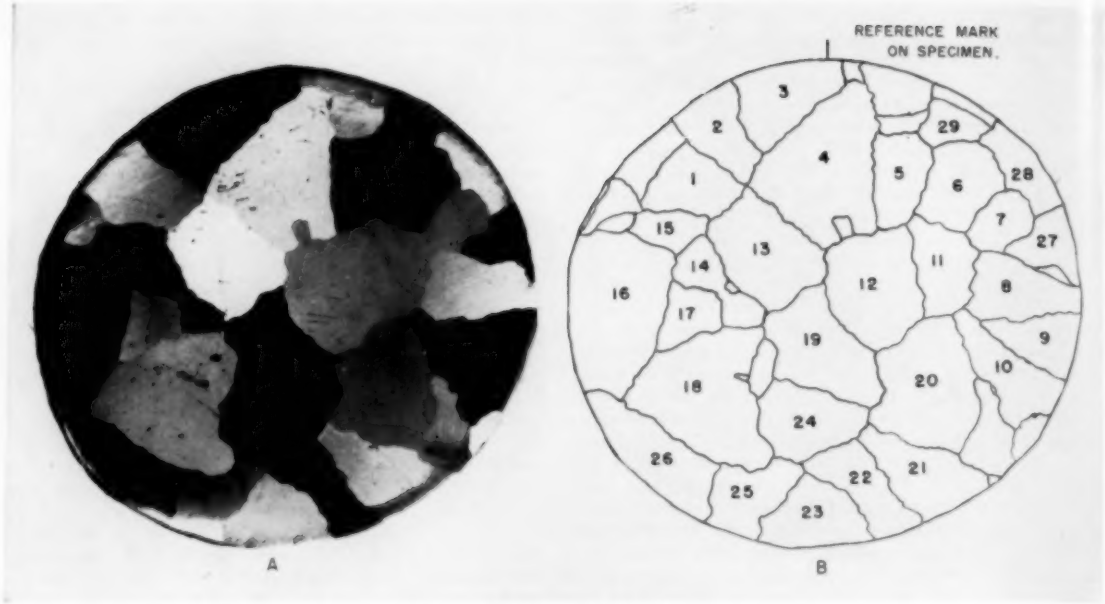

FIGURE 2. *Tin specimen 1144.*

A, Etched with 5-percent ferric chloride solution, approximately × 4; B, sketch for identification of grains.

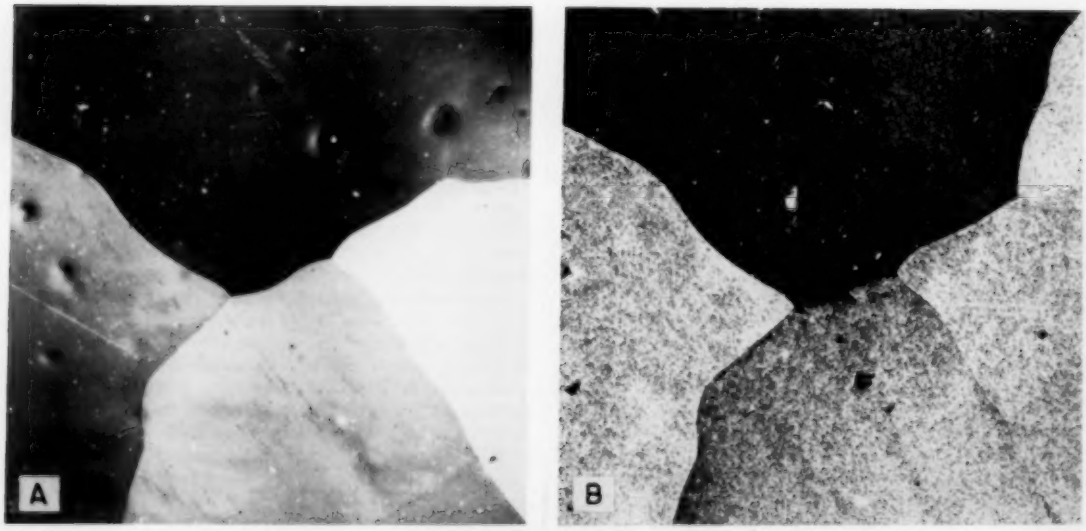

FIGURE 3. *Surface of tin 1144 after etching with 5-percent ferric chloride solution.*

A, Light etch, × 50; B, deep etch, × 50.

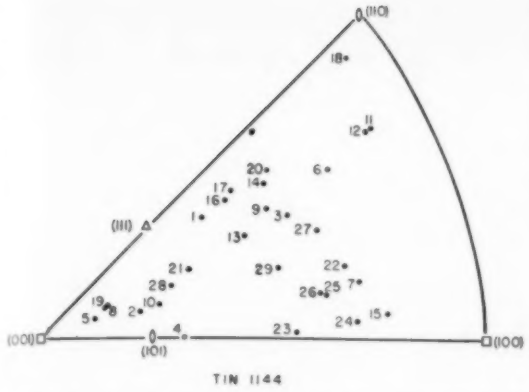

TIN 1144

FIGURE 4. *Crystallographic orientations of surface normal with respect to individual crystals in the polished surface of tin 1144.*

Numbers 1 to 29 correspond to the numbers identifying the crystals in figure 2.

TABLE 1. *Photometer minima, tin 1144, light etch*

Grain	ΔI	ψ_c	ψ_c'	Orientation		$\Delta\psi$
				ϕ_c	δ	
		Degrees	*Degrees*	*Degrees*	*Degrees*	*Degrees*
1	19.4	19.6	290	289	48	1
2	1.8	69.8	250	294	26	−44
3	25.8	69.5	250	248	63	2
4	6.9	80.7	171	186	36	−15
5	4.7	72.3	72	84	15	−12
6	33.7	65.4	245	241	73	4
7	36.6	21.9	112	113	72	−1
8	3.2	80.0	170	184	18	−14
9	26.6	67.2	157	160	60	−3
10	1.9	6.6	277	280	31	−3
11	39.2	51.8	322	320	82	2
12	39.8	53.3	323	320	81	3
13	21.4	61.6	332	326	54	6
14	25.2	7.8	278	276	62	2
15	43.4	31.4	301	299	76	2
16	14.6	52.3	232	228	54	4
17	19.9	5.0	275	272	56	3
18	42.8	82.7	263	260	85	3
19	1.6	0.8	91	120	19	−29
20	29.8	55.1	55	53	64	2
21	12.0	1.4	181	172	40	9
22	47.2	12.5	12	12	70	0
23	39.4	30.7	121	122	76	−1
24	40.7	87.8	268	268	78	0
25	33.3	27.8	208	213	71	−5
26	24.8	34.2	214	216	71	−2
27	25.3	68.1	338	336	67	2
28	2.1	42.2	312	304	35	8
29	24.7	1.2	91	92	58	−1

Average $|\Delta\psi|=6.3°$.

If we arbitrarily take $\Delta I=3$ as the value below which valid judgments of extinction angle cannot be made, grains 2, 10, 19, and 28 are excluded, and

Average $|\Delta\psi|=4.0°$.

The following symbols are used in the tables:

ΔI=Change of intensity of light falling on sensitive tube as grain is rotated from a position giving maximum intensity to an extinction position.

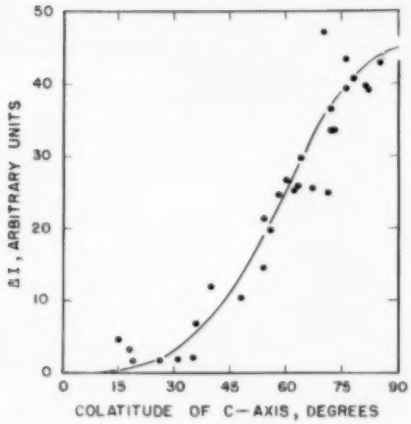

FIGURE 5. *Relation of ΔI to angle between surface normal and c-axis (colatitude) in grains of lightly etched tin 1144.*

ψ_c=Extinction angle: The average angle obtained by a rotation of the microscope stage from a reference line on the surface of the specimen to the position of the first extinction.

ϕ_c=Azimuth of the *c*-axis (the optic axis) of tin, measured from the same fiducial line as that used in measuring extinction angles.

ϕ_a=Azimuth of the projection of the cubic axis making the greatest angle with the surface normal.

ψ_c'=Adjusted extinction angle: ψ_c plus such a multiple of 90° as to give a value near ϕ_c or ϕ_a, as the case might be.

ψ_0=Adjusted average of extinction angle and polarization figure crossings when the latter were usable.

$\Delta\psi$=Difference between the adjusted extinction angle and the azimuth of the active axis; ψ_c' or ψ_0 minus ϕ_c or ϕ_a, as the case might be.

δ=Colatitude of the active axis: The angle between the active axis and the normal to the surface.

α=Angle between surface normal and [110] direction in Al.

β=Angle between surface normal and [111] direction in Al.

γ=Angle between surface normal and [100] direction in Al.

Table 1 also includes the photometer data and the extinction angles for the lightly etched specimen, with the differences between the *c*-axis azimuths and the extinction angles. The average difference was 6.3°. However, if $\Delta I=3$ is arbitrarily taken as the value below which valid judgments of extinction angle cannot be made, four grains are excluded, and the average difference is 4.0°. The results show that, with the exception of these four dim grains, there was excellent agreement of extinction angle with azimuth of the *c*-axis. Figure 5 is a graph of

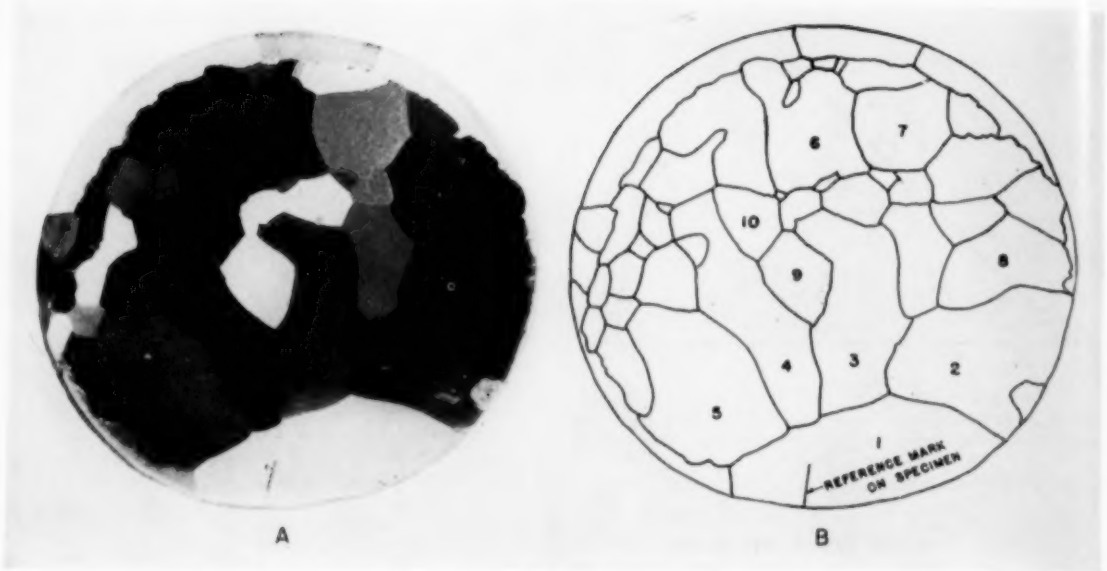

FIGURE 6. *Aluminum specimen 1143.*

A, Etched with Tucker's reagent, × 4; B, sketch for identification of grains.

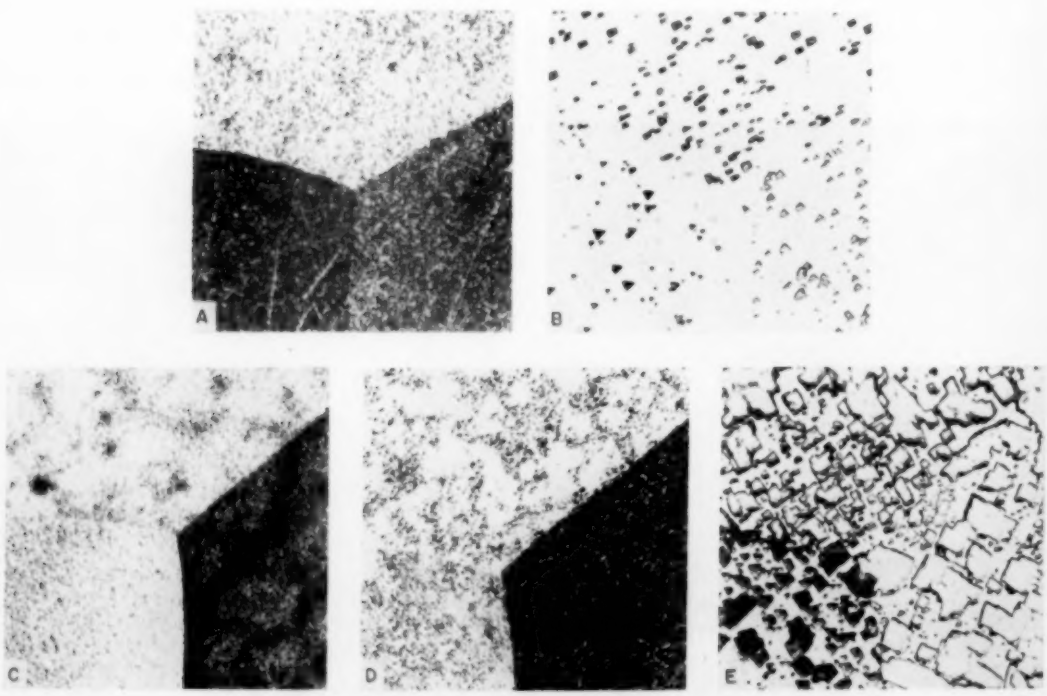

FIGURE 7. *Surface of aluminum 1143 after certain treatments.*

A and B, Etched with Tucker's reagent, × 50 and × 500, respectively; C, anodized, × 50; D and E, etched with modified Tucker's reagent, × 50 and × 500, respectively.

ΔI versus δ, the angle between the surface normal and the c-axis for this specimen of tin. The curve drawn was for the equation

$$\Delta I = 45 \sin^4 \delta,$$

for which no theoretical justification was attempted. However, it exhibited reasonable symmetry and behavior at the end points, and the probable error in the value of the colatitudes of the data points compared with those of points on this curve was less than 5°.

Measurements were also taken from specimen 1144 after the surface had been deeply etched. The average difference between extinction angle and c-axis azimuth more than doubled, and the ΔI relationship to the c-axis colatitude developed so much scatter that it could hardly be called more than a trend.

4.2. Aluminum

The aluminum specimen, 1143, was a coarse-grained cast specimen that had been polished by conventional metallographic procedure. Its granular structure is shown in figure 6. The intensity measurements were made after treating the polished surface in four ways: surface 1 was the result of etching with Tucker's reagent [*15*]; surface 2 was, after repolishing, anodized in an electrolyte recommended by Pearson, Machland, and Hay [*16*]; surface 3 was a repetition of the anodizing treatment; and surface 4 was the result of a deep etch with a modified Tucker's reagent [*17*]. These surfaces may be seen in figure 7. To show that the faces of the deep pits in this case were parallel to cubic planes, the positions of the specular reflections of ordinary light from them were measured with an optical goniometer [*18*]. The results checked satisfactorily.

The crystallographic orientation of the surface normal for the aluminum grains is shown in the stereographic triangle, figure 8. The stereographic coordinates, azimuth and colatitude, for the cubic axis making the greatest angle with surface normal, are given with photometer data from surface 4 in table 2. Table 3 presents the intensity and orientation relationship, which is shown graphically in figure 9.

For the etch-pit conditions, surfaces 1 and 4, the agreement between the extinction angle and the

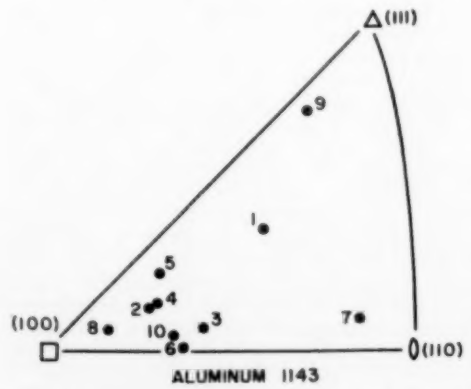

FIGURE 8. *Crystallographic orientations of surfaces normal with respect to individual crystals in the polished surface of aluminum 1143.*

Numbers 1 to 10 correspond to the numbers identifying the crystals in figure 6.

TABLE 2. *Photometer minima Al 1143, second etch pit condition*

Grain	ΔI	ψ_e	ψ	Orientation		$\Delta\psi$
				ϕ_a	δ	
		Degrees	*Degrees*	*Degrees*	*Degrees*	*Degrees*
1	29.6	17.2	17	19	75	−2
2	65.8	62.7	63	62	83	+1
3	90.5	84.0	354	357	87	−3
4	27.8	57.5	148	147	84	+1
5	45.3	23.6	24	21	80	+3
6	165	59.8	150	147	90	+3
7	201	29.9	120	119	86	+1
8	59.1	11.0	281	281	88	0
9	22.1	80.4	350	355	65	−5
10	107	54.9	325	325	88	0
Average $\lvert\Delta\psi\rvert$=1.9°.						

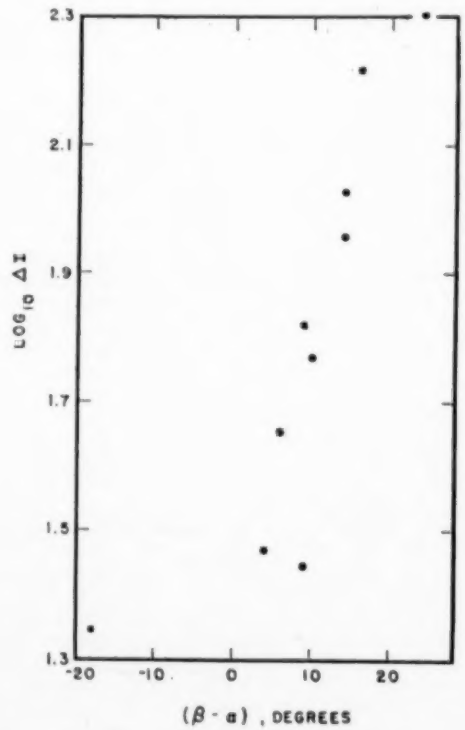

FIGURE 9. *Relation of ΔI of aluminum grains to the difference in angles between surface normal and the nearest [110] and [111] axes.*

TABLE 3. *Intensity and angle relationships in Al 1143, second etch-pit surface*

Grain	ΔI	α	β	γ	$\beta-\alpha$	$\log_{10}\Delta I$
		Degrees	*Degrees*	*Degrees*	*Degrees*	
7	201	8	32	39	24	2.3032
6	165	28	44	17	16	2.2175
10	107	29	45	16	14	2.0294
3	90.5	26	40	20	14	1.9566
2	65.8	33	42	14	9	1.8182
8	59.1	38	48	8	10	1.7716
5	45.2	32	38	17	6	1.6561
1	29.6	22	26	31	4	1.4713
4	27.8	32	41	15	9	1.4440
9	22.1	29	11	43	−18	1.3440

aizmuth of the cubic axis of greatest colatitude was good. The average difference for surface 1 was 4.2° and for surface 4, 1.9°. No doubt the intensity was related in some way to the orientation of the surface with respect to the grain's crystallography, but no empirical relationship could be found that was satisfactory over the entire range of the limited amount of data at hand. For convenience, one treatment of this data is presented in figure 9. However, no real functional relationship is implied.

The qualitative aspects of the reflection of plane polarized light from the aluminum with etch pits correlated well with the multiple reflections observed from the pit models made with front-surfaced mirrors because the faces of the etch pits are but slightly imperfect cubic planes.

A few limited experiments were made with three mirror models. One was a single-plane front-surfaced aluminized mirror with a stem normal to the plane. One was a "cube corner," three mutually perpendicular mirrors, with a stem making equal angles with the faces. The third consisted of two mirrors at right angles with a stem perpendicular to their line of intersection and making equal angles with each face. From experiments conducted with these models, it appears that there is a useful analogy between the orientation of the plane of the reflected polarized light and the orientation of the image of a linear object multiply reflected by the same mirror system.

Reflection from the single-plane mirror, normal incidence, showed no rotation of the plane of polarization. Nor did reflection from the three mutually perpendicular plane mirrors, no matter what the position of the model as it was rotated about its stem, corresponding to a [111] direction. Study of the light reflected from the model made of two perpendicular mirrors, however, was more complex. When the line of intersection (corresponding to a cubic axis) of the two surfaces was parallel to or at right angles to the plane of polarization of the incident light, the plane was not changed upon reflection. When the line of intersection was at 45° to the plane of the incident light, the plane of the reflected light was rotated 90°. Or, in general, for a rotation of $\theta°$ of the model about its stem, corresponding to a [110] direction, there was a $2\theta°$ rotation of the plane. These results were implied in the equations pertaining to multiple reflection of polarized light published

RAY DIAGRAM FOR RIGHT—ANGLE MIRROR

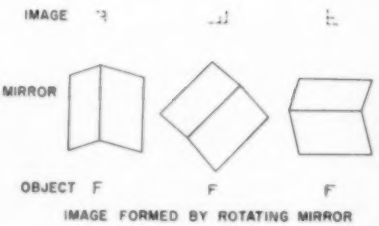

FIGURE 10. *Image formation by right-angle mirror.*

by Olwen Jones in 1924 [*19*]. This turning of the plane of polarization is analogous to the rotation of the image of an object placed before such a rotating mirror, as illustrated in figure 10.

In observations with the etched specimen, the greatest ΔI was observed from grains with their surface normals near [110]. In accordance with reflection from the two-mirror model, the intensity of the light passing through the crossed analyzer rose and fell four times per revolution. In the metallographic specimen, the grain with its surface normal nearest [111] had the smallest ΔI, that is, gave the smallest increase in light above the faint light at extinction. This agrees well with the three-mirror model, which did not rotate the plane of polarization in any position, and therefore always showed extinction when viewed through a crossed analyzer. The results of the experiments with the mirror models would lead one further to expect a minimum ΔI from grains with normals near [100]. This, however, was not observed to be very pronounced. A possible explanation could be that pits of this type were subject, on the average, to a greater degree of imperfection because more cubic faces would be involved in each such pit than in the two simpler cases.

The anodized films, surfaces 2 and 3, were reasonably light, just heavy enough to give smooth, nearly uniform cover. Polarized light, upon reflection from these surfaces was markedly affected, both as

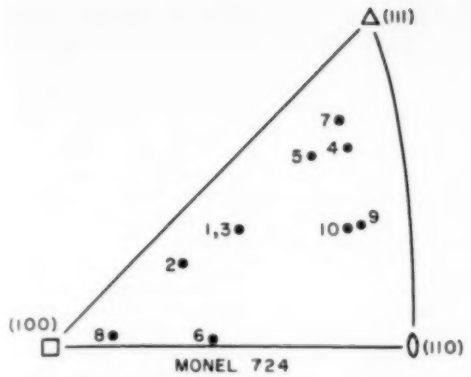

FIGURE 11. *Crystallographic orientations of surface normal with respect to individual crystals in the polished surface of monel 724.*

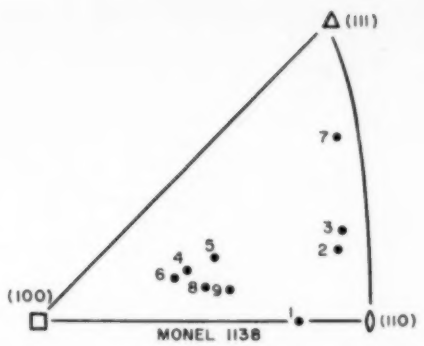

FIGURE 12. *Crystallographic orientations of surface normal with respect to individual crystals in the polished surface of monel 1138.*

to extinctions and to striking colors when examined through the sensitive tint plate. There was no apparent correlation, however, between this activity and the crystallographic orientation of the underlying metal. A film-orientation correlation was reported, however, by Pearson, Machland, and Hay [*16*], employing a heavier film than was used in this study.

4.3. Monel

The surfaces of the two monel specimens, 724 and 1138, were polished mechanically and etched with two reagents: A, a cyanide-persulate aqueous solution and B, monel contrast solution [*20*]. Each solution was used twice alternately on specimen 724; only the cyanide solution was used on specimen 1138. As pointed out in section 3.2, orientations of grains used were determined by the twin-trace method; the positions of the surface normal relative to the crystallographic directions in the grains are shown in stereographic triangles in figures 11 and 12. The stereographic coordinates, azimuth and colatitude, of the cubic axis of greatest colatitude are given in table 4 for monel 724, along with photometer data and extinction angles based both on photometer minima and polarization figure crossings. These data were taken from the surface with the second cyanide etch, preparation 3. Table 5 compares the intensity of reflection and the precision of the cubic axis azimuth-extinction angle correlation for the four surface preparations of this specimen. Table 6 lists the grains in the four cases in order of decreasing ΔI. It is apparent that the several sets of measurements of reflection showed much variation, especially in terms of intensity and its change, ΔI. In all four cases there was reasonable agreement of extinction angle with the azimuth of the cubic axis of greatest colatitude, but the average differences in the cases where the cyanide etch was used were less than half

TABLE 4. *Optical data, monel 724, surface III*

Grain	ΔI	ψ_0	Orientation		$\Delta\psi$
			Φ_n	δ	
		Degrees	*Degrees*	*Degrees*	*Degrees*
1	21.6	27	34	77	−7
2	7.9	347	345	79	2
3	29.0	286	280	76	6
4	5.8	323	321	67	2
5	5.1	357	3	68	−6
6	49.5	250	251	89	−1
7	5.3	346	353	55	−7
8	1.8	207	214	89	−7
9	43.5	82	83	76	−2
10	23.1	172	168	76	4
Average $\lvert\Delta\psi\rvert = 4.4°$.					

TABLE 5. *Comparison of approximate intensity of reflection and precision of results with various surfaces on monel 724*

Surface	Etch	Maximum I for grain 9	ΔI for grain 9	Average $\lvert\Delta\psi\rvert$
				Degrees
1	Cyanide	50.5	43.7	5.1
2	Contrast	21.5	20.5	10.2
3	Cyanide	51.2	43.5	4.4
4	Contrast	285.0	279.0	13.0

TABLE 6. *Grains of monel 724 ranked by intensity values.*

Rank	Surface condition			
	1 grain	2 grain	3 grain	4 grain
1	9	6	6	9
2	1	9	9	10
3	6	10	3	1
4	3	3	10	7
5	10	5	1	3
6	5	1	2	4
7	7	7	4	5
8	2	2	7	2
9	4	4	5	6
10	8	8	8	8

TABLE 7. *Photometer minima for grains of Monel 1138*

Grain	ΔI	ϕ_o	ϕ'_o	Orientation		$\Delta\phi$
				ϕ_o	δ	
		Degrees	*Degrees*	*Degrees*	*Degrees*	*Degrees*
1	40.2	36	36	39	89	−3
2	41.2	23	293	291	80	2
3	44.9	60	330	330	81	0
4	14.8	3	93	89	84	4
5	15.6	28	28	35	82	−7
6	23.3	81	351	346	83	5
7	9.7	41	311	324	69	−13
8	17.2	86	86	81	85	5
9	31.2	36	36	32	84	4
Average $\lvert\Delta\phi\rvert$=4.8°						

as large as those in the contrast etch cases. In all cases, however, there were large shifts in ranking the grains in terms of intensity, as can be seen in table 7. Hence, there was obviously no correlation of intensity with orientation, except the vague observation that the grain with surface normal nearest the [100] direction was always of smallest ΔI, whereas the two grains with normals nearest [110] were always near the top of the list in ΔI.

The other monel specimen, 1138, was etched with the cyanide reagent only. The surface normals of the grains are located in the stereographic triangle in figure 12, and the coordinates of the cubic axis of greatest colatitude are given in table 7, along with the photometer and microscope data. These results are comparable with those from monel 724, showing good agreement of extinction position with the azimuth of the cubic axis of greatest colatitude, and only a hint of correlation of intensity with angles between the surface normal and the [110] direction.

It should be stated that the correlations were usually poor when the normals to the surface were far from the [110] direction. This was observed for several grains in a different area of specimen 1138, for which data are not presented here. The extinction angles had a fair degree of reproducibility but did not always correspond with the azimuths of the cubic axis of greatest colatitude. In these cases they often corresponded to the azimuths of the axis most nearly normal to the surface. This was in agreement with some of the observations reported in the paper by Vacher [2], where specific data on a few such grains with anomalous extinctions were presented. This disturbing behavior did not appear in the case of aluminum or tin.

5. Discussion

The practical value of the polarizing microscope for the determination of the orientation of crystal grains in metallographic specimens and the source or mechanism of the optical anisotropy will be discussed in the light of the foregoing results.

5.1. Value of Polarized-Light Measurements in Determining Crystal Orientation

An examination of the results presented above reveals varying degrees of correlation between certain characteristics of reflected polarized light and the crystallography of the grains in the reflecting metal surface. It is true, however, that a complete orientation determination of a grain in a metallographic specimen cannot be made alone from polarized-light observations such as these. The first difficulty encountered is the obtaining of a suitable specimen surface, that will not cause the pertinent phenomena to be masked by the extraneous optical effects of scratches, irregular pits, nonuniform films, cold-working, inadequate etching, etc. If a nearly perfect, lightly etched surface with polarizing activity is obtained, the observation with crossed polarizing elements of the four extinction angles as the specimen is rotated will give within a few degrees four possible positions 90° apart for the azimuth of the "active" axis. This is the optic axis of a uniaxial material, or the axis making the greatest angle with the normal for a material showing anisotropic effects due to etch pits with facets parallel to cubic planes; or stated another way, when the polarizingly active specimen is in an extinction position on the microscope stage, the plane containing the surface normal and the active axis will coincide with either the plane of polarization of the polarizer or that of the analyzer.

If the surface quality is such that polarization figures can be observed, this ambiguity is cut in half. The four settings of the specimen, observed conoscopically, which give the cross figure, correspond to the extinction positions. As the specimen is rotated the isogyres spread apart and move toward the edges of the field in the quadrants containing the projection of the optic axis of a uniaxial material [9]. In this study the observation of polarization figures with uniaxial tin was found to be very difficult, but such observations were made quite successfully with etched monel, where the position of the cubic axis of greatest colatitude governed the behavior of the isogyres just as the optic axis is expected to do in theory. Locating the projection of the active axis in this way reduces its possible azimuth to two positions 180° apart. Polarization figures were not observed with aluminum either etched or anodized. In general, the degree of surface perfection required for the formation of these figures is even higher than that required for consistent extinction angle observations. Apparently the presence of textured films, pits, etc., precluded their use with the aluminum and tin specimens. The other quantity measured, change of intensity of polarized light as the specimen is rotated, is less reliable in its relation to orientation, probably because of its very great dependence upon surface condition. Nevertheless, if we can generalize from the observations of tin, it appears that for uniaxial materials with carefully prepared surfaces,

the order of grains ranked in terms of decreasing A/I will correspond very closely to the order of those ranked in terms of decreasing colatitude of the optic axis, approximating a fourth-power sine law.

On the other hand, the case for cubic materials is more complex and apparently is subject to more disturbing factors. This is shown by the great variations and inconsistencies of the intensities observed with monel. The observations with etch pits on aluminum were somewhat encouraging, and lead one to suppose that if suitable etchants that consistently create pits with known faces, preferably cubic, are employed [*18*], empirical relationships might be found for some isotropic materials.

It is apparent that the measurement of extinction angle and intensity is not sufficient to permit one to obtain a complete orientation determination. This procedure can be of great value, however, as an aid when other methods are being employed, as, for example, the twin-trace method or the etch-pit reflection method. Ambiguities often arise in twin-trace studies; and, with the method of reflections of ordinary light from etch pits, large deficiencies of precision are often an impediment. The additional information supplied by polarized-light examination will be an aid in resolving the difficulties encountered in such cases. In connection with the back-reflection Laue method, polarized-light data will facilitate the assignment of indices or the positioning of the specimen so that more readily interpreted patterns can be obtained.

5.2. Cause of the Optical Anistropy of Metals Having Cubic Structure

In section 1 brief reference is made to the question of the source of the polarization phenomena. Observations reported here showed distinct cases of polarization activity due both to a surface film (the anodized surface) and to surface contour (the etch pits). It is not surprising that an effect on the reflected polarized light can be due to either mechanism. The question would still remain, however, whether the effect of the film on the light was due to intrinsic anisotropy or to underlying metal-surface contour. It has been shown here that, when surface contour (etch pits) alone was involved, there was good correlation of the optical effects and the crystal orientation. The data from lightly anodized surfaces, however, gave no such correlation. It is therefore evident that the anisotropy of these light films was not related in any simple manner to the underlying surface contour, if such contour was a function of the crystal orientation, as in the case of the etch pits. Hence, it seems probable that these films are inherently anisotropic but that their orientation is related in an as yet undefined manner to the orientation of the underlying grains.

The results from monel were very much less definite than those from aluminum, but they showed a slight resemblance to the latter. Their lack of consistency can perhaps be attributed to the variation of degree of attack on cubic faces by the etching reagents.

When working with tin the conditions were somewhat different. The fact that the metal itself was anisotropic was the controlling factor in its behavior. Because of the softness of the metal, a very light etch improved the results by removing disturbing surface features such as polishing scratches, but the heavy etch worked against a correlation because of excessive irregular attack or an accumulation of an obscuring film of etch products.

6. Summary

Metallographic specimens of tin, aluminum, and monel were prepared, and the crystallographic orientations of many of the grains in each specimen were determined. The reflection of plane polarized light normally incident upon the specimens after various surface treatments was examined by means of a polarizing microscope and an electronic photometer. In some cases convergent light was used and polarization figures were observed. Very significant correlation was found in most cases between the extinction angle and the azimuth of the active axis. Moreover, in the case of tin, the change of intensity of the light from a grain was approximately proportional to the fourth power of the sine of the angle between the optic axis and the surface normal. In the case of aluminum and monel, the relationship of intensity to orientation was not so clear. The results support the hypothesis that the source of the optical anisotropy of polarized-light reflection from cubic metals is an oriented- surface contour.

The authors acknowledge capable assistance of Ellen A. Buzzard in preparing the metallographic specimens and express their gratitude to Mrs. Buzzard and Ruth E. Dowden for aid in the preparation of many of the drawings and photographs used.

7. References

[*1*] D. H. Woodard, Stages in the deformation of Monel metal as shown by polarized light, Am. Inst. Min. Met. Engrs, Metal Trans. **185**, 722 (1949).

[*2*] H. C. Vacher, A correlation of polarized light extinctions with crystal orientation in 70 nickel-30 copper alloy, J. Research NBS **49**, 149 (1952) RP2351.

[*3*] J. Woodrow, B. W. Mott, and H. R. Haines, Analysis of polarized light reflected from absorbing materials at normal incidence, Proc. Phys. Soc. London [B] **65**, 603 (1952).

[*4*] G. K. T. Conn and F. J. Bradshaw, Polarized light in metallography, p. 72 (Academic Press, Inc., New York, N. Y., 1952).

[*5*] F. A. Jenkins and H. E. White, Fundamentals of optics, p. 560 (McGraw-Hill Book Co., New York, N. Y., 1950).

[*6*] B. W. Mott and H. R. Haines, Examination of metals under polarized light. I. Theory and apparatus, Research **4**, 24 (1951).

[*7*] G. K. T. Conn and F. J. Bradshaw, Polarized light in metallography, p. 66 (Academic Press, Inc., New York, N. Y., 1952).

[8] F. A. Jenkins and H. E. White, Fundamentals of optics, p. 537 (McGraw-Hill Book Co., New York, N. Y., 1950).
[9] E. N. Cameron and L. H. Green, Polarization figures and rotation properties in reflected light and their application to the identification of ore minerals, Econ. Geol. **45**, 719 (1950).
[10] C. S. Barrett, The structure of metals, p. 39 (McGraw-Hill Book Co., New York, N. Y., 1943).
[11] A. B. Greninger, Determination of orientation of metallic crystals by means of back-reflection Laue photographs, Trans. Am. Inst. Mining Met. Engrs. **117**, 61 (1935); A back-reflection Laue method for determining crystal orientation, Z. Krist **91**, 424 (1935).
[12] C. S. Barrett, The structure of metals, p. 167 (McGraw-Hill Book Co., New York, N. Y., 1943).
[13] L. V. Foster, A polarizing vertical illuminator, J. Opt. Soc. Am. **28**, 124 (1938).
[14] C. H. Hack and F. H. Clark, The metallography of tin and tin alloys, Metals Handbook, 1948 ed., p. 1069 (Am. Soc. Metals, Cleveland 3, Ohio).
[15] F. Keller, The metallography of aluminum alloys, Metals Handbook, 1948 ed., p. 798 (Am. Soc. Metals, Cleveland 3, Ohio).
[16] E. C. Pearson, G. Machland, and R. H. Hay, An electrolytic etch technique for aluminum and its application to some metallographic problems, Can. Inst. Metals **45**, 598 (1952).
[17] G. E. G. Tucker and P. C. Murphy, A method for determining orientation in aluminum single crystals and polycrystalline aggregates, J. Inst. Metals **81**, 235 (1953).
[18] C. S. Barrett, The structure of metals, p. 173 (McGraw-Hill Book Co., New York, N. Y., 1943).
[19] O. Jones, Reflection of plane polarized light by etched metals, Phil. Mag. **48**, 207 (1924).
[20] D. I. Sinizer, The metallography of nickel and nickel alloys, Metals Handbook, 1948 ed., p. 1045 (Am. Soc. Metals, Cleveland, Ohio).

WASHINGTON, November 3, 1953.

rnal of Research of the National Bureau of Standards Vol. 53, No. 1, July 1954 Research Paper 2511

Separation of Iodide, Bromide, and Chloride From One Another and Their Subsequent Determination

Thomas J. Murphy, W. Stanley Clabaugh, and Raleigh Gilchrist

A method is described for separating iodide, bromide, and chloride from one another. First, the iodide ion is oxidized to elementary iodine by hydrogen peroxide in weakly acid solution and the iodine removed by distillation. Next, bromide is oxidized to bromine without affecting the chloride ion by use of a controlled concentration of nitric acid as oxidizing agent. After removal of bromine by distillation, chloride remains in the residual solution.

Determination of the individual halides depends on the quantity of each. If in trace amounts, a turbidimetric method is used; if in larger amounts, potentiometric titration with silver nitrate is used.

A description of the apparatus used is also given.

1. Introduction

Many of the methods described in the literature for the separation of iodide, bromide, and chloride from one another and for their subsequent determination yield unsatisfactory results. In the separation of iodide only from a mixture of the three halides, the published methods do report accurate results. Iodide is usually separated by oxidizing it with nitrous acid or ferric sulfate in a dilute solution of sulfuric acid [1] [1] and volatilizing the liberated iodine. The separation of bromide from chloride is a more difficult matter. In 1928 Wales [2] studied the methods reported in the literature and found the method of Winkler [3] to be the most promising. Winkler treated a mixture of bromide and chloride with sulfuric acid and permanganate and distilled out the bromine. In 1931 Freeman [4] reported this method to be unsatisfactory and recommended a modification, but in 1942 he [5] reported unsatisfactory results with his own revision. He stated that in this method, as well as in the others studied, the principal cause of error was the formation of free chlorine, which caused high results, or the formation of bromate, which caused low results. In the best method that he studied for the separation and determination of iodide, bromide, and chloride, the recovery of bromide was only 95 percent.

Because of this lack of a reliable method, a study was undertaken and a method developed by which the three halogens can be quantitatively separated from one another. The method yields accurate results regardless of the relative concentrations of the three halides.

2. Discussion

2.1. Separation of Iodide from Bromide and Chloride

In weakly acid solution it is possible to oxidize iodide to iodine with hydrogen peroxide without oxidizing either bromide or chloride. In solutions containing iodide, bromide, and chloride and hydrogen peroxide, the following are the significant reactions which can occur. The free-energy values, in kilocalories per mole, are calculated from values reported by Latimer [6], as follows:

(1)	$H_2O_2 + H^+ + 2I^- = I_2 + 2H_2O$;	ΔF°_{298}	$= -53.284$
(2)	$H_2O_2 + I_2 = O_2 + 2H^+ + 2I^-$;		$= +2.844$
(3)	$H_2O_2 + 2H^+ + 2Br^- = Br_2 + 2H_2O$;		$= -31.785$
(4)	$H_2O_2 + Br_2 = O_2 + 2H^+ + 2Br^-$;		$= -18.655$
(5)	$H_2O_2 + 2H^+ + 2Cl^- = Cl_2 + 2H_2O$;		$= -17.560$
(6)	$H_2O_2 + Cl_2 = O_2 + 2H^+ + 2Cl^-$;		$= -32.880$
(7)	$H_2O_2 = H_2O + \frac{1}{2}O_2$;		$= -25.220$

The large negative values of ΔF show that all of the reactions except reaction (2) tend to take place. At a pH of 5, reactions (1) and (2) proceed at about the same rate [7], the net results of the reaction being the decomposition of hydrogen peroxide. As the acidity is increased, reaction (1) takes place at a faster rate and reaction (2) at a slower rate until at a pH of 1 the rate of reduction of iodine is negligible. If the iodine formed is removed from the solution, reaction (1) can go to completion. However, as the acidity is increased it is possible to oxidize a small amount of bromide to bromine (reaction 3). Reaction (4) is much faster than reaction (3) [8], but as the acidity is increased reaction (3) is favored. As the rate of reaction between bromine and peroxide is rapid in neutral or weakly acid solution and the rate of oxidation of bromide slow, it follows that any bromine formed by reaction (3) would be reduced rapidly, with the resultant decomposition of hydrogen peroxide (reaction 7). However, if some of the bromine produced by reaction (3) were removed either as bromine or iodine monobromide (through reaction with the liberated iodine in reaction (1) before conversion to bromide by reaction (4), it would be possible to lose some of the bromine. This actually proves to be the case. For example, when 3 g of sodium bromide in 100 ml of water was treated with 3 ml of hydrogen peroxide and 2 ml of phosphoric acid, and the solution boiled, bromine vapor could be seen distilling over. However, when the bromide content was decreased to 1 g of sodium bromide in 200 ml of water and the acidity adjusted to a pH of 1 with phosphoric acid, no bromine could be seen distilling over, and a test of the distillate showed it to contain only 0.2 mg of bromide. This error would be negligible for large amounts of iodide in the presence of small amounts of bromide. How-

[1] Figures in brackets indicate the literature references at the end of this paper.

ever, to determine small amounts of iodide in the presence of a large amount of bromide, the distillate obtained must be again treated with hydrogen peroxide and phosphoric acid and redistilled. When this is done no bromine is detected in the distillate. When large amounts of both iodide and bromide occur together, bromine may be lost as iodine monobromide, if the acidity is not controlled carefully. When enough phosphoric acid is added at the start so that the resultant pH will be 1 after the iodine is removed, considerable bromide is lost as iodine monobromide. But when peroxide is added first, the solution heated to boiling, and the acid added slowly as the iodine distills out, only a negligible amount of bromide is lost.

Reactions (5) and (6) both take place at about the same rate, with the resultant decomposition of hydrogen peroxide [9]. At low acidity, only a negligible amount of chlorine distills, even from fairly concentrated chloride solutions. Thus under proper conditions it is possible to separate quantitatively iodide from bromide and chloride.

2.2. Separation of Bromide from Chloride

It has been found that nitric acid in suitable concentration will quantitatively oxidize bromide to bromine without oxidizing chloride to chlorine. Kebler [10] and Chamot and Mason [11] both used this reaction for the qualitative separation of bromide from chloride, but apparently no attempt was made to find out if the reaction could be made quantitative under proper conditions. Experiments showed that in diluted nitric acid (1+9)[3] the oxidation was complete but slow and that in diluted nitric acid (1+2) chlorine begins to distill. It was observed experimentally that satisfactory results were obtained when the range of nitric acid concentration was from (1+6) to (1+3). The nitric acid concentration used in the experimental work was (1+5). However, it was found that under these conditions a small amount of chloride is lost as chlorine. For example, when 20 ml of nitric acid was added to 100 ml of water containing 1 g of potassium chloride and 25 ml of the solution distilled into hydrazine sulfate solution, the distillate was found to contain 0.5 mg of chloride. In more dilute solutions of chloride and of acid the error is even less. This error would be negligible for large amounts of bromide in the presence of small amounts of chloride, but a second treatment and distillation is necessary in the case of large amounts of chloride in the presence of small amounts of bromide. This indicates that it is possible to separate quantitatively bromide from chloride.

3. Reagents Used

Potassium Iodide. The potassium iodide used was prepared by Mark Swanson, formerly of the Bureau. The method of preparation is not known. It was found to contain 0.0003 percent of bromide and 0.0003 percent of chloride.

Sodium Bromide. A survey of available bromide salts showed that they all contained chloride. The sodium bromide used in these experiments was prepared from sodium carbonate and hydrobromic acid as follows:

An approximately 30-percent solution of sodium carbonate, prepared from sodium carbonate containing 0.002 percent of chloride, was filtered through a glass filter of fine porosity. Sodium bicarbonate was precipitated from this solution by saturation with carbon dioxide. The mixture was cooled in an ice bath, and the salt was caught on a porous glass filter, washed with cold water, and sucked dry. The sodium bicarbonate so obtained was redissolved and the solution acidified with specially prepared hydrobromic acid, containing 0.0004 percent of chloride, to the end point of methyl red. The solution was boiled to expel carbon dioxide, evaporated to a small volume on the steam bath, cooled, filtered, and the resulting salt washed with 95-percent ethyl alcohol. This product was found to contain 0.0002 percent of iodide and 0.006 percent of chloride.

Potassium Chloride. The potassium chloride used was of ACS reagent quality and was found to contain 0.0006 percent of iodide and 0.0002 percent of bromide.

Phosphoric Acid. The phosphoric acid used was of ACS reagent quality and was found to contain less than 0.0005 percent of combined halides as chloride.

Hydrogen Peroxide. The hydrogen peroxide used was 30-percent peroxide of ACS reagent quality. It was found to contain less than 0.0005 percent of combined halides as chloride.

Nitric Acid. The nitric acid used was of ACS reagent quality. It was found to contain less than 0.00001 percent of combined halides as chloride.

Hydrazine Sulfate. The hydrazine sulfate was supplied commercially. It was found to contain less than 0.0005 percent of combined halides as chloride.

Silver Nitrate. The silver nitrate used was of ACS reagent quality. It was found to contain less than 0.00005 percent of combined halides as chloride.

Potassium Permanganate Reagent Solution. A survey of commercial samples showed them all to be high in chloride content. The following method of purification was used:

Seventy-five grams of potassium permanganate was dissolved in 1,250 ml of water, and 10 ml of nitric acid was added. The solution was heated to about 45° C, and a stream of halide-free air was passed through the solution. At intervals the evolved gases were passed through a 2-percent solution of hydrazine sulfate for ½ hour, and this solution was tested for chloride with silver nitrate. The treatment was continued until chlorine was no longer detected. This solution, which contained about 0.9 g of potassium permanganate in 15 ml, was found to contain less than 0.0001 percent of chloride.

[3] Throughout this paper, whenever the use of an acid is prescribed with no indication of strength or dilution, the acid to be used is the concentrated acid. Dilutions are indicated by the volumes of acid and water mixed to prepare a dilute reagent. Diluted nitric (1+r) means a diluted acid prepared by mixing 1 volume of the concentrated acid with r volumes of distilled water.

4. Preparation and Standardization of Solutions

4.1. Silver Nitrate on a Weight Basis (Approximately 0.1 Molal)

About 70 g of silver nitrate was dissolved in 4 liters of water. Two 50-ml portions and a 60-ml portion were measured by means of a weight buret. The portions were concentrated on a steam bath to a volume of about 10 ml, and 10 ml of 1 *N* hydrochloric acid was added to each. The solutions were diluted to 150 ml and stored in the dark overnight. The precipitates were collected in filtering crucibles of fine porosity, washed with very dilute hydrochloric acid (1+999), dried at 120° C, and weighed. The concentration was found to be 0.010625 g of silver per gram of solution.

4.2. Silver Nitrate on a Volumetric Basis (Approximately 0.01 Normal)

The same procedure as above was followed except that the 50-ml and 60-ml portions were accurately measured volumetrically instead of being weighed. The solution was found to be 0.10256 *N* and was diluted tenfold before use.

4.3. Iodide

Twenty grams of the potassium iodide was dissolved in 2 liters of distilled water. Weighed portions of the solution of about 45 g to 60 g were diluted to 100 ml, and 0.1 molal silver nitrate was added by means of a weight buret to within about 1 percent of the equivalence point. The titration was completed with 0.01 *N* silver nitrate potentiometrically. The concentration was found to be 0.0077132 g of iodide per gram of solution.

4.4. Bromide

Twenty grams of the sodium bromide was dissolved in 2 liters of distilled water. The same procedure was used as for the standardization of the iodide solution. The concentration was found to be 0.0078208 g of bromide per gram of solution.

4.5. Chloride

Twenty grams of the potassium chloride was dissolved in 2 liters of distilled water. The same procedure was used as for the standardizations of the iodide and bromide solutions, except that the solution was cooled in an ice bath during the titration. The concentration was found to be 0.0047904 g of chloride per gram of solution.

5. Procedure Used for Separating Iodide, Bromide, and Chloride

5.1. Halides Present as Major Constituents

The distilling apparatus was assembled as in figure 1. Twenty-five milliliters of a 2-percent solution of hydrazine sulfate was placed in flask G and 25 ml of a 0.5-percent solution of hydrazine sulfate was placed in flask I. About 4 in. of mercury was placed in gas washing bottle K and 50 ml of 1 *N* silver nitrate was placed in gas washing bottle L. When this system was connected to a vacuum line, the silver nitrate solution served to wash any halide from the air, and the mercury maintained the pressure on the system about 4 in. below atmospheric pressure. In this manner no halogen was lost through the glass joints, as air would have been drawn in through a loosely fitting joint.

By means of weight burets and the standardized halide solutions, synthetic mixtures of halide salts were obtained containing varying amounts of each halide. The amounts added were such that a total of about 1 g of combined halide salts was present.

The standardized solutions were added directly from weight burets to flask A to avoid error due to transfer. This apparatus and method of adding the known amounts of halide solutions were used throughout all the separations, unless otherwise noted.

Separation of Iodide. The synthetic halide mixture in flask A was diluted to about 200 ml. The system was closed and connected to a vacuum line. The vacuum was regulated so that air slowly bubbled through the mercury. One milliliter of 30-percent hydrogen peroxide was added through delivery funnel B, and the solution was heated to boiling. Diluted phosphoric acid (1+99) was placed in the delivery funnel and slowly dropped into the solution until iodine began to be evolved. The addition of

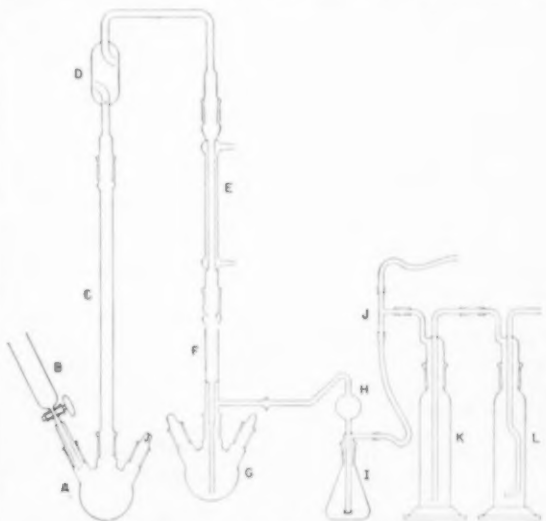

FIGURE 1. *Distilling apparatus.*

A, 300 ml, 3-neck distilling flask with standard taper joints; B, delivery funnel, about 60-ml capacity, with standard taper joint and stopcock; C, tube about 50 cm long with standard taper joints; D, spray trap, Kjeldahl cylindrical type with standard taper joints; E, condenser, West type, about 30 cm long with standard taper joints; F, distilling tube, ball joint on side arm, standard taper joints elsewhere. Delivery tube extends to bottom of flask G; G, 200 ml, 3-neck distilling flask with standard taper joints; H, distilling tube with ball joint on entrance arm and bulb to prevent suck-back. Delivery tube reaches to bottom of flask I and has a gas-bubbling disc at its end; I, 125-ml flask with standard taper stopper; J, connection to vacuum line; K, gas washing bottle, 125-ml capacity, containing about 4 inches of mercury; L, gas washing bottle, 125-ml capacity, containing about 40 ml of 1 *N* $AgNO_3$. The delivery tube has a fritted disc at the end.

The joints on the 3-neck flasks not in use are capped with standard-taper caps. A plug of glass wool is inserted into the neck of both K and L. Rubber connections are used where standard taper or ball joints are not specified.

phosphoric acid was stopped and the liberated iodine removed by distillation. More diluted phosphoric acid was added and the iodine liberated again removed. This addition of phosphoric acid and removal of iodine was continued until iodine was no longer liberated from the solution. The amount of diluted phosphoric acid necessary will depend on the quantity of iodide present. Usually, 10 to 25 ml of the diluted acid is required. The distillation was continued until all of the iodine was distilled into flask G.[3] It was necessary to keep the hydrazine sulfate solution in flask G warm because iodine does not react readily with the cool solution. The rate at which the iodine distilled was kept slow, so that only about 25 ml to 30 ml of solution distilled. About 1 ml of diluted phosphoric acid (1+99) and 0.2 ml of 30-percent hydrogen peroxide were added through the delivery funnel and the color of the solution noted. If a color developed, the iodine formed was removed by distillation and the treatment repeated until no color was developed.[4] The solution in flash I was poured into flask G. Tubes F and H and flask I were rinsed and the washings caught directly in flask G. The flask and contents were reserved for the determination of iodide.

Separation of Bromide. The apparatus was reassembled as above, with another 3-neck flask for G. Sixty milliliters of diluted nitric acid (1+1) was added through delivery funnel B, and the solution was refluxed until all the hydrogen peroxide was decomposed. (With a little practice, this can be determined by noting a change in the bubble formation.) The bromine produced was slowly distilled, and the distillation continued for 15 minutes after the residual solution was colorless and no trace of bromine could be seen anywhere in the system. The rate of distillation was kept slow, and the volume in flask A was never allowed to drop below 120 ml. The solution in flask I was poured into flask G. Tubes F and H and flask I were rinsed and the washings caught directly in flask G. The flask and contents were reserved for the determination of the bromide.

Separation of Chloride. As the iodide and bromide originally present had already been removed, the only halide remaining in flask A was the chloride. The flask and contents were reserved for the determination of chloride.

5.2. Iodide as the Major Constituent, Bromide and Chloride as Minor Constituents

Separation of Iodide. The method of separation used was the same as for the separation of iodide under 5.1, except that the concentration and method of addition of the phosphoric acid were different. In this instance 10 ml of diluted phosphoric acid (1+9) was added directly instead of dropping in the more diluted acid (1+99).

Separation of Bromide. The apparatus was assembled as in 5.1, except that tube H and flask I were omitted and that 0.5-percent hydrazine sulfate solution was used in flask G. A piece of platinum gauze and 60 ml of diluted nitric acid (1+1) were added to the solution in flask A. The purpose of the platinum gauze was to catalyze the decomposition of the hydrogen peroxide present. The solution was refluxed until the peroxide was decomposed, and then for 30 minutes longer. The solution was slowly distilled until no visual evidence of bromine remained or until 25 ml had distilled if no bromine was noted. Tube F was rinsed and the washings caught directly in flask G. The flask and contents were reserved for the determination of bromide.

Separation of Chloride. If more than 0.1 percent (1 mg) of chloride was present, the chloride was determined without further treatment. If less than 0.1 percent (1 mg) of chloride was present, the following method was used:

The apparatus was assembled as in the separation of bromide. Fifteen milliliters of potassium permanganate reagent solution was added to flask A through the delivery funnel. The solution was heated to boiling, refluxed for 30 minutes, 25 ml slowly distilled into flask G, and this solution saved for the determination of chloride. This isolation of the small amount of chloride is advantageous because the chloride is thus concentrated in a small volume of solution that is free from substances such as nitric acid that might have a solvent effect on the silver chloride.

5.3. Bromide as the Major Constituent, Iodide and Chloride as Minor Constituents

Separation of Iodide. The apparatus was assembled as in the separations of bromide and chloride in 5.2. Using this modified apparatus, the iodide was separated as in 5.2 except that at the end of this separation a second apparatus similar to the first was set up in which flask G of the first apparatus became flask A′ of the second one. One-half gram of dipotassium hydrogen phosphate, 2 ml of 30-percent hydrogen peroxide, and 10 ml of diluted phosphoric acid (1+9) were added to this flask. The resulting solution was heated to boiling, refluxed for 30 minutes, and 25 ml was slowly distilled into flask G′. The solution in this flask was saved for the determination of iodide. The solution in flask A′ was poured into flask A.

This is, in effect, a second treatment and separation of the iodide, necessary because of the small amount of bromide that comes over in the first separation. The role of the dipotassium hydrogen phosphate is not clear, but halogens appear to distill from solutions that contain it faster than from those that do not.

Separation of Bromide. The method outlined for the separation of bromide in 5.1 was followed, except that a piece of platinum gauze was added to hasten the decomposition of the peroxide, and 30 ml of concentrated nitric acid was used instead of 60 ml of diluted nitric acid (1+1).

Separation of Chloride. The procedure outlined for the separation of chloride in 5.2 was followed.

[3] The side necks of flask A were gently heated with a torch to drive over the iodine that condensed there.

[4] On turning off the heat, it was necessary to open the stopcock on B and to disconnect the vacuum to prevent the solution in G from sucking back.

5.4. Chloride as Major Constituent, Iodide and Bromide as Minor Constituents

Separation of Iodide. The iodide was separated as in 5.3, except that a second treatment and separation were not necessary.

Separation of Bromide. The method outlined for the separation of bromide in 5.2 was followed, except that at the end of this separation a second apparatus similar to the first was set up in which flask G of the first apparatus became flask A′ of the second apparatus. One-half gram of dipotassium hydrogen phosphate, 50 ml of water, and 15 ml of nitric acid were added to the solution in flask A′ and the same procedure followed as in the first separation. This second treatment served to separate the bromide from the small amount of chloride that distilled in the first separation. After the second separation the solution in flask A′ was poured into flask A.

Separation of Chloride. The procedure outlined for the separation of chloride in 5.1 was followed.

5.5. Halides Present as Minor Constituents

Separation of Iodide. The procedure outlined for the separation of iodide in 5.3 was followed, except that a second treatment and separation were not necessary and that 0.5 g of dipotassium hydrogen phosphate was added to flask A before the separation.

Separation of Bromide. The procedure outlined for the separation of bromide in 5.2 was followed.

Separation of Chloride. The procedure outlined for the separation of chloride in 5.2 was followed.

6. Determination of the Separated Halides

In the above procedures the separated halides were determined by two different methods, depending on the concentration of the halide. When the halide was in excess of 1 mg, a potentiometric titration method was used, and when present in less than this amount, a turbidimetric method was used.

6.1. Potentiometric Method

The potentiometric method was based on a variation of the method of Lange and Schwartz [12]. The apparatus consisted of the following items: Vacuum-tube voltmeter with full scale of 100 mv; silver electrode; calomel electrode; salt bridge, consisting of a glass tube fitted with fine porous frits at the ends and filled with a solution containing 1 part of glycerine and 1 part of a saturated aqueous solution of ammonium nitrate; and magnetic stirring apparatus.

The 3-neck flask containing the separated halide was placed on the stage of the magnetic stirrer, and a Teflon-coated stirring bar was placed in the flask. The salt bridge was inserted into a side neck of the 3-neck flask so that it reached below the surface of the solution. The silver electrode was inserted through the other side neck in a similar manner. The other end of the salt bridge was immersed in the calomel electrode, and the silver and calomel electrodes were connected to the voltmeter. When chloride was being determined, it was necessary to cool the flask in an ice bath during the titration. During all determinations it was necessary to shield the flask from light. This was accomplished by enclosing the assembly in black paper.

Standardized silver nitrate was added from a weight buret until the end point was approached, usually to within 1 percent of the theoretical amount required. The titration was completed by using 0.01 *N* silver nitrate. The change in electromotive force produced by the addition of known amounts of the silver nitrate solution was recorded, and the end point was determined by the method of plotting $\Delta E/\Delta v$ with respect to the volume, v, of solution added. From the weight of the first silver nitrate solution and the volume of the second, the amount of halide was calculated.

6.2. Turbidimetric Method

When the halide content was small (less than 1 mg), a turbidimetric method was used after suitable dilution. The method was as follows:

The solution in flask G was diluted so as to contain from 0.01 to 0.05 mg of halide in 50 ml of solution. Controls containing varying amounts of halides (e. g., 0.01, 0.02, 0.03 mg of halide) and the same amount of hydrazine sulfate as in 50 ml of the diluted sample solution were prepared. One milliliter of nitric acid and 1 ml of 0.1 *N* silver nitrate were added to the 50-ml portion of the sample solution and to the controls. The turbidities produced were compared visually in Nessler tubes.

7. Results

Table 1 shows the results obtained for the separation and determination of known amounts of halides when at least 1 mg of each halide was present. The separations were all performed according to the procedure outlined in section 5.1. The determinations were all by the potentiometric method.

Table 2 shows the results obtained for the separation and determination of known amounts of halides when one of the halides was present as a major constituent, with the other two halides as minor constituents. The separations were all performed according to the procedures outlined in sections 5.2., 5.3., and 5.4. The major constituent was not determined because the results shown in table 1 prove that large amounts of halides can be recovered. The minor constituents (halides) were determined by the turbidimetric method.

Table 3 shows the results obtained for the isolation and determination of small known amounts of the halides in the order of 1 mg or less of each. The separations were all done as in the procedure given in section 5.5. The determinations were all by the turbidimetric method.

The results given in tables 2 and 3 were corrected for any halide present in the reagents.

As shown in table 1, there was a standard deviation of 0.0002 g for the iodide determinations, 0.0002 g for the bromide determinations, and 0.0003 g for the chloride determinations. Because all determinations reported in tables 2 and 3 were made by a

TABLE 1. *Results obtained when halide was a major constituent*

Approximate composition	Solution No.	Iodide			Bromide			Chloride		
		Present	Found	Error	Present	Found	Error	Present	Found	Error
		g	*g*	*g*	*g*	*g*	*g*	*g*	*g*	*g*
33⅓% KI, 33⅓% NaBr, 33⅓% KCl	1	0.2377	0.2378	0.0001	0.2475	0.2472	0.0003	0.1142	0.1143	0.0000
	2	.2844	.2846	.0002	.2715	.2716	.0001	.1871	.1868	.0003
	3	.2714	.2719	.0005	.2764	.2765	.0001	.1761	.1761	.0000
	4	.2533	.2532	.0001	.2676	.2680	.0004	.1517	.1514	.0003
15% KI, 15% NaBr, 70% KCl	5	.1437	.1438	.0001	.1277	.1276	.0001	.2923	.2917	.0006
	6	.0763	.0765	.0002	.0804	.0804	.0000	.3958	.3953	.0005
15% KI, 60% NaBr, 25% KCl	7	.1191	.1190	.0001	.4599	.4598	.0000	.1012	.1012	.0000
	8	.1100	.1099	.0001	.4656	.4655	.0001	.1328	.1322	.0006
60% KI, 15% NaBr, 25% KCl	9	.4090	.4089	.0001	.0829	.0828	.0001	.1264	.1266	.0002
	10	.4596	.4595	.0001	.0870	.0870	.0000	.1029	.1030	.0001
2% KI, 2% NaBr, 96% KCl	11	.0078	.0077	.0001	.0098	.0098	.0000	.4849	.4849	.0000
	12	.0098	.0098	.0000	.0113	.0115	.0002	.4784	.4781	.0003
96% KI, 2% NaBr, 2% KCl	13	.7658	.7658	.0000	.0098	.0097	.0001	.0078	.0077	.0001
	14	.7531	.7530	.0001	.0088	.0088	.0000	.0061	.0061	.0000
2% KI, 96% NaBr, 2% KCl	15	.0070	.0070	.0000	.7743	.7742	.0001	.0062	.0063	.0001
	16	.0061	.0061	.0000	.7716	.7714	.0002	.0052	.0053	.0001
Standard deviation				0.0002			0.0002			0.0003

TABLE 2. *Results obtained when two of the halides were minor constituents, and the third a major constituent*

Approximate composition	Solution No.	Iodide		Bromide		Chloride	
		Added	Found	Added	Found	Added	Found
		mg	*mg*	*mg*	*mg*	*mg*	*mg*
0.1% I, 0.1% Br, rest KCl	1	1.0	1.0	1.0	1.0	------	------
	2	1.0	1.0	1.0	1.0	------	------
0.1% I, 0.1% Cl rest NaBr	3	1.0	1.0	------	------	1.0	1.0
	4	1.0	1.0	------	------	1.0	1.0
0.1% Br, 0.1% Cl, rest KI	5	------	------	1.0	1.0	1.0	1.0
	6	------	------	1.0	1.0	1.0	1.0
0.01% I, 0.01% Br, rest KCl	7	0.1	0.1	0.1	0.1	------	------
	8	.1	.1	.1	.1	------	------
0.01% I, 0.01% Cl, rest NaBr	9	.1	.1	------	------	0.1	0.1
	10	.1	.1	------	------	.1	.1
0.01% Br, 0.01% Cl, rest KI	11	------	------	.1	.1	.1	.1
	12	------	------	.1	.1	.1	.1
0.001% I, 0.001% Br, rest KCl	13	.01	.01	.01	.01	------	------
	14	.01	.01	.01	.01	------	------
0.001% Br, 0.001% Cl, rest KI	15	------	------	.01	.01	.01	.01
	16	------	------	.01	.01	.01	.01

visual turbidimetric method, standard deviations were not calculated, as they would be meaningless. For all practical purposes, the recovery of added halides in these determinations may be regarded as 100 percent.

8. References

[1] F. A. Gooch and F. W. Mar, Am. J. Sci. **39,** 293 (1890).
[2] H. Wales, J. Assoc. Offic. Agr. Chemists **12,** 302 (1929).
[3] L. W. Winkler, Z. angew. Chem. **28,** 477 (1915).
[4] N. E. Freeman, J. Assoc. Offic. Agr. Chemists **14,** 338 (1931).
[5] N. E. Freeman, J. Assoc. Offic. Agr. Chemists **25,** 833 (1942).
[6] W. M. Latimer, Oxidation potentials, 2d ed. (Prentice-Hall, Inc., New York, N. Y., 1952).
[7] W. C. Bray and H. A. Liebhafsky, J. Am. Chem. Soc. **53,** 38 (1931).
[8] R. S. Livingston and W. C. Bray, J. Am. Chem. Soc. **45,** 2048 (1923).
[9] R. S. Livingston and W. C. Bray, J. Am. Chem. Soc. **47,** 2069 (1925).

TABLE 3. *Results obtained when halide was a minor constituent*

Solution No.	Iodide		Bromide		Chloride	
	Added	Recovered	Added	Recovered	Added	Recovered
	mg	*mg*	*mg*	*mg*	*mg*	*mg*
1	1.0	1.0	1.0	1.0	1.0	1.0
2	1.0	1.0	1.0	1.0	1.0	.9
3	.10	.10	.10	.10	.10	.10
4	.10	.10	.10	.10	.10	.10
5	.01	.01	.01	.01	.01	.01
6	.01	.01	.01	.01	.01	.01

[10] L. F. Kebler, J. Anal. App. Chem. **6,** 569 (1892).
[11] E. M. Chamot and C. W. Mason, Mikrochem. **5,** 85 (1927).
[12] I. M. Kolthoff and N. H. Furman, Potentiometric titrations, 2d ed., p. 148 (John Wiley & Sons, Inc., New York, N. Y., 1940).

WASHINGTON, April 13, 1954.

Journal of Research of the National Bureau of Standards Vol. 53, No. 1, July 1954 Research Paper 2512

Relative Humidity-Temperature Relationships of Some Saturated Salt Solutions in the Temperature Range 0° to 50° C[1]

Arnold Wexler and Saburo Hasegawa

The relative humidity-temperature relationships have been determined in air in equilibrium with saturated salt solutions of lithium chloride, $LiCl \cdot H_2O$; magnesium chloride, $MgCl_2 \cdot 6H_2O$; sodium dichromate, $Na_2Cr_2O_7 \cdot 2H_2O$; magnesium nitrate, $Mg(NO_3)_2 \cdot 6H_2O$; sodium chloride, NaCl; ammonium sulfate, $(NH_4)_2SO_4$; potassium nitrate, KNO_3; and potassium sulfate, K_2SO_4, over a temperature range of 0° to 50° C, using the dewpoint method. The relative humidity is a continuous function of temperature, and, except for sodium chloride, is monotonic. The curve for sodium chloride increases from 74.9-percent relative humidity at 0° C to a maximum of 75.6 percent at 30° C and then gradually decreases to 74.7 percent. The maximum change in relative humidity with temperature, about 15-percent relative humidity as the temperature increases from 0° to 50° C, occurs with saturated salt solutions of sodium dichromate and magnesium nitrate.

1. Introduction

Saturated salt solutions are very useful in producing known relative humidities, principally for testing and calibrating selected hygrometers and hygrographs at temperatures above 0° C. The saturated salt solution is made up as a slushy mixture with distilled water and chemically pure salt in a glass or enameled tray and is enclosed in a sealed metal or glass chamber. When equilibrium conditions, usually hastened by forced air circulation or stirring, are attained, the chamber space is at a constant relative humidity. Some saturated salt solutions produce relative humidities that are roughly independent of temperature.

The equilibrium values of relative humidity of the saturated solutions of several salts used in calibration and testing are listed in NBS Circular 512 [1][2] and are based partly on vapor-pressure data given in the International Critical Tables [2] and partly on dewpoint measurements made at NBS. The relative humidity-temperature relationships of these, as well as several other, saturated salt solutions have been redetermined and are the subject of this paper.

The measurement of vapor pressure or vapor pressure lowering of a salt solution may be made in several ways. The differential methods are based on the determination of the difference in vapor pressure between the solution and solvent, using a sensitive differential manometer. In the dynamic method, the boiling point of the solution is determined under reduced pressure. The transpiration, or gas-saturation, method involves the gravemetric measurement of the water-vapor content of an inert gas saturated by passage over or through the salt solution. The dewpoint method consists in reducing the temperature of a mirror surface until condensation occurs.

The dewpoint method was utilized in this investigation. With this method, measurements could readily be made in the presence of an air atmosphere under conditions similar to those occurring in the use of saturated salt solutions for humidity-control purposes. Furthermore, other than using chemically pure salts of reagent grade and distilled water, no special precautions were taken. Thus the salts contained trace impurities, and the water was air saturated.

2. Description of Apparatus

The experimental setup shown in figure 1 was used to determine the equilibrium vapor pressure of a saturated salt solution. The bottom of a 2-liter Wolff flask, A, was filled to a depth of 2 inches with a saturated solution of a salt, B, made up as a slushy mixture with a pure reagent grade chemical and distilled water. A dewpoint apparatus, C, was inserted through one side neck of the flask; an air stirrer, D, was inserted through the central neck of the flask; and two copper-constantan thermocouples, E and F, were inserted through the other side neck of the flask. The Wolff flask was immersed in a liquid bath, O. Automatic temperature control of the bath was achieved by a system in which thermistors, in a bridge circuit, detected the temperature unbalance and a heater, H, supplied heat in proportion to the unbalance. Below room temperature, a cooling system, I, was used to reduce the bath temperature.

The shaft of the air stirrer, D, was supported in a close-fitted bearing and driven, through a belt and pulley, by an external remotely positioned motor.

Thermocouple, E, measured the air temperature within the Wolff flask, thermocouple, F, measured the temperature of the saturated salt solution, and thermocouple, H, measured the temperature of the liquid bath. These thermocouples were made with cotton-covered Bakelite-insulated wire. To insure that no spurious electromotive force would be

[1] This investigation was financially supported by the Aerology Branch, Bureau of Aeronautics, Department of the Navy.

[2] Figures in brackets indicate the literature references at the end of this paper.

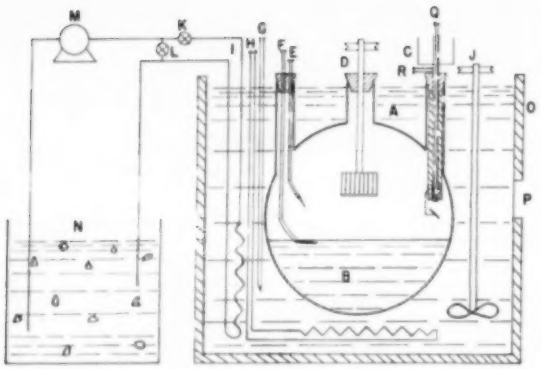

FIGURE 1. *Experimental setup.*

A, 2-liter Wolff flask; B, saturated salt solution; C, dewpoint apparatus; D, air stirrer; E, thermocouple for measuring air temperature; F, thermocouple for measuring temperature of saturated salt solution; G, thermocouple for measuring bath temperature; H, bath heater; I, cooling system; J, liquid bath stirrer; K, cooling system control valve; L, cooling system by-pass valve; M, cooling system pump; N, Stoddard's solvent mixed with dry ice; O, liquid thermostated bath; P, position external to bath from which a light is projected on the dewpoint mirror and from which the dewpoint mirror is observed with a telescope.

introduced because of electrolytic action, each junction was coated and protected with polystyrene cement. The thermocouple leads were covered with grounded equipotential shields. A precision potentiometer was used to measure the thermocouple electromotive force with a precision of better than 1 microvolt.

A light was projected on the dewpoint mirror and the mirror was viewed, through a telescope, from position, P, external to the liquid bath.

Details of the dewpoint apparatus are shown in figure 2. A brass cup, A, 3 inches in diameter and 3 inches deep, was attached to one end of a ¼-inch-outside-diameter copper tube, B, $\frac{1}{32}$-inch in wall thickness. A dewpoint mirror, H, was soldered to the other end of the copper tube. This mirror, ¼-inch-outside-diameter and ⅛ inch thick, was machined from copper, with a recess equal to the wall thickness of the copper tube so that it would fit snuggly in the end of the tube. The reflective surface of the mirror was first ground and polished, then plated with chromium, and finally lapped to within one-half fringe of optical flatness. A 1-mm-diameter hole was drilled in the center of the mirror, from the rear, to within about $\frac{1}{64}$ inch of the front reflective surface. A copper-constantan thermocouple, C, B&S gage No. 30, was inserted into the hole and soldered to the mirror.

An insulated-wire heater, E, was wound around the copper tube close to the mirror end. This heater was controlled by a variable transformer from a 60-cycle a-c power source. Glass-wool insulation, G, was wrapped around the copper tube and retained in position by a Bakelite tube, F, ¾-inch outside diameter. A galvanometer mirror, I, attached to the Bakelite tube by a metal bracket, J, allowed convenient viewing of the dewpoint mirror.

The addition of dry ice and alcohol to the brass cup, A, figure 2, served as a cold source for cooling

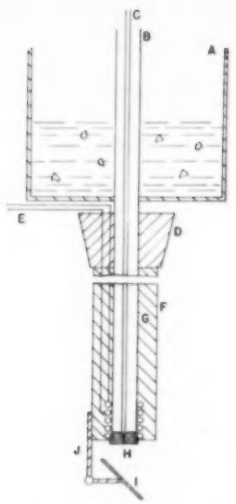

FIGURE 2. *Dewpoint apparatus.*

A, Brass cup; B, copper cooling tube; C, thermocouple; D, rubber stopper; E, heater; F, Bakelite tube; G, glass wool insulation; H, dewpoint mirror; I, viewing mirror; J, support bracket.

the dewpoint mirror, H, through conduction along the copper tube, B. By decreasing the voltage applied to heater, E, the temperature of the dewpoint mirror could be lowered gradually until dew or frost was detected. By increasing the voltage applied to heater, E, the temperature of the mirror could be raised slowly until all dew or frost disappeared. The dewpoint mirror temperature corresponding to the instant of appearance and disappearance was measured by thermocouple, C.

3. Experimental Procedure

The procedure employed in making observations was to adjust the liquid-bath temperature to some desired value and then permit the Wolff flask, with its contents to come to temperature equilibrium. After equilibruim had been established, an observer would manipulate the dewpoint heater control and simultaneously view the dewpoint mirror until he had obtained five successive appearances and disappearances of dew or frost on the dewpoint mirror. A second observer would then repeat the process under the same operating conditions. Occasionally, the two observers would take repeat sets of observations. In this fashion, for any one salt, data were obtained at 10-deg. intervals from 0° to 50° C.

4. Results

For purposes of this investigation, it was assumed that the dewpoint corresponded to the mean of the observed temperature at which dew first appeared and then disappeared. For a given observer, each dewpoint therefore corresponded, usually, to the average of a minimum of 10 temperature observa-

TABLE 1. *Observed temperature-relative humidity data*

Lithium chloride $LiCl \cdot H_2O$							
Temperature ..... °C	0.23	9.56	19.22	29.64	39.64	46.76
Relative humidity ..... %	11.7	13.4	12.4	11.8	11.8	11.4
Magnesium chloride $MgCl_2 \cdot 6H_2O$							
Temperature ..... °C	0.42	9.82	19.53	30.18	39.96	48.09
Relative humidity ..... %	35.2	34.1	33.4	33.2	32.7	31.4
Sodium dichromate $Na_2Cr_2O_7 \cdot 2H_2O$							
Temperature ..... °C	0.60	10.14	19.82	30.04	37.36	47.31
Relative humidity ..... %	60.4	57.8	55.5	52.4	50.4	48.0
Magnesium nitrate $Mg(NO_3)_2 \cdot 6H_2O$							
Temperature ..... °C	0.39	9.85	19.57	30.47	40.15	48.10
Relative humidity ..... %	60.7	57.5	55.8	51.6	49.7	46.2
Sodium chloride NaCl							
Temperature ..... °C	0.92	10.23	20.25	30.25	39.18	48.39
Relative humidity ..... %	75.0	75.3	75.5	75.6	74.6	74.9
Ammonium sulfate $(NH_4)_2SO_4$							
Temperature ..... °C	0.39	10.05	20.04	30.86	39.97	47.96
Relative humidity ..... %	83.7	81.8	80.6	80.0	80.1	79.2
Potassium nitrate KNO_3							
Temperature ..... °C	0.62	10.17	20.01	30.70	40.35	48.12
Relative humidity ..... %	97.0	95.8	93.1	90.6	88.0	85.6
Potassium sulfate K_2SO_4							
Temperature ..... °C	0.54	10.08	19.81	30.44	39.94	48.06
Relative humidity ..... %	99.0	98.0	97.1	96.8	96.1	96.0

tions. The dewpoint, for a salt at a test temperature, was taken as the mean of the dewpoints obtained by each observer.

The ambient temperature was assumed to be the mean of the air temperature and the salt temperature within the Wolff flask. As these temperatures were relatively stable for appreciable periods of time, only one such set of temperature readings was obtained by each observer for his corresponding set of dewpoint observations.

The relative humidity in equilibrium with the saturated salt solution is given by

$$RH = \frac{e_d}{e_a} \times 100,$$

where e_d is the vapor pressure of pure water at the dewpoint temperature, and e_a is the vapor pressure of pure water at the ambient temperature. The vapor pressures given in the Smithsonian Tables [3] were used in this computation.

The mean relative humidity at each observed test temperature is presented in table 1 for eight different saturated salt solutions ranging in relative humidity from about 11 percent to 99 percent. The data for each salt were plotted, and the best smooth curve obtainable by eye was drawn through the plotted points. The faired values from this smooth curve are given in table 2. They represent the best estimates of the relative humidities obtained with these salts at the selected temperatures.

TABLE 2. *Faired values of relative humidity versus temperature*

Temperature	Relative humidity of saturated salt solution							
	$LiCl \cdot H_2O$	$MgCl_2 \cdot 6H_2O$	$Na_2Cr_2O_7 \cdot 2H_2O$	$Mg(NO_3)_2 \cdot 6H_2O$	NaCl	$(NH_4)_2SO_4$	KNO_3	K_2SO_4
°C	%	%	%	%	%	%	%	%
0	14.7	35.0	60.6	60.6	74.9	83.7	97.6	99.1
5	14.0	34.6	59.3	59.2	75.1	82.6	96.6	98.4
10	13.3	34.2	57.9	57.8	75.2	81.7	95.5	97.9
15	12.8	33.9	56.6	56.3	75.3	81.1	94.4	97.5
20	12.4	33.6	55.2	54.9	75.5	80.6	93.2	97.2
25	12.0	33.2	53.8	53.4	75.8	80.3	92.0	96.9
30	11.8	32.8	52.5	52.0	75.6	80.0	90.7	96.6
35	11.7	32.5	51.2	50.6	75.5	79.8	89.3	96.4
40	11.6	32.1	49.8	49.2	75.4	79.6	87.9	96.2
45	11.5	31.8	48.5	47.7	75.1	79.3	86.5	96.0
50	11.4	31.4	47.1	46.3	74.7	79.1	85.0	95.8

TABLE 3. *Scatter of data about smooth curves*

Nominal temperature	Relative-humidity deviation of data from curve of saturated salt solution							
	$LiCl \cdot H_2O$	$MgCl_2 \cdot 6H_2O$	$Na_2Cr_2O_7 \cdot 2H_2O$	$Mg(NO_3)_2 \cdot 6H_2O$	NaCl	$(NH_4)_2SO_4$	KNO_3	K_2SO_4
°C	%	%	%	%	%	%	%	%
0	0	+0.3	0	+0.2	+0.1	0	−0.5	0
10	0	−.3	0	−.3	−.1	0	+.4	+.1
20	0	−.2	+.2	+.8	0	0	−.2	−.1
30	0	+.3	−.1	−.3	0	0	+.1	+.2
40	+.2	+.5	−.1	+.5	−1.0	+.4	+.1	−.1
50	−.1	−.2	+.2	−.6	0	0	0	+.1
Average..	0	±0.3	±0.1	±0.6	±0.2	±0.1	±0.2	±0.1

The plots of relative humidity versus temperature yield curves that are continuous and, generally, vary little with temperature over the temperature range of 0° to 50° C. These plots are shown as solid-line curves in figures 3 to 10. The maximum variation of relative humidity with temperature occurs with saturated solutions of sodium dichromate and magnesium nitrate. For these salts there is an absolute decrease in relative humidity of about 15 percent as the temperature increases from 0° to 50° C. The scatter of the mean experimental values above the smooth curves is given in table 3. The greatest scatter of the data occurs with sodium chloride and is ± 0.6 percent relative humidity. For the other salts, the scatter is equal to or less than ± 0.3 percent relative humidity.

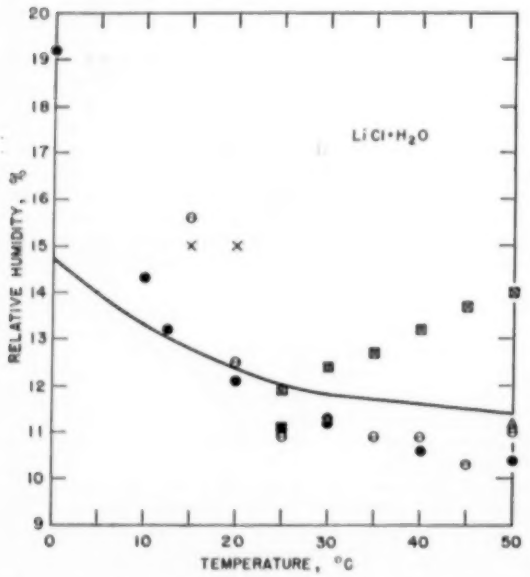

FIGURE 3. *Comparison of the faired NBS results with results of other experimenters.*

Figures 3 to 10, inclusive, show a comparison of the faired NBS results, as solid-line curves, with the results of other experimenters. The following symbol notation is used throughout these figures:

- ICT [2]
- Foote, Saxton, and Dixon [4]
- Leopold and Johnston [5]
- Sakal [6]
- Adams and Merz [7]
- Burns [8]
- O'Brien [9]
- Speranskii [10, 15]
- Prideaux [11]
- Edgar and Swan [12]
- Stokes and Robinson [13]
- van't Hoff [14]
- Carr and Harris [16]
- Lescoeur [17]
- Derby and Yngve [18]
- Konduirev and Berezovskii [19]
- Ewing, Klinger, and Brandner [20]
- Johnson and Molstad [21]
- Huttig and Reuscher [22]
- Gokcen [23]

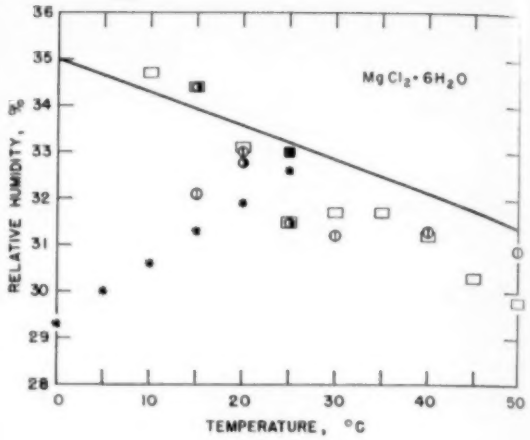

FIGURE 4.
(See fig. 3)

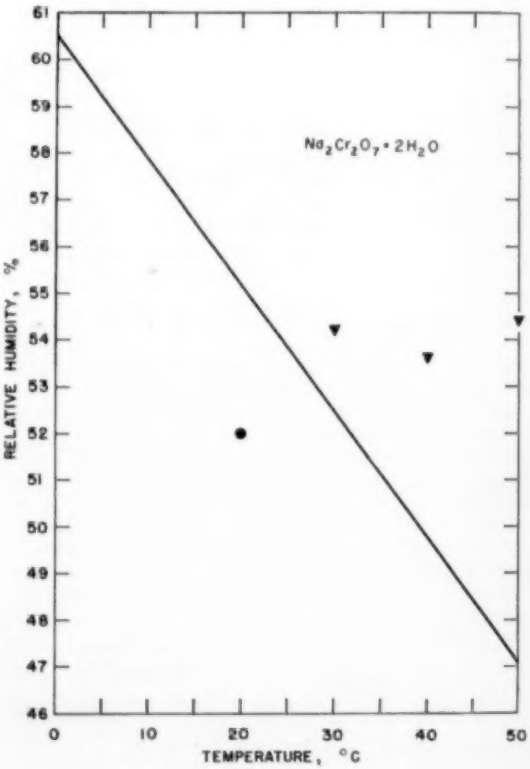

FIGURE 5.
(See fig. 3)

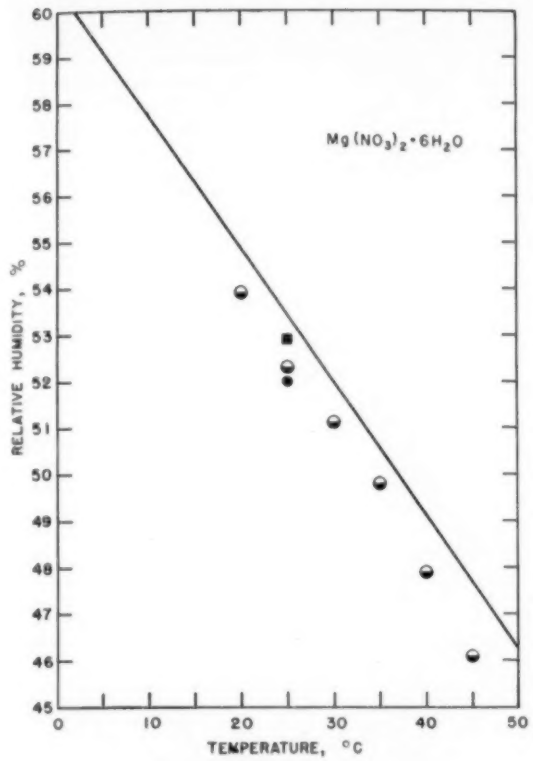

FIGURE 6.
(See fig. 3)

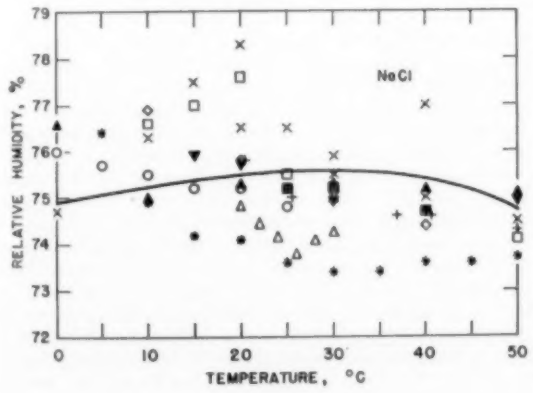

FIGURE 7.
(See fig. 3)

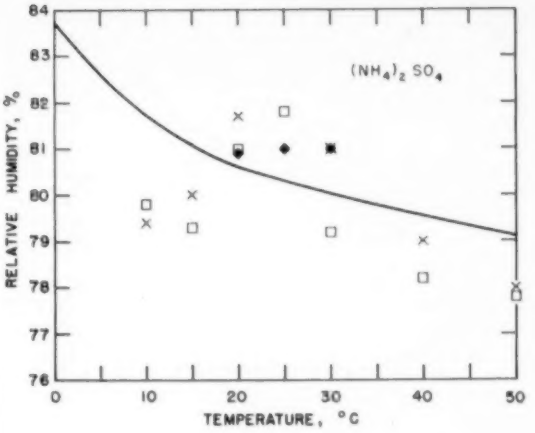

FIGURE 8.
(See fig. 3)

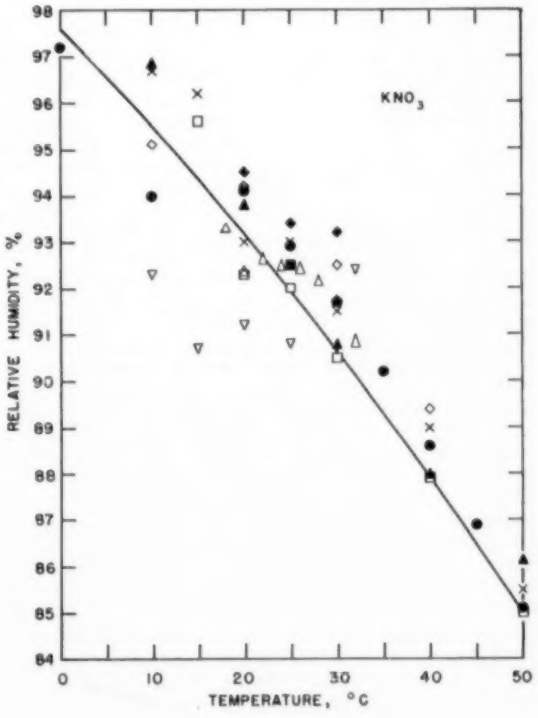

FIGURE 9.
(See fig. 3)

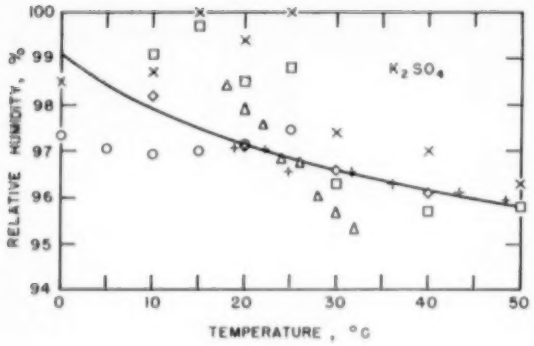

FIGURE 10.
(See fig. 3)

5. Discussion

5.1. General

There are several advantages to the use of the dewpoint method in determining the equilibrium relative humidity over a saturated salt solution. The experimental setup can be relatively simple, requiring only a temperature-controlled liquid bath for maintaining the salt solution and its containing vessel at some fixed temperature and a dewpoint detector. The dewpoint can be measured in the presence of an air (or other noncondensible) atmosphere. Methods that depend on the direct measurement of vapor pressure, either absolute or differential, require careful elimination of all gases and vapors except the water vapor from above the salt solution as well as the elimination of any dissolved gases in the solution because these would produce a serious error in the vapor pressure. The absolute accuracy of the vapor-pressure measurement increases with decreasing dewpoint for a given accuracy in the dewpoint measurement. For example, if the dewpoint is measured with an accuracy of 0.1 deg C, the corresponding accuracy in vapor pressure is 0.008 mm Hg at −20° C, 0.034 mm Hg at 0° C, 0.109 mm Hg at 20° C, and 0.296 mm Hg at 40 °C. The accuracy, in terms of percentage of vapor pressure, is 0.8 percent at −20° C, 0.7 percent at 0° C, 0.6 percent at 20° C, and 0.5 percent at 40° C. Thus, the percentage accuracy in vapor-pressure determination by the dewpoint method, for a given dewpoint accuracy, is roughly independent of dewpoint or vapor pressure. The dewpoint method is an indirect method; it yields a temperature from which the vapor pressure is obtained by recourse to tables. One of the inherent limitations of the method lies in the basic accuracy of the tables. For most work, and particularly for this investigation, the standard tables are considered to have adequate accuracy.

5.2. Errors

In determining relative humidity by the dewpoint method, the principal errors arise in the measurement of the dewpoint temperature and the ambient temperature. The precision of the temperature measurement, using calibrated single-junction copper-constantan thermocouples and a calibrated precision potentiometer, was 0.01 deg C, but the accuracy was probably no better than 0.05 deg C. As (1) the thermocouple for measuring the dewpoint was imbedded only several hundredths of an inch below the surface of the dewpoint mirror, (2) the body of the mirror was copper, and (3) the rates of heating and cooling were uniform and slow, it seems reasonable to assume that any temperature differentials within or across the mirror were negligible, say, no more than 0.01 to 0.02 deg C. Because of the relatively low thermal conductivity of liquid water, the temperature differential across the thickness of a dew film was possibly of greater magnitude. In cooling, the mirror was colder than the exposed dew surface and in heating, it was warmer. Two factors tend to reduce the importance of this. First, by averaging the temperatures at which dew is first observed to appear and then disappear, the errors due to the differentials across the dew, because they are of opposite sign, tend to cancel. Second, by keeping the thickness and quantity of dew small, the differentials can be reduced to a minimum.

The manually operated and visually observed dewpoint hygrometer required a certain degree of skill for successful use. After some experience in its use, it was possible to control the rate of heating and cooling so that the mirror temperature could be followed easily with a potentiometer, the appearance and disappearance of dew could be detected readily, and the thickness of the dew deposit kept as small as desirable. An observer could repeat a series of, say, five dewpoint determinations, at any one time, with an average deviation of a single determination from the mean of 0.04 deg C, with an average deviation of the mean of 0.01 C, and with an average range of 0.13 deg C. The average difference in temperature between the appearance and disappearance of dew was 0.5 deg C, whereas the maximum difference ever observed was 2 deg C. The dewpoint appeared to be independent of the various observed differences in temperature between the appearance and disappearance of dew.

The dewpoint (the average, usually, of five repeat determinations) obtained by any one observer had an average deviation from the mean of two or more observers of 0.07 deg C. The average deviation of the mean dewpoint of all observers for a salt solution at any temperature was 0.04 deg C. The mean range in dewpoint for all of the test conditions for two or more observers was 0.16 deg C.

Because the dew was visually detected, it is likely that different observers used different criteria for defining the appearance or disappearance of dew.

This may account to some extent for the spread in dewpoint from one observer to another.

Below 0° C, either frost or dew (supercooled water) may be deposited on the surface of the dewpoint mirror. In all cases (which included dewpoints as low as −23° C) the deposit first detected was dew. If the mirror temperature was not permitted to fall too far below the dewpoint, then dew remained on the mirror throughout the determination. If the mirror temperature dropped appreciably below the dewpoint, the dew changed to frost.

The ambient temperature was taken as the mean temperature of the salt solution and air. These latter two temperatures differed from each other because of the heat sources and sinks associated with the setup. The fan used for stirring the air within the chamber introduced heat through agitation; conduction along the shaft added or abstracted heat, depending on whether the room temperature was above or below that of the test chamber. The dewpoint hygrometer served as a serious heat sink, for, by the very nature of its operation, it has to be maintained below test-chamber temperature. Although the insulation surrounding the conduction rod aided appreciably in reducing the magnitude of the heat loss, there was still enough loss to produce a temperature differential between the salt solution and air. The test-chamber temperature may therefore have an average uncertainty, because of this differential, of 0.09 deg C.

The root-mean-square uncertainty in the dewpoint determination is 0.07 deg C and in the ambient (test chamber) temperature is 0.10 deg C. The corresponding uncertainty in relative humidity varies from a maximum of 1.2 percent for the high-humidity saturated salt solutions to 0.2 percent for the low-humidity saturated salt solutions.

5.3. Comparison of Results With Those of Other Investigators

The NBS results are compared with those of other investigators in figures 3 to 10, in which the NBS results are shown as solid-line curves. The results of some workers were reported for a limited temperature range or, occasionally, for only one temperature. Wherever necessary, results that were presented in terms of vapor pressure were converted into relative humidity.

It is apparent from these figures that there is a certain degree of scatter among the values reported by other researchers as well as some disagreement between the NBS results and those values. In general, these other results fall within a band of values that is, on an average, roughly within ±1½-percent relative humidity of the NBS results.

5.4. Use of Saturated Salt Solutions

When saturated salt solutions are employed for humidity control, experience has shown that certain precautions must be observed in order that the theoretical values may be used without the need of measurement. It is necessary to enclose the saturated salt solution in a sealed chamber. The chamber and the fixtures therein must be made of nonhygroscopic materials, preferably metal or glass, else the time required for humidity equilibrium to be achieved may be very great, sometimes of the order of days or weeks. The chamber, salt solution, and ambient air should be brought to temperature equilibrium. It is desirable for the salt solution to occupy as large a surface area as possible and for some means of air ventilation or circulation to be provided. In the latter regard, if at all possible, the motor that drives the fan or blower should be external to the chamber. Otherwise, the heat dissipated by the motor will gradually raise the internal chamber temperature and introduce some uncertainty in the equilibrium relative humidity. The time required for humidity equilibrium to be reached with saturated salt solutions depends on several factors: (1) the ratio of free surface area of the solution to chamber volume, (2) the amount of air stirring, and (3) the presence of hygroscopic materials. It is conjectured that agitating the saturated salt solution may increase the rate at which equilibrium is achieved.

As ideal conditions are rarely obtained in practice, it is probable that the theoretical values of relative humidity are seldom reached. In general use, saturated salt solutions should not be expected to control the relative humidity to closer than about 1-percent relative humidity of the theoretical values.

6. References

[1] Arnold Wexler and W. G. Brombacher, Methods of measuring humidity and testing hygrometers, NBS Circular 512 (1951).

[2] International Critical Tables **1,** 68 (McGraw-Hill Book Co., New York, N. Y., 1927).

[3] Smithsonian Meteorological Tables, 6th Revised Edition (1951).

[4] H. W. Foote, Blair Saxton, and J. D. Dixon, The vapor pressures of saturated aqueous solutions of certain salts, J. Am. Chem. Soc. **54,** 563 (1932).

[5] H. Geneva Leopold and John Johnston, The vapor pressure of the saturated aqueous solutions of certain salts, J. Am. Chem. Soc. **49,** 1974 (1927).

[6] W. Sakai, The study of urea, *i.* The hygroscopic properties of (the) double substance. The vapor pressure of saturated solution(s) of salts, J. Soc. Chem. Ind. Japan, **43,** Suppl. binding 104 (1940).

[7] J. R. Adams and A. R. Merz, Hygroscopicity of fertilizer materials and mixtures, J. Ind. Eng. Chem. **21,** 305 (1929).

[8] Robert Burns, Conditioning of insulating materials for test, Bell Telephone System Monograph B–986 (1937). Source of material not given.

[9] F. E. M. O'Brien, J. Sci. Instr., **25,** 73 (1948).

[10] A. Speranskii, The vapor pressure and integral heat of solution of saturated solutions, Z. physik. Chem. **78,** 86 (1912).

[11] E. B. R. Prideaux; The deliquescence and drying of ammonium and alkali nitrates and a theory of the absorption of water vapor by mixed salts, J. Soc. Chem. Ind. **39,** 182–5T (1920).

[12] G. Edgar and W. O. Swan, Factors determining the hygroscopic properties of soluble substances, I. Vapor pressure of saturated solutions, J. Am. Chem. Soc. **44,** 570 (1922).

[13] R. H. Stokes and R. A. Robinson, Ind. Eng. Chem. **41,** 2013 (Sept. 1949).
[14] J. H. van't Hoff, E. F. Armstrong, W. Hinrichsen, F. Weigert, and G. Just, Gips und Anhydrit, Z. physik. Chem. **45,** 257 (1903).
[15] A. Speranskii, Vapor pressure of saturated solutions, Z. physik. Chem. **70,** 519 (1910).
[16] D. S. Carr and B. L. Harris, Ind. Eng. Chem. **41,** 2014 (Sept. 1949).
[17] M. H. Lescoeur, Researches sur la dissociation des hydrates salines et des composés analogues, Ann. Chem. Phys. (7) **2,** 85 (1894).
[18] I. H. Derby and Victor Yngve, Dissociation tensions of certain hydrated chlorides and the vapor pressures of their saturated solutions, J. Am. Chem. Soc. **38,** 1439 (1916).
[19] N. V. Konduirev and G. V. Berezovskii, Vapor pressure of saturated solutions and hydrates of magnesium chloride, J. Gen. Chem. (USSR) **5,** 1246 (1935).
[20] Warren W. Ewing, Ernest Klinger, and John D. Brandner, Vapor pressure-temperature relations and the heats of hydration, solution and dilution of the binary system magnesium nitrate-water, J. Am. Chem. Soc. **56,** 1053 (1934).
[21] Ernest F. Johnson, Jr., and Melvin C. Molstad, Thermodynamic properties of aqueous lithium chloride solutions. An evaluation of the gas-current method for determination of thermodynamic properties of aqueous salt solutions, J. Phys. & Colloid Chem. **55,** 257 (1951).
[22] F. H. Huttig and F. Reuscher, Studien zur Chemie des Lithiums. I. Über die Hydrate des Lithiumchlorids und Lithiumbromids, Z. anorg. Chem. **137,** 155 (1924).
[23] Nevzat A. Gokcen, Vapor pressure of water above saturated lithium chloride solution, J. Am. Chem. Soc. **73,** 3789 (1951).

WASHINGTON, February 19, 1954.

Journal of Research of the National Bureau of Standards Vol. 53, No. 1, July 1954 Research Paper 2513

Disintegration Rate of Carbon-14

R. S. Caswell, J. M. Brabant,[1] and A. Schwebel

The energy emission rates of C^{14} samples have been measured with an extrapolation ionization chamber. From the energy emission rates, the disintegration rates are determined through knowledge of the average beta-ray energy emitted per disintegration. From earlier data on the isotopic abundance, a value for the half-life of C^{14} of 5,900 $\pm$250 years is obtained.

In view of the large discrepancies existing between various determinations of disintegration rate (and consequently of the half-life) of carbon-14 [1],[2] a measurement by an independent method has seemed desirable. In the present work an extrapolation chamber measurement of the energy emission of a C^{14} sample is combined with the average energy per disintegration from beta-ray spectrometer measurements to yield the disintegration rate. The half-life is then determined by using previously reported measurements of isotopic abundance [1]. The disintegration rate is found by the relation $\dot{E}_m = \dot{n}\overline{E}$, where $\dot{E}_m$ is the energy produced per second per gram of material, n is the number of disintegrations per second per gram, and $\overline{E}$ is the average energy per disintegration. Using the number of C^{14} atoms per gram, n, (from mass-spectrometer measurement) the half-life is determined by the relation $\dot{n} = -0.693n/T_{1/2}$.

The type of extrapolation chamber used here has previously been used in combination with 4-pi beta counting to determine the average energy of beta-ray spectra [2, 3]. The excellent agreement between average energies determined in this way and average energies calculated from spectrometer data or from beta-decay theory (using experimental values for E_{max}) demonstrates that the extrapolation chamber does measure $\dot{E}_m$ to good accuracy. Nuclides previously studied range in energy from Ca^{45} ($\overline{E}$= 0.075 Mev) to Y^{90} ($\overline{E}$=0.895 Mev).

The theory of the extrapolation chamber has been discussed elsewhere [2, 4]. The energy production rate for an air-cavity water-electrode chamber is given by the Bragg-Gray cavity theorem [5]: $\dot{E}_m = J_m W_{air} \rho_m$, where J_m is the number of ion pairs formed per gram of air per second, ρ_m is the mass stopping power of the water relative to air, and W_{air} the average energy required to produce an ion pair in air. In the present experiment, one electrode was aluminum and the other was a dilute, thoroughly mixed water solution of C^{14} (as Na_2CO_3). In this case $E_m = 2J_m W_{air} \rho_m / B$, where B is called the "backscattering correction factor." B has been evaluated experimentally by comparison with a water backscattering electrode (solidified with agar), and by extrapolation chamber studies of the variation of backscattering with atomic number [2]. B is found to be remarkably independent of beta energy (varying by less than 2% from P^{32} to S^{35}) and is taken as 1.125 for C^{14}. The relative stopping power of water to air, ρ_m, is taken as 1.13, which is the ratio of the number of electrons per gram of the two media (1,11), corrected for the difference in stopping power caused by the effective ionization potentials of water and air. Failla and Rossi [6] have reported a value of W_{air}= 32.5 ev per ion pair for S^{35}, which should be very close to the value for C^{14} because both nuclides have the same spectrum shape and nearly the same beta energy. This value agrees with that calculated by Wang [7] from the formula of Gerbes by averaging over the energy of the electrons from the initial energy until brought to rest. For this report, we take W_{air}=32.5 ev per ion pair. A recent review by Binks [8] of a large number of measurements of W_{air} indicates 33 ev per ion pair may be preferable. If so, the results of this experiment should be changed accordingly.

The average beta energy of C^{14} was numerically calculated to be 49.7 kev, using 155 kev for the maximum energy [9] and considering the beta spectrum as "allowed" [10].

The amount of C^{14} in the water solution, n, was determined by comparison with standard ampoules prepared by Manov [1,11] and on which mass spectrometer measurements have been made in four laboratories. The standard sample is taken as having 3.132×10^{11} atoms of C^{14} per milliliter of solution. The value of n for the experimental sample is determined by evolving CO_2 from both standard and experimental solutions and observing the relative ionization currents in a CO_2-filled ionization chamber.

Three runs were made, giving values of $\dot{n}$ of 12.55 μc/ml, 4.53 μc/ml, and 1.49 μc/ml, respectively. The corresponding values of n were 1.25×10^{17} atoms/ml, 4.53×10^{16} atoms/ml, and 1.47×10^{16} atoms/ml, respectively. These runs yield values for the half-life of C^{14} of 5,900 years, 5,940 years, and 5,840 years, respectively. The third run is of somewhat lower accuracy than the first two because of the low activity of the sample.

In terms of the disintegration rate values assigned to the standard ampoules by Manov and Curtiss [11] based on CO_2-CS_2 gas counting, the disintegration rates, $\dot{n}$, for the present samples should have been 13.8 μc/ml, 5.01 μc/ml, and 1.62 μc/ml, respectively. These values are systematically about 9 percent higher than the values obtained in the present work. This comparison (which is independent of

[1] Now at University of California, Berkeley, Calif.

[2] Figures in brackets indicate the literature references at the end of this paper.

isotopic abundance measurements) shows a discrepancy of 9 percent.

This discrepancy is of the same order as the uncertainties in the gas-counting method itself as shown by disintegration-rate intercomparisons [1] and indirectly by the half-life determinations (table 1). The recent work of Crane [12] suggests the possibility of multiple counts in CO_2-CS_2 counters due to production of pulses by both electrons and negative ions.

Table 1 shows a comparison of recent half-life values obtained by gas counting, calorimetric measurement, and the present method. "n" was determined by mass spectrometer measurement in all cases except for the calorimeter. In the calorimetric measurement we have used our value (49.7 kev) for the average energy of the beta spectrum. Probable errors in the present measurements are taken as: W_{air}, ± 3 percent; J_m, ± 1 percent, B, ± 1.5 percent; ρ_m, ± 1 percent; n, ± 1.6 percent; $\overline{E}$, ± 1 percent, giving an over-all probable error in the half-life of about 250 years.

TABLE 1. [13]

Authors	Method of disintegration rate determination	$T_{1/2}$
		Years
Hawkings, Hunter, Mann, and Stevens.	CO_2+CS_2 (GM counter)	6,360±200
Engelkemeir and Libby	CO_2+argon-alcohol (GM counter)	5,580±45
Jones	CO_2+argon-alcohol (GM counter)	5,589±75
Manov and Curtiss [11]	CO_2+CS_2 (GM counter)	5,370±200
Miller, et al.	CO_2+CS_2 (GM counter)	6,400
	CO_2+methane (prop. counter)	5,600
Jenks and Sweeton	Calorimeter (and gas density measurement for n).	6,090
Present work	Extrapolation chamber	5,900±250

The present value is in best agreement with the calorimeter measurements, which also depend upon energy emission rather than a direct disintegration-rate determination. The present value is not in good agreement with either group of gas-counting measurements (about 5,500 years and 6,400 years). In view of the excellent beta-ray spectrometer data on C^{14}, it appears very unlikely that any uncertainty in $\overline{E}$ can account for the difference. No large error should be present in (W_{air} ρ_m/B) because this quantity has been independently checked in the previous average energy measurements. For example, Ca^{45} has an average energy about 1.5 times that of C^{14} and also has an "allowed" spectrum. With the same value of (W_{air} ρ_m/B) used here, the disintegration rate of a Ca^{45} source determined by extrapolation chamber coincided with a value determined by 4-π counting within 1 percent.

In conclusion, a reinvestigation of disintegration rate measurements by several independent methods appears desirable. Considerable emphasis should be placed on calorimeter measurements of disintegration rate because they involve a minimum of uncertainty. These measurements should be done on a sample of high specific activity in conjunction with isotopic abundance measurements. Further studies of this nature are under way in the Radioactivity Section at the National Bureau of Standards.

We are indebted to the University of Kentucky and to T. I. Davenport of the National Bureau of Standards for the loan of the equipment used.

References

[1] G. G. Manov, National Research Council Nuclear Science Series Preliminary Report No. 13 (1953).
[2] R. S. Caswell, Phys. Rev. **86,** 82 (1952).
[3] J. M. Brabant, L. W. Cochran, and R. S. Caswell, Phys. Rev. **91,** 210A (1953).
[4] G. Failla, H. H. Rossi, R. K. Clark, and N. Baily, U. S. Atomic Energy Commission Document 2142.
[5] L. H. Gray, Proc. Roy. Soc. (London) **156A,** 578 (1936).
[6] G. Failla and H. H. Rossi, U. S. Atomic Energy Commission Report NYO–4008 (1952).
[7] T. J. Wang, Nucleonics **7,** No. 2, 55 (1950).
[8] W. Binks, Report for British Committee on Radiological Units BRU/40 (to be published in Acta Radiologica).
[9] K. Way et al., NBS Circular 499.
[10] C. S. Wu and A. Schwarzschild, Phys. Rev. **91,** 483A (1953).
[11] G. G. Manov, and L. F. Curtiss, J. Research NBS **46,** 328 (1951) RP2203.
[12] H. R. Crane, Bul. Am. Phys. Soc. **29,** 39 (1954).
[13] R. C. Hawkings, R. F. Hunter, W. B. Mann, and W. H. Stevens, Can. J. Research **B27,** 545 (1949); A. G. Engelkemeir and W. F. Libby, Rev. Sci. Instr. **21,** 550 (1950); W. M. Jones, Phys. Rev. **76,** 885 (1949); W. W. Miller, R. Ballentine, W. Bernstein, L. Friedman, A. O. Nier, and R. D. Evans, Phys. Rev. **77,** 714 (1950); G. H. Jenks and F. H. Sweeton, Phys. Rev. **86,** 803 (1952).

WASHINGTON, March 1, 1954.

rnal of Research of the National Bureau of Standards Vol. 53, No. 1, July 1954 Research Paper 2514

Testing of Large Optical Surfaces With Small Test Plates

James B. Saunders

A procedure for testing large optical surfaces with relatively small optical standards is described. Simplified formulas are used to apply a statistical method for obtaining increased precision. A practical example is used to illustrate the procedure for testing surfaces that may be assumed to have revolution symmetry.

1. Introduction

With the increased use of massive optical parts, there is need for a practical method of testing large optical surfaces with relatively small standards, such as are available in the average optical shop. The conventional test of observing fringes between the standard and unknown at various positions on the surface enables the optician to form a rough estimate of the nature of the surface. For more precise values either extensions of the present conventional tests or new methods must be used. Present shop methods of testing optical surfaces are not practical for massive optical elements as standard test plates of the sizes required for conventional test methods are seldom available.

A test for shape of very large optical surfaces, by means of interference of light, may be made with a standard test plate (flat or spherical) that is much smaller than the surface to be tested. The principles involved are not new and may be considered elementary, but those who perform the tests on optical surfaces during the polishing are not as a rule sufficiently versed in mathematics to apply the principles outlined in the present paper to the best advantage. They can, however, apply observed data to a set of simple formulas and compute the ensuing results.

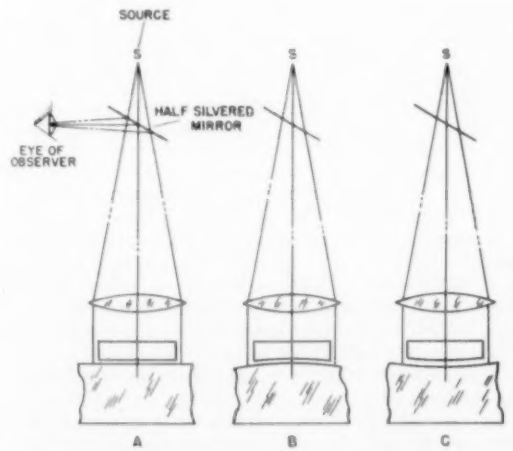

FIGURE 1. *Optical arrangements for testing (A) flat surfaces, (B) convex surfaces, and (C) concave surfaces.*

A procedure is described in which an ordinary-sized standard test plate can be used to measure the shape of surfaces that are much larger than the standard. Use is made of statistical methods for improving the computed results. Simplified formulas will be developed that may be applied by opticians, after a short training period, even though they may not be able to follow the mathematical derivations and theory. The application of the general formulas to a typical set of data will then be made to illustrate the testing of a surface by means of a smaller standard optical flat. The method is not limited to plane surfaces. The sphericity of very large spherical or aspherical surfaces may be measured with standard test plates of approximately the same radius, if the viewing system permits the use of normal incident light. Figure 1, (A, B, C) shows simple optical arrangements for testing plane, convex, and concave surfaces, respectively.

The basic principle may also be applied to the testing of off-axis curved, or nonsymmetrical, surfaces, with modifications of the formulas. However, as these are encountered only rarely, the present paper will be limited to surfaces of revolution.

We will consider a Fizeau viewer (fig. 1) that has an aperture equal to or greater than the area of the standard surface. Spherical surfaces are referred to the spherical master with which they are tested, and plane or approximately plane surfaces are referred to planes. The equations and measurements are identical for plane and spherical surfaces. This discussion will deal with the testing of an approximately plane surface against a standard optical flat. The unknown surface is assumed to be a figure of revolution about an axis normal to and passing through a known point on it. In general, this point will be at or near the center, if the surface is circular.

2. Experimental Procedures

If the standard flat is adjusted normally to the collimated beam of light and the unknown is placed close to and approximately parallel to the standard, interference fringes may be observed with monochromatic light of known wavelength. Measurements made on the fringe pattern permit a computation of the shape of the unknown relative to a plane (sphere for spherical surfaces) over the visible region of interference. If adjustments permitted, the entire area of the unknown could be covered by

moving the standard step by step without rotation, in a plane parallel to the standard plane. The aggregate of the resultant fringe patterns, when properly assembled to form a composite pattern of the whole surface, would be quite similar to what would have been obtained with a standard surface that covered the whole of the unknown.

As it is virtually impossible to make the above assumed adjustments, corrections for rotation and changes in separation of the unknown, relative to the original surface of the standard, must be made by measuring these changes and applying the required corrections. The corrections are always subject to errors of observation. If several successive positionings of the standard, relative to the unknown, are required to measure the shape along a diameter, these errors accumulate. Consequently, it is desirable to reduce these errors. The "Method of Averages," [1] which is easy to apply and yields simple working formulas, is used since it provides adequate precision.

In general, large optical surfaces are ground and polished by machines that produce figures of revolution about a known point, usually located at the center of the surface. If the surface is one of revolution,[2] its departure from a straight line that is tangent to it at the center of revolution is a measure of its departure from its tangent plane and consequently determines the shape of the entire surface relative to any other chosen plane. The axis of abscissas (see fig. 2) is chosen as the intersection of a plane through the axis of rotation of the surface with the plane that is tangent to the surface at its center. The unit of abscissas is chosen as the separation of equally spaced reference marks along a chosen diameter of the surface. The chosen diameter is the axis of abscissas. The axis of ordinates is the axis of revolution of the surface. The unit of ordinates is one-half the wavelength of the light used.

The following steps are the chosen procedure for acquiring the data necessary to compute the shape of the surface. The master flat is placed on, and concentric with, the surface (positions A and A', fig. 2). The magnitude of the air wedge between the two surfaces is adjusted to produce a satisfactory number of fringes in the field (see fig. 3). The direction of this wedge is adjusted to make the fringes approximately normal to the line along which the chosen reference points lie. Except for plane surfaces this wedge varies from one reference point to the next. Consequently, if linear interpolation is used in estimating fractions of fringes at the reference points, the error in estimation varies with the fraction observed. For most observers this error is a minimum when the fraction is 0.0 or 0.5, that is, when the reference point falls on the center of a dark or a bright fringe. Best accuracy is obtained by reading abscissas corresponding to the center of all fringes—both dark and bright—and from these data, by nonlinear interpolation, compute the relative

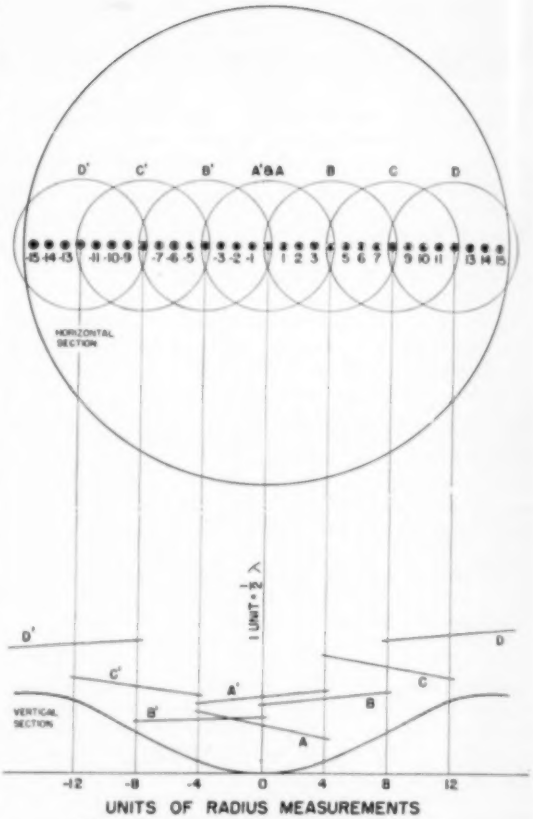

FIGURE 2. *Coordinate system of reference.*

The vertical section (below) cuts the horizontal section (above) along the line of reference points—dots concentric with small circles. Circles A, A' B, B', etc. represent the several positions of the standard test plate. The corresponding straight lines below represent sections through the standard surface of reference.

orders at the chosen reference points. The procedure will be explained in greater detail with the held of the fringe configuration shown in figure 3.

The fringes (relative orders of interference) in position A are evaluated at the several equally spaced reference points by the method indicated above. The standard is then moved to position B, which overlaps an appropriate amount of the area covered in its first position, A. Again the fringe readings at all reference points, covered by the standard in this new position, are evaluated. The standard is then moved to position C and the corresponding fringe readings noted. This procedure is repeated until the surface covered by the master extends to the edge of the unknown surface of revolution. The positions represented by primed letters are a second independent set, useful in checking the precision of the method.

In general, the fringe values at the reference points will not be integral. Consequently, the fractional parts must be obtained by interpolation and, in marginal cases, by extrapolation. Linear interpolation

[1] J. B. Scarborough, Numerical mathematical analysis, p. 446 (Johns Hopkins Press, Baltimore, Md., 1950).

[2] W. A. Granville, Elements of differential and integral calculus, p. 264 (Ginn & Co., New York, N. Y., 1911).

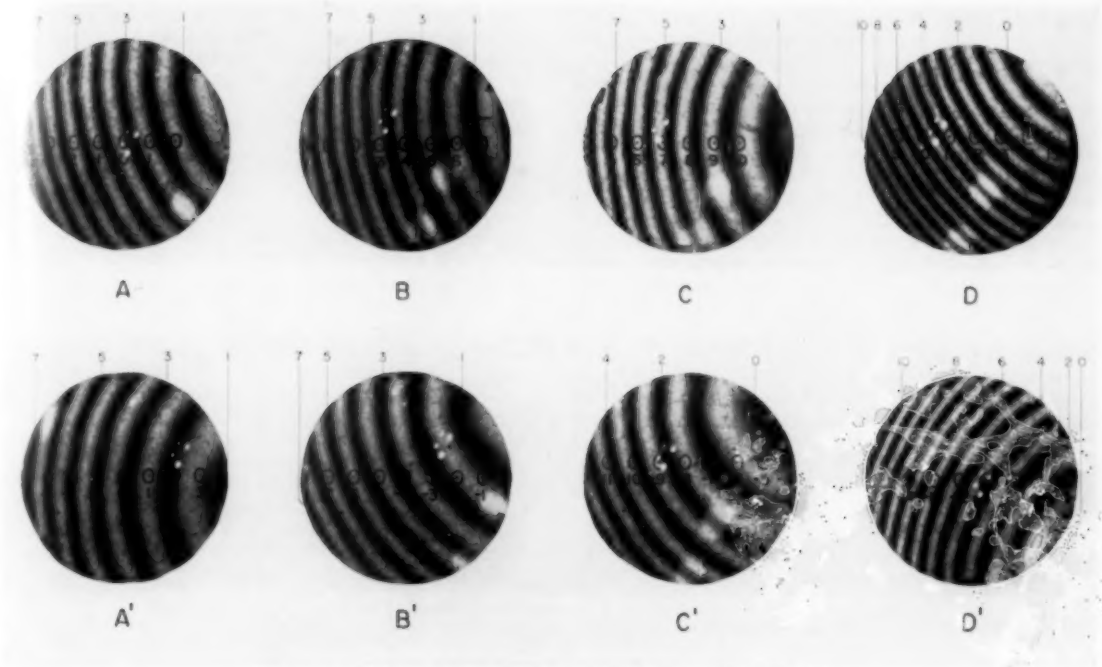

FIGURE 3. *Fringes for the several positions of the standard test plate.*

The numbers above each picture represent relative orders of interference.

or extrapolation is accurate only when the fringes are equally spaced along the straight line on which the reference points are chosen. If they are equally spaced, the surface is plane and no further test is necessary. In general, the fringes will be curved and nonlinear interpolation should be used if highest accuracy is to be obtained. Of the several methods of performing nonlinear interpolation, the graphical method is simplest and, for these purposes, adequate. The details of this are best shown by a description of its application to actual data. This will be given in a later section, where the shape of the surface of a glass disk will be computed from photographs of interference fringes that are obtained when the glass disk is tested interferometrically against a standard flat.

3. Derivation of Formulas

A set of formulas are now derived for use in the above-mentioned computation. In figure 4 the curved line represents the surface to be measured. The chosen reference plane is represented by the axis of abscissas. The chosen reference points are indicated by circles on the curved line. The several positions of the master plane relative to the coordinate system are represented by straight lines at various angles. The coordinates of all chosen reference points, which are marked on the surface of the unknown, are (R, Y_R). The observed fringe (a relative order of interference) at (R, Y_R) is designated A_R for the first position of the standard, B_R for the second position of the standard, C_R for the third position, and so forth. The slopes and intersections of the straight lines with the axis of ordinates are represented by M_A and A_0, respectively, for the A position, M_B and B_0 for the B position, M_C and C_0 for the C position, and so forth.

The slope-intercept form of the equation for the straight line representing the standard in the X position ($X=A, B, C$, etc.) is

$$Y_R+(X_R-X_0)=M_XR. \tag{1}$$

In position A, for example, the ordinates of the line are $(A_R+Y_R)=A_0+M_AR$, where A_R is the separation of the two optical surfaces. The absolute values for X_R are unknown, but differences in X_R, for any given position of the standard, are directly observable. Consequently, the integral part of the smallest X_R will be subtracted from all X_R's for purpose of computation. The quantity (X_R-X_0) is unaffected by this operation.

We will evaluate M_X and X_0 by applying the method of averages (footnote 1) to the data. The grouping of observations will be made in such manner that there is no overlapping of the two groups of points except when an odd number of reference points are to be applied to an evaluation. When the number of reference points in the two groups is odd, two observations are considered to be made at each of the points, and the two observations made at the central

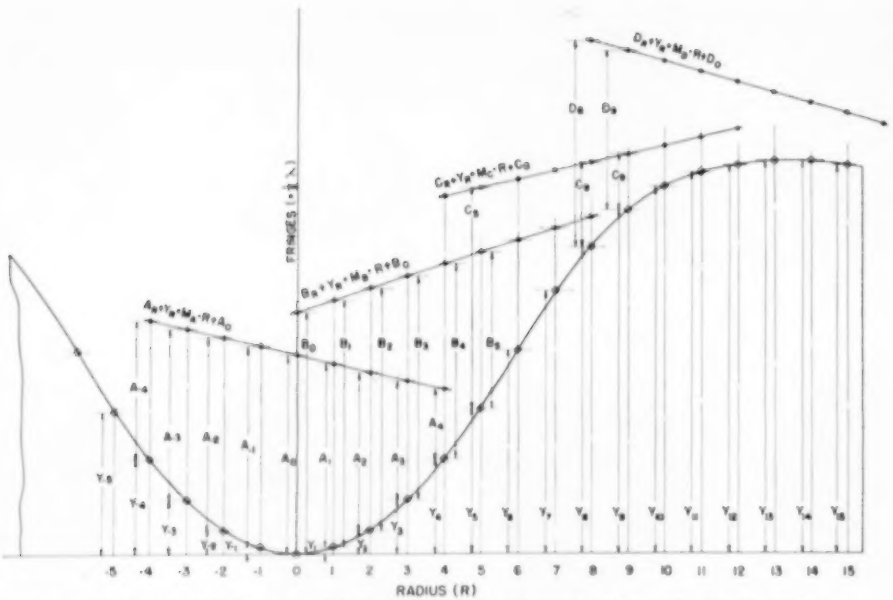

FIGURE 4. *Analytical representation of the surface and standard for mathematical analysis.*
The slanting straight lines represent the several positions of the standard and the adjacent formulas the equations of its corresponding belt.

point are divided between the two groups. The two groups then have an equal number of observations, and all observations are thereby assigned equal weights. When the total number of reference points is even, there is no overlapping of groups for an equal number of points to be allocated to each of the two groups for equal weighting of datum.

In applying the method of averages (footnote 1), we require that the algebraic sum of errors be zero for each of the two groups of observations. This requirement is represented by the following equations:

$$\left.\begin{aligned}\sum_{R_1}^{R_2}(Y_R+X_R)&=M_X\sum_{R_1}^{R_2}R+\frac{1}{2}N_X X_0,\\ \sum_{R_3}^{R_4}(Y_R+X_R)&=M_X\sum_{R_3}^{R_4}R+\frac{1}{2}N_X X_0,\end{aligned}\right\}\tag{2}$$

where summations in the first of this pair of equations are from the lowest value of $R(=R_1)$ to the largest value of $R(=R_2)$ in this group and summations in the second equation are from the lowest value of $R(=R_3)$ in the second group to the largest value of $R(=R_4)$ in the second group. Equality of R_2 and R_3 will result when the number of reference points is odd, whereas they will differ by unity when the total number of reference points is even. The number of reference points used in each evaluation is N_X.

Solving for M_X and X_0 from the pair of equations (2), we get

$$M_X=\frac{\sum_{R_3}^{R_4}(Y_R+X_R)-\sum_{R_1}^{R_2}(Y_R+X_R)}{\sum_{R_3}^{R_4}R-\sum_{R_1}^{R_2}R}\tag{3}$$

$$X_0=\frac{2\left[\sum_{R_1}^{R_2}R\sum_{R_1}^{R_2}(Y_R+X_R)-\sum_{R_1}^{R_2}R\sum_{R_1}^{R_2}(Y_R+X_R)\right]}{N_X\left[\sum_{R_1}^{R_2}R-\sum_{R_1}^{R_2}R\right]}\tag{4}$$

Equations (1), (3), and (4), together with the assumption that the surface to be measured has revolution symmetry, permit a computation of Y_R for all chosen reference points and consequently the shape of the surface.

The foregoing analysis permits a statistical evaluation of M_X and X_0 for all values of X (i. e., A, B, C, . . .) except the quantity A_0. An error in A_0 represents an error in the position of the reference plane and since this has no effect on the computed shape of the surface, the observed A_0 is assumed to be free from error.

As the surface is assumed to have revolution symmetry,

$$Y_R=Y_{-R}.\tag{5}$$

From eq (1) $Y_R=M_A R+(A_0-A_R)$, and $Y_{-R}=-M_A R+(A_0-A_{-R})$. On eliminating M_A and Y_R from these three equations, we have

$$Y_R=A_0-\tfrac{1}{2}(A_R+A_{-R}).\tag{6}$$

As M_A does not enter into the computation, it need not be evaluated.

4. Illustrative Example

Equations (1), (3), (4), and (6) form a set of fundamental equations from which all values for Y_R may be computed.

To clarify any possible lack of understanding in the development and application of these formulas, we will apply them to a set of observations and will compute the resultant shape of a surface. In this case the large circle in figure 2 represents the periphery of a 31.1-cm-diameter disk that is to be measured by means of a standard whose diameter is 8.2 cm. The seven circles, centered on one diameter of the large disk, represent the several successive positions of the standard. The eight circular fringe patterns shown in figure 3 (forming two independent sets, primed and unprimed) were obtained by photographing the fringe patterns formed by light reflected normally from the top surface of the large disk and the standard flat when in the several positions indicated in figure 2. The differences in values of the ordinates ($Y_R - Y_{-R}$), obtained from the two sets of photographs, is a measure of the accuracy obtainable. These differences are due to errors of observation and to an error in the choice of the center point. If the unknown is ground and polished on a spindle that is not concentric with it, the axis of rotation of the unknown surface will not be centered at the chosen origin of coordinates. However, the average value of Y_R and Y_{-R} from the two sets of data, primed and unprimed, respectively, will be almost free from the error of centering.

In order to obtain more precise values for X_R, the following procedure is followed: Reference marks with their associated R-values, or abscissas, are placed on the glass surface along the chosen reference line. These reference points are indicated by black dots centered in the small circles shown in figure 2. The standard is placed in the desired position and the air wedge adjusted so that a desirable number (5 to 10) of fringes cross the reference line. The present author prefers to have the fringes approximately perpendicular to the reference line. Considerable departure from this, however, is usually tolerated. The fringe pattern is photographed.[3] This is repeated for all desired positions of the standard. A fine straight line, using a needle point and a straight edge, is drawn across the photograph through the nine reference points on it. The positions of the centers of the references points are marked by pricking the photograph with a needle. This is to permit accurate readings on their positions. If no distortion is introduced in the photographic reproduction, the separation of all adjacent points will be equal. The intersections of all fringes, both dark (i. e., integral orders of interference) and light (integral plus half orders), with the reference line are marked also by pricking the photograph. The direction of increasing orders of interference is ascertained from tests and notations made when the fringes are photographed. The relative orders of interference, beginning with 1, are indicated by inserting numbers on the dark fringes. In figure 3 these numbers appear above each of the fringe patterns. The lesser visible numbers, adjacent to the reference points, represent the abscissas (or R-values) of the several reference points that were marked on the unknown surface.

In general, the scale of the photographic reproduction will differ from that of the chosen abscissa scale. For interpolation purposes any convenient scale may be used to measure the relative positions of points on the photograph. A centimeter scale with millimeter marks was used for this compilation. We will define the scale used as the P-scale and the readings from it as P-values. The P-values corresponding to all reference points and fringes are read off the centimeter scale and inserted in column 1 of table 1, which represents a typical data sheet. The corresponding R-values (numbers associated with the fiduciary reference points and appearing in the photographs) are inserted in column 2; the A_R-values, corresponding to integral and half-integral orders of interference, are inserted in their respective places in column 3. If an observed P-value, corresponding to an R-value, falls precisely on a fringe (reference point centered on a fringe), two identical P-values are inserted as for $R=-2$ and $A_R=5.5$ in the case given here.

The object of this listing and the following computations is to obtain more precise A_R-values (orders of interference) than can be obtained by direct interpolation or reading from the photographs.

A direct plot of the P-values versus A_R-values first entered in column 3, table 1 (the blank spaces to be filled later), shown as small black dots in figure 5, may be made. A smooth curve is then drawn through these points. The values for A_R in column 3, which correspond to R-values in column 2, are located on the curve. The corresponding ordinates represent the interpolated A_R-values desired. The values with asterisks, shown in table 1, are more precise values obtained by an interpolation process described in the following paragraphs.

The values for A_R, determined above from the direct plot, are not as precise as the directly observed values from which the plot was made. More precise

TABLE 1. *Arrangement of data for computation*

Values for A_R in column 3 that are followed by an asterisk are interpolated values from the curve of figure 5.

P	R	A_R	0.7 P	(0.7 P+A_R)
0.21	−4	8.23*	0.15	8.38*
.44	.....	8	.31	8.31
.93	.....	7.5	.65	8.15
1.39	.....	7	.97	7.97
1.54	−3	6.80*	1.08	7.88*
1.85	.....	6.5	1.29	7.79
2.40	.....	6	1.68	7.68
2.94	−2	5.50*	2.06	7.56*
2.94	.....	5.5	2.06	7.56
3.54	.....	5	2.48	7.48
4.29	.....	4.5	2.94	7.44
4.29	−1	4.42*	3.00	7.42*
4.80	.....	4	3.36	7.36
5.43	.....	3.5	3.80	7.30
5.64	0	3.33*	3.95	7.28*
6.05	.....	3	4.24	7.24
6.85	.....	2.5	4.80	7.30
7.00	1	2.41*	4.90	7.31*
7.70	.....	2	5.39	7.39
8.37	2	1.62*	5.86	7.48*
8.60	.....	1.5	6.02	7.52
9.67	.....	1	6.77	7.77
9.73	3	0.98*	6.81	7.79*
10.80	.....	.5	7.56	8.06
11.08	4	.39*	7.76	8.15*

[3] A micrometer eyepiece may be used to read the data directly and thus dispense with photography.

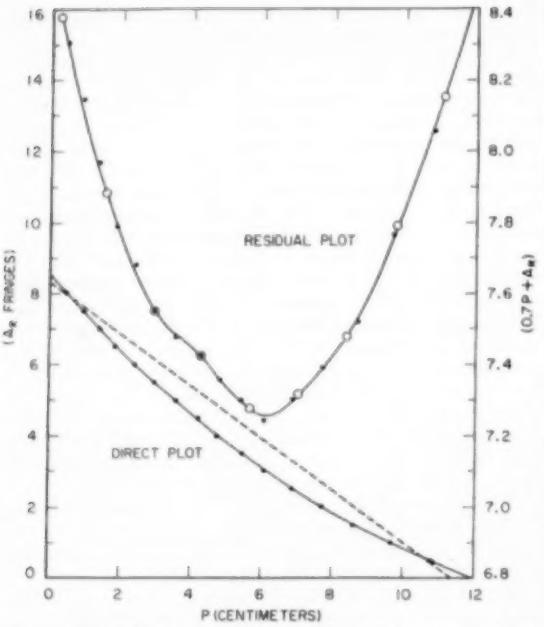

FIGURE 5. *Direct and residual plot of data for nonlinear interpolation of fringe orders.*

values may be obtained from a residual plot.[4] To obtain data for the residual plot, a column of values (table 1, column 4), computed with a slide rule, is added to the table of observed quantities. This column is a product of corresponding P-values and an appropriately chosen constant. This constant represents the slope of a straight line that crudely approximates the plotted points. It is indicated in figure 5. The approximate slope of this line is 0.7. A relatively large error in the choice of the slope contributes little or no error in the final results. Values of $0.7P$ are accordingly computed to two decimal places. The sums of corresponding values from columns 3 and 4, except where vacancies exist in column 3, are entered in column 5. These values are plotted, on an appropriately chosen scale, against corresponding P-values, and a smooth curve that best fits the points is drawn in by inspection (residual plot, fig. 5). One may now locate the points, shown as circles, on this curve, whose abscissas are those observed for the chosen reference points. The corresponding ordinates are read off and inserted in the $(0.7P+A_R)$ column. These values are marked with an asterisk for distinction. The corresponding values of $0.7P$ are subtracted from $(A_R+0.7P)$, and the resultant A_R values, shown also with asterisks, are inserted in the vacant places of the A_R column. These are the desired orders of interference at the several reference points. Values for $X_R(X=B,C,D, \ldots)$ are obtained from all photographs in this manner.

[4] H. M. Goodwin, Elements of the precision of measurements and graphical methods, p. 60 (McGraw-Hill Book Co., New York, N. Y., 1920).

TABLE 2. *Computation sheet for statistical evaluation of* ata
The average of corresponding values in columns 3 and 5 represents the ost acceptable results

R	A_R	Y_R	B_R	Y_{-R}
−4	8.23	.....	.....	.....
−3	6.80	.....	.....	.....
−2	5.50	.....	.....	.....
−1	4.42	.....	.....	.....
0	3.33	0.00	8.71	0.00
+1	2.41	−.09	7.13	−.09
2	1.62	−.23	5.75	−.27
3	0.98	−.56	4.49	−.56
4	.39	−.98	3.32	−1.04
5	.....	−1.57	2.34	−1.58
6	.....	−2.30	1.49	−2.28
7	.....	−3.16	0.77	−3.13
8	.....	−4.26	.29	−4.20
9	.....	−5.67	.....	−5.39
10	.....	−7.05	.....	−6.74
11	.....	−8.64	.....	−8.28
12	.....	−10.30	.....	−9.96
13	.....	−12.37	.....	−11.86
14	.....	−14.51	.....	−13.93
15	.....	−16.86	.....	−16.21

In order to determine the shape of the surface from the fringe readings and their corresponding abscissas, or R-values, these quantities are now applied to the formulas of eq (3), (4), and (6). Table 2 is a typical computation sheet. From eq (6) one computes $Y_4=3.33-\frac{1}{2}(8.23+0.39)=-0.98$, and likewise for all values of Y_R in the range covered by the standard in position A (column 3 of table 2). In order to proceed to the evaluation of Y_R for other values of R, eq (3) and (4) are used. Values for B_R, found in the same manner as described previously for A_R, are inserted in column 4, table 2. This permits a summation to be made of all terms shown in eq (3) and (4) and consequently an evaluation of M_B and B_0. As the number of reference points covered by the standard in each of the two positions, A and B, is odd (i. e., from $R=0$ through $R=4$, or 5 points), they are each assumed to represent 2 observations, making the total number of observations 10, which may now be divided into 2 equal groups. With this in view, it will be seen that $\sum_{R_0}^{R_5} R=2\times0+2\times1+1\times2=4$, and likewise for all summations shown in eq (3) and (4). The resultant values for M_B and B_0 are, respectively, −1.580 and +8.67. Slide-rule computation is adequate except for final precision. In general, the computed parameter B_0 will differ slightly from the observed value found in table 2. On substituting these values for M_X and X_0 in eq (1), and using values for R and B_R in columns 1 and 4, values for Y_R may be computed from $R=5$ through 8. These operations are now repeated, using consecutively the C and D data, to compute additional values for Y_R to the edge of the surface. These values are inserted in column 3, table 2. A similar treatment of the primed data yields an independent set of value for Y_{-R} shown in column 5, table 2, which should agree approximately with the above set. An average of Y_R and Y_{-R} values for each value of R is the accepted value. This averaging operation tends to decrease the effects of error in choice of the axis of rotation of the unknown surface as well as observational errors.

WASHINGTON, December 3, 1953.

Journal of Research of the National Bureau of Standards Vol. 53, No. 1, July 1954 Research Paper 2515

Bacher and Goudsmit Theory of Complex Spectra

R. E. Trees

The Bacher and Goudsmit theory expresses the energy of a state of an atom in terms of a linear combination of energies of states of other ions of the same atom. This theory is tested in the spectra with d- and s-electrons and general conclusions drawn about its accuracy.

In deriving their theory, Bacher and Goudsmit formally introduced many-particle interactions. They showed (to a limited extent) that this was equivalent to a second procedure in which the zero-order wave functions were assumed to be independent of the ionization and successive orders of perturbations were included.

Recently it has been shown that a linear theory, which is a combination of the Slater theory and an empirically derived correction, predicts the separations of terms in any one configuration with about the same accuracy as the Bacher and Goudsmit theory; in this theory, the wave functions are allowed to depend on the degree of ionization. It is shown that the Bacher and Goudsmit theory can be interpreted in a third way that is consistent with this linear theory.

In the light of this latter interpretation, Racah has suggested an empirical modification of the Bacher and Goudsmit theory that often leads to better results; this suggestion has been incorporated in the present paper.

1. Introduction

Bacher and Goudsmit have shown that it is possible to express the energy levels of an atom correctly to second order by taking linear combinations of the energy levels of the ions of that atom.[1] They gave explicit formulas for these linear combinations for atoms containing s- and p-electrons, and tested the theory in the spectra of oxygen, nitrogen, and carbon. The theory usually predicted the absolute term values with an error less than 2500 K.[2] Separations of terms in a given configuration were often given very much better, sometimes within a few hundred kaysers.

In section 2 the theory of Bacher and Goudsmit is derived briefly from a new viewpoint. Bacher and Goudsmit derived their formulas by formally introducing many-body interactions; no explicit form was given for these interactions. They were able to show that in the first and second approximations this was equivalent to using zero-order wave functions that were independent of the degree of ionization, and, with these, making first- and second-order perturbation calculations of the energy, respectively. In the present paper, a third derivation is given, in which the zero-order wave functions of the Slater theory are allowed to vary regularly with the degree of ionization; an explicit two-body interaction is also introduced. This interpretation is justified by the observation that there is a smooth variation of the one-particle and two-particle parameters in a linear theory.[3] The more specific and easily understood meaning of this interpretation in terms of a linear theory is given in section 5; it is equivalent to assuming that the parameters in different ions of the same atom are given by series expansions in powers of the degree of ionization. It is shown that the BG nth approximation accounts for terms up to and including the nth power for the one-particle parameters and terms to the $(n-1)$th power for the two-particle parameters.

In section 3 a few formulas applicable to terms in d^n, $d^n s$, and $d^n s^2$ configurations are obtained by using tables of coefficients of fractional parentage and recoupling transformations given by Racah.[4] In section 4 an application of these formulas is made in the spectra of titanium, vanadium, chromium, and zirconium. It is found that separations of terms in the same configuration are given very closely (the error is less than 400 K). Separations of terms in different configurations may be given very poorly, however, as an error of 6000 K is found in titanium ($Z=22$). The latter type of error is found to decrease very rapidly in spectra of more highly ionized atoms: in chromium spectra ($Z=24$) the error is only 600 K, one-tenth the error found for the related titanium spectra. The error is also found to decrease for spectra with higher nuclear charge as it is only 2000 K in zirconium ($Z=40$).

Racah has pointed out that a power-series expansion, of the type described previously, converges more rapidly if spectra are chosen having the same degree of ionization. A comparison with experiment, using this empirical modification of the original theory of Bacher and Goudsmit, is also given in section 4.

As indicated previously, the Bacher and Goudsmit theory can be interpreted in terms of a linear theory in which the radial parameters are given by series expansions in the degree of ionization. Checking these expansions is the easiest way to check all the data against the Bacher and Goudsmit theory. The

[1] R. F. Bacher and S. Goudsmit, Phys. Rev. **46**, 948 (1934); referred to in the present paper as "BG".

[2] "Kayser" is the name adopted by the Joint Commission for Spectroscopy for the unit of wave number, cm^{-1}, and is abbreviated "K".

[3] R. E. Trees and M. M. Harvey, J. Research NBS **49**, 397 (1952) RP2378. In section 1 of RP2378 the literature is reviewed, and the methods of analyzing spectra with the Slater theory, for including effects of configuration interaction, and of making allowance for polarization energy with the $L(L+1)$ correction are also outlined and applied. In referring to a "linear theory", the $L(L+1)$ correction is combined with the Slater theory, and the radial integrals are regarded as parameters.

[4] G. Racah, Phys. Rev. **62**, 438 (1942); **63**, 367 (1943). These papers are referred to herein as II and III, respectively.

301746—54——4

conclusions reached from the direct application of the theory already cited above, have been verified by using all available data with this method. The detailed calculations needed for this verification are omitted for brevity.

In section 6 the effect of weak configuration interaction in which one electron is excited is considered, and in section 7 the effect of irrationality of the energy eigenvalues is analyzed. The purpose is to illustrate in more detail the direct application of the theory of BG and to indicate where a direct application might lead to results that differ from those obtainable with a linear theory. Such differences are probably too small to be detected within the accuracy obtainable at present with any theory, but more complete comparisons of theory with the presently available experimental data are needed to verify this conclusion.

2. Bacher and Goudsmit Theory

2.1. General Theory

In this section is given a new derivation of the theory in which it is assumed that the interaction parameters vary smoothly. The Hamiltonian of the n–electron system is taken as

$$H=H_1+H_2, \tag{1}$$

where

$$H_1=\sum_{i=1}^{n}\left(\frac{1}{2\mu}p_i^2-\frac{Ze^2}{r_i}\right)$$

and

$$H_2=\sum_{i<j=1}^{n}\frac{e^2}{r_{ij}}.$$

H_1 and H_2 are examples of what are called "type-one" and "type-two" terms, respectively, (H_1 is a sum of functions, each depending on the coordinates of a single electron, and H_2 is a sum of functions for two electrons). A particular selection P of r of the n–electrons will be indicated by P_r. The sum of the Hamiltonians $H(P_r)$ of the r–electron systems for all possible choices P is a symmetric function of the n–electrons, and the n–electron Hamiltonian H is expressible identically as a linear combination of such symmetric sums for two or more values of r,

$$H=\sum_r C_r\sum_P H(P_r); \tag{2}$$

The conditions that this be an identity are the following:

$$\sum_r C_r\binom{n}{r}\binom{r}{1}=\binom{n}{1} \quad \text{and} \quad \sum_r C_r\binom{n}{r}\binom{r}{2}=\binom{n}{2}. \tag{3}$$

In general, $\binom{a}{b}$ is the binomial coefficient when $a\geq b\geq 0$,

$$\binom{a}{b}=\frac{a!}{(a-b)!b!},$$

and zero for $b<0$ or $a<b$. The values of the coefficients C_r will be indeterminate if there are more than two nonzero C_r-values. The method of choosing best values of the C_r in such cases will be considered below.

The eigenfunction $\psi(\gamma)$ of the n-electron system is assumed to have in its specification a definite configuration $l_1, l_2, \ldots, l_n$, and P_r is specified by r of these l-values; the electrons are regarded as distinguishable, even though some may be equivalent. The electrons in the selection P_r have allowed eigenfunctions $\psi(\alpha)$ of the r-electron Hamiltonians $H(P_r)$; the residual $(n-r)$ electrons have allowed eigenfunctions $\psi(\beta)$ of the $(n-r)$-electron Hamiltonian. The l-values of the electrons are included in the specifications α, β, and γ, along with S- and L-values for the combined system and any other quantum numbers needed to specify the coupling.[5] The function formed by vector coupling the $(n-r)$-electron eigenfunction to the r-electron eigenfunction is indicated by $\psi(\alpha,\beta,\gamma)$. A linear combination of these functions can be formed that will be identical with $\psi(\gamma)$; this was first pointed out by Bacher and Goudsmit,

$$\psi(\gamma)=\sum_{\alpha\beta}(\alpha\beta,\gamma]\gamma)\psi(\alpha,\beta,\gamma). \tag{4}$$

$(\alpha,\beta,\gamma]\gamma)$ is called the coefficient of fractional parentage. The calculation of the coefficients of fractional parentage is a mathematical problem that has been considered in detail by Racah. He has tabulated these coefficients for configurations of equivalent p- and d-electrons in III; their use will be illustrated in section 3.

A partial energy $E(\alpha)$ of the choice P_r is introduced that is associated with the r-electrons while they are part of the n-electron system and combined to form the state α. This energy cannot be observed, and must be approximated from the observed energy of the r-electron ion of the atom in the state α, which is defined as $W(\alpha)$. The average energy of the choice P_r when present in the original n-electron configuration γ is determined with the help of (4),

$$\overline{E}(\gamma;P_r)=\sum_{\alpha\beta}(\alpha\beta,\gamma]\gamma)^2E(\alpha). \tag{5}$$

The corresponding approximate energy can be calculated from the observed energies in the r-electron ion,

$$\overline{W}(\gamma;P_r)=\sum_{\alpha\beta}(\alpha\beta,\gamma]\gamma)^2W(\alpha). \tag{6}$$

The energy of the n-electron system is then given identically by an expression similar to (2),

$$E(\gamma)=\sum_r C_r\sum_P\overline{E}(\gamma;P_r). \tag{7}$$

[5] There may be more than one term allowed with a given (SL)-value in the configuration considered (the configuration may be that contained in α, β or γ). In such cases the function obtained by a legitimate coupling procedure will not be an eigenfunction of the Hamiltonian, even though it has an allowed symmetry, if it mixes with other allowed eigenfunctions in that configuration having the same (SL)-value. In such cases a purely formal difficulty arises because the characterization by parentage is indeterminate, and the theory given by Bacher and Goudsmit must be amplified by more or less arbitrary additions. In sections 2, 3, and 4 of the present paper these cases are omitted. These omitted cases are considered in sections 5 and 7.

The corresponding approximate energy is calculated from the approximate average energies (6),

$$W(\gamma)=\sum_r C_r \sum_p \overline{W}(\gamma;P_r). \tag{8}$$

The energies W and $\overline{W}$ used above are the same as the W used in BG for both expressions. Quantities such as $W(\alpha)$, $W(\alpha,\beta)$, etc., on the right side of eq (7) to (14) in BG are sometimes energies of observed spectral terms, but in general they are linear combinations of the observed energies; in the present notation they would be replaced by $\overline{W}(\gamma;P_1)$, $\overline{W}(\gamma;P_2)$, etc. Directly observed energies are indicated by W, as in the right-hand side of (25) and (26) of BG.

The difference between the exact value (7) and the approximate value (8) is estimated by separating the E's and W's into their type-one and type-two parts, and by assuming that the following expansions can be made:

$$\begin{aligned} W_1(\alpha)&=E_1(\alpha)\{1+a_1(\gamma)(n-r)+a_2(\gamma)(n-r)^2+\ldots\} \\ W_2(\alpha)&=E_2(\alpha)\{1+b_1(\gamma)(n-r)+b_2(\gamma)(n-r)^2+\ldots\}. \end{aligned} \tag{9}$$

The coefficient $a_t(\gamma)$ in (9) will be eliminated from the difference between (7) and (8) if

$$\sum_{r=1}^{n-1} C_r (n-r)^t \binom{n}{r}\binom{r}{1}=0, \tag{10}$$

and the coefficient $b_t(\gamma)$ will be eliminated if

$$\sum_{r=1}^{n-1} C_r (n-r)^t \binom{n}{r}\binom{r}{2}=0. \tag{11}$$

A choice of C_r-values defines an approximation of the same order as the largest value of t for which (10) is satisfied (it is assumed that (10) and (11) are satisfied for all smaller values of t and that relations (3) are satisfied). For instance, in a second approximation, the type-one energies are expanded in a series containing powers up to and including the squares of $(n-r)$, whereas the type-two energies are expanded only to first power in $(n-r)$. Formulas (3), (10), and (11) are not independent. They may be combined into a definition that is easily shown to be equivalent to that just given, by requiring the coefficients C_r to satisfy the following $(m+1)$ equations in order to define an mth approximation

$$\sum_{r=1}^{n-1} C_r (n-r)^t \binom{n}{r}\binom{r}{1}=\delta_{t0}\binom{n}{1} \qquad (t=0,1,\ldots,m). \tag{12}$$

In the derivation of BG, many-body interactions are formally introduced. According to the present notation, this is equivalent to considering not only type-one and type-two terms as being present in (1) but also type-three, type-four, etc., terms. This leads immediately, by generalizing (3), to the definition of the m^{th} approximation given by Bacher and Goudsmit. According to their definition the C_r-values satisfy the following $(m+1)$ equations:

$$\sum_{r=1}^{n-1} C_r \binom{n}{r}\binom{r}{k}=\binom{n}{k} \qquad k=1,2,\ldots,(m+1). \tag{13}$$

To show the definitions (12) and (13) are equivalent, the following expansion is utilized for powers $t>0$ of an integer p: [6]

$$p^t=\sum_{\kappa=1}^{t}\alpha_\kappa(t)\binom{p}{\kappa}, \tag{14}$$

where

$$\alpha_\kappa(t)=\kappa^t-\kappa(\kappa-1)^t+\frac{\kappa(\kappa-1)(\kappa-2)^t}{2!}-\ldots.$$

Inserting (14) in (12) leads to the result

$$n\sum_{\kappa=1}^{t}\alpha_\kappa(t)\binom{n-1}{\kappa}\sum_{r=1}^{n-1} C_r\binom{n-\kappa-1}{r-1}=0 \quad (t=1,\ldots,m). \tag{12a}$$

Equation (13) is equivalent to the formula

$$\sum_{r=1}^{n-1} C_r\binom{n-k}{r-k}=1 \qquad (k=1,2,\ldots,(m+1)). \tag{13a}$$

It follows therefore by repeated application of the binominal coefficient relation,

$$\binom{n-\kappa-1}{r-1}=\binom{n-\kappa}{r-1}-\binom{n-\kappa-1}{r-2},$$

and the use of (13a) that the left side of (12a) vanishes, as it should, whenever (13) is satisfied. When $t=0$ in (12), the equation is the same as (13) when $k=1$, so the equivalence of the two sets of defining equations is demonstrated. A special m^{th} approximation is defined by the following set of C_r-values:

$$\left.\begin{aligned} C_r&=(-)^{m-r+1}\binom{n-m-1}{m-r+1} \quad (r=1,2,\ldots,(m+1)) \\ C_r&=0 \qquad\qquad\qquad\qquad (r=(m+2),\ldots,(n-1)) \end{aligned}\right\}. \tag{15}$$

If there are only two nonzero values of C_r, and these are C_1 and C_2, then they are defined by (15), and relation (8) has the explicit form

$$W_1(\gamma)=\sum_p \overline{W}(\gamma;P_2)-(n-2)\sum_{p_4}\overline{W}(\gamma;P_1). \tag{16}$$

Relations (8) and (12) of BG are special cases of (16), for which n has the values 4 and 5, respectively. As an alternative, it can be assumed that C_1 and C_{n-1} are the nonzero coefficients, and then the fol-

[6] A treatise on the calculus of finite differences, G. Boole, edited by F. J. Moulton (Macmillan & Co., London, 1880).

lowing formula is obtained by solving (12) or (13) (the specification γ will be omitted for brevity):

$$W_1(n)=\frac{1}{n-2}\sum_p \overline{W}(P_{n-1})-\frac{1}{n-2}\sum_p \overline{W}(P_1). \quad (17)$$

2.2. The Second Approximation

If C_1, C_2, and C_3 are taken as the nonzero coefficients of the second approximation, the following formula is obtained from (15):

$$W_2(n)=\sum_p \overline{W}(P_2)-(n-3)\sum_p \overline{W}(P_2)+$$

$$\frac{1}{2}(n-3)(n-2)\sum_p \overline{W}(P_1). \quad (18)$$

Relations (9) and (13) of BG are special cases of this formula for which n has the values 4 and 5, respectively. In appendix I of BG, perturbation theory was used to show that (18) is equivalent to a calculation that is correct up to and including the second order. In general, reference to "the theory of Bacher and Goudsmit" in the present work applies chiefly to this second approximation.

The complete set of one-electron functions used in appendix I of BG was that appropriate to the ionized state of the atom with only a single electron outside of a closed shell. The same zero-order functions were used for the atom in all other states of ionization, and the second-order effect was evaluated with them. This is a poor zero-order approximation for some spectra,[7] so that "second-order effect," in the sense used by Bacher and Goudsmit, is not synonymous with polarization energy. The latter energy is usually defined as that part of the observed energy that cannot be explained by a calculation in which the one-electron functions are determined by the Hartree-Fock method for each state of ionization. No investigation has been made to determine the variation in accuracy of a second-order calculation with change of the zero-order eigenfunctions, but Bacher and Goudsmit often obtained poor values in their calculations because the higher-order effects became more important as the zero-order functions became worse approximations.

The influence of polarization on the separation of terms in a single configuration containing d- and s-electrons may be represented by a correction proportional to $L(L+1)$.[8] Racah has shown that this correction may be derived by assuming a special type of linearity for the polarization energy, and he has outlined a proof of this assumption of linearity.[9] The proof is based on the assumption that in the configuration d^n the $L(L+1)$ correction arises from interactions with configurations $d^{n-2}l^2$ and $d^{n-2}l'$ that have two electrons of the original configuration excited. The linear behavior then follows from (54) of BG. Alternatively, it can be demonstrated by comparing (33a) of III with (33c) of III, and assuming that the perturbing configurations are sufficiently far away so that the energy denominators in the second-order perturbation can be assumed constant. The proof shows that the $L(L+1)$ correction is accounted for initially in the first approximation, so that it is on the same footing as the Slater energy. An interaction in which only one electron is excited is included fully for the first time in the second approximation, as shown by (53) and (59) of BG. Any deviation from linear behavior that is produced by such an interaction must be assumed negligible if the $L(L+1)$ correction is used to account for polarization.

In section 4 it is shown that the Bacher and Goudsmit theory leads to close agreement with the observed separation for two terms in the d^2 s configuration in both titanium and zirconium, the errors being 357 K and 293 K, respectively. Bacher and Goudsmit noted that the separation of terms in the same configuration are well predicted in spectra containing $2s$- and $2p$-electrons.[10] It is concluded that the error of the Bacher and Goudsmit theory in predicting separations of terms in the same configuration will generally be less than 400 K and that the accuracy is therefore about the same as that obtained with a linear theory.

A large part of the polarization energy is the same for all terms of a given configuration. The energy common to all terms can be investigated with self-consistent field and other variational methods, but it is not easy to get a reliable picture of the behavior from the few calculations that have been made. One approximation, used fairly often with minor variations, ascribes an energy of 5000 to 10000 K either to each electron or to each pair of equivalent electrons; interactions between pairs of nonequivalent electrons are neglected in the latter approximation. The energy is independent of Z but depends a little on the types of electrons that are paired.[11] This part of the polarization energy is very large, and the departures from the described behavior could be appreciable.

The Bacher and Goudsmit theory can be tested in this respect by calculating the separations of terms in different configurations. In section 4 it is shown

[7] Similarly defined parameters change by 10 to 30 percent in successive ions when they are evaluated by least squares; they would have the same value if the zero-order functions were the same in all ions. A similar problem is considered by A. Rahman, Physica **19**, 377 (1953). See also E. P. Wigner, Phys. Rev. **94**, 77 (1954).

[8] R. E. Trees, Phys. Rev. **84**, 1089 (1951).

[9] G. Racah, Phys. Rev. **85**, 381, (1952), and private communications.

[10] Tables XVII and XVIII of BG, calculation II. It is noted in BG that agreement better than 200 to 300 K must be regarded as fortuitous so that the ultimate significant accuracy is regarded as about the same as obtained with the $L(L+1)$ correction. Many separations of terms in the same configuration are predicted with errors greater than 1000 K in BG, and this must be attributed to the neglect of configuration interaction, or to the fact that the theory is less accurate for spectra with $2s$- and $2p$-electrons.

[11] F. Seitz, Modern theory of solids, p. 247ff (McGraw-Hill Book Co., New York, N. Y., 1940). Seitz evaluates energy per electron rather than per pair of equivalent electrons, but his remarks on page 248 justify the latter interpretation. Self-consistent field calculations of O, O^+, and O^{++}, including exchange and configuration interaction (D. R. Hartree, W. Hartree, B. Swirles, Phil. Trans. Roy. Soc. [A] **238**, 229 (1939)), support an interpretation based on pairs, a value of 7000 K being associated with each pair of equivalent $2p$-electrons. Although a strong dependence on multiplicity is expected (page 250), this is shown only to a minor extent in the oxygen calculations; if present, it would be accounted for in the previous consideration of the separations of terms in the same configuration. An additional point that should be noted is that comparison of the self-consistent field calculations in oxygen (noted above), with and without configuration interaction, indicates that configuration interaction is important.

that there is an error of 6000 K in predicting the energy difference between a term in the $3d^3$ configuration and one in the $3d^2\,4s$ configuration of titanium, and a corresponding error of 2000 K in similar zirconium spectrum with $4d$- and $5s$-electrons, and also that this error decreases rapidly as ionization increases in the spectra with $3d$- and $4s$-electrons because the spectra of titanium, vanadium, and chromium show errors of 6000, 1800, and 600 K, respectively. Bacher and Goudsmit found an error of about 2000 K in the spectra with $2s$- and $2p$-electrons; the decrease of the error with increase of Z was slight in these spectra.[12]

The spectra considered here contain four electrons outside of closed shells and are the easiest spectra to analyze with relation (18). A more complete exploration of the theory would consider also spectra with five or more electrons.

2.3. Higher Approximations

A third approximation may be obtained from (15), in which C_1, C_2, C_3, and C_4 are nonzero;

$$W_3(n)=\sum_p \overline{W}(P_4)-(n-4)\sum_p \overline{W}(P_3)+\frac{(n-4)(n-3)}{2}\sum_p \overline{W}(P_2)-\frac{(n-4)(n-3)(n-2)}{3.2}\sum_p \overline{W}(P_1). \quad (19)$$

Relation (14) of BG is a special case of this formula for which $n=5$. Bacher and Goudsmit considered this approximation equivalent to a calculation by perturbation theory correct to third order, but they were not able to carry out the complex calculation that would be necessary to demonstrate this rigorously. Separations of terms in spectra of oxygen and nitrogen were calculated a little better in the W_3 than in the W_2 approximation.[13] In section 5 the relative accuracy of W_3 and W_2 is discussed from another viewpoint (formulas (56) and (60)), and it is concluded that higher approximations can only account for a small part of the error already noted in the W_2 approximation.

Any interpretation used to justify the method of Bacher and Goudsmit leads to the conclusion that it is more accurate the more similar the binding of the electrons (and the structure of the configurations) for the different energy levels utilized in the formulas. For example, in calculating term values for l^n all configurations specifying a choice of r-elections would belong to l^r. On the other hand, in calculating term values for $l^{n-1}\,s$ the selection of r-elections is specified by either the l^r or the $l^{r-1}\,s$ configuration, so that there are twice as many different configurations to be considered. According to this argument, a given order of approximation would probably predict terms in the l^n configuration best, terms in $l^{n-1}\,s$ next best, and terms in $l^{n-2}\,s^2$ least accurately. This argument has some confirmation which was pointed out by Bacher and Goudsmit.[14] Bacher and Goudsmit also have noted that the method is inadequate for configurations such as $2s^22p^24s$, in which the total energy of the excited electron is less than the electrostatic energy of the inner ones. In such cases, even the separations of terms in the same configurations would not be given accurately. Similiarly, the method gives poor predictions for negative ions.[15]

3. Formulas for Spectra With d- and s-Electrons

3.1. The l^n Configuration

When the configuration specified in γ is l^n, equation (6) has the form

$$\overline{W}(l^n\gamma SL;\,l^r)=\sum_{\alpha_1 S_1 L_1 \alpha_2 S_2 L_2}(l^r(\alpha_1 S_1 L_1)l^{n-r}(\alpha_2 S_2 L_2), SL]l^n\gamma SL)^2\,W(l^r\alpha_1 S_1 L_1). \quad (20)$$

If this relation is used in (17) for $\overline{W}(P_{n-1})$, the sum over P introduces a factor $\binom{n}{r}=\binom{n}{n-1}=n$, and (17) becomes,

$$W_1(l^n\gamma SL)=\frac{n}{n-2}\sum_{\alpha_1 S_1 L_1}(l^{n-1}(\alpha_1 S_1 L_1)lSL]l^n\gamma SL)^2\cdot W(l^{n-1}\alpha_1 S_1 L_1)-\frac{n}{n-2}\,W(l). \quad (21)$$

The first term on the right defines the separation of terms in the l^n configuration; it has the same form as a relation given by Racah for calculating matrix elements of a general scalar operator G defined between pairs of interacting electrons.[16] Similiarly, by utilizing (20) with $r=2$, relation (16) becomes

$$W_1(l^n\gamma SL)=\frac{n(n-1)}{2}\sum_{S_1 L_1 \alpha_2 S_2 L_2}(l^2(S_1 L_1)l^{n-2}(\alpha_2 S_2 L_2), SL]l^n\gamma SL)^2\,W(l^2 S_1 L_1)-n(n-2)\,W(l). \quad (22)$$

[12] Table XIV of BG. In discussing this table, Bacher and Goudsmit noted that the errors decreased slightly as Z increased, but from a later discussion it is apparent that they considered this effect of Z as being of minor importance.

[13] Separations of terms in the same configuration were sometimes given with a smaller error by W_3 than by W_2, as may be seen by comparing calculation III with calculation II in table XVIII of BG; however, in an almost equal number of cases the agreement was worse. Absolute term values calculated with W_3 for the $2s^2\,2p^3$ configuration of oxygen were generally in error by less than 1000 K (table XIV of BG), whereas the W_3 approximation indicated term values in the $2s^2\,2p^4$ configuration with a larger error, about 1400 K (table XV of BG). Bacher and Goudsmit note that the $2s^2\,2p^4$ configuration is calculated better in the W_2 approximation, regarding the s-electrons as part of the closed shell, than in the W_3 approximation. The relative errors of absolute term values will naturally decrease for the higher approximation as the absolute value of the energy to the closed shell is much greater.

[14] Table XIV of BG. Absolute term values for the $2p^4$ configuration of oxygen are predicted within a few hundred kaysers, which may be the best significant agreement obtainable. Errors for $2p^3\,2s$ are about 1000 K, and they are about 2000 K for $2s^2\,2p^2$.

[15] In footnote 7 of BG it is noted that the calculated electron affinity of oxygen is 8000 K and that the observed value is 18000 K. The discontinuity in binding energy of negative ions has been discussed by Ta-You Wu in Phys. Rev. **89**, 629 (1952).

[16] G. Racah, Phys. Rev. **76**, 1349 (1949). Formula (1).

This is the same as an alternative formula given by Racah for calculating matrix elements of a scalar operator.[17]

It is noted in III that the formula corresponding to (22) needs very long calculations and is of practical use only in a few particular cases. Although the direct use of (20) is impractical, except when $r=n-1$ (or in the trivial case where r is unity), a step-by-step procedure, starting with $r=n-1$ and decreasing r a unit at a time, is generally practical. With this procedure, only tables of the coefficients $(l^{n-1}(\alpha_1 S_1 L_1)l, SL\|l^n\gamma SL)$ are needed. These coefficients are defined by (9) III and (11) III, and the coefficients have been tabulated in III for p^n and d^n configurations.

As an example, the second approximation (18) will be evaluated in detail for a $d^4\ ^5$D term by using (20) in a step-by-step procedure. By using table III of III, relation (20) becomes

$$\overline{W}(d^4\ ^5\mathrm{D};f^2) = 3/10\,W(d^3\ ^4\mathrm{P}) + 7/10\,W(d^3\ ^4\mathrm{F}). \quad (23)$$

The W's on the right are formally evaluated with (20), by using table II of III:

$$\overline{W}(d^3\ ^4\mathrm{P};f^2) = 8/15\,W(d^2\ ^3\mathrm{P}) + 7/15\,W(d^2\ ^3\mathrm{F}), \quad (24)$$

$$\overline{W}(d^3\ ^4\mathrm{F};f^2) = 1/5\,W(d^2\ ^3\mathrm{P}) + 4/5\,W(d^2\ ^3\mathrm{F}). \quad (25)$$

These results are then substituted back in (23):

$$\overline{W}(d^4\ ^5\mathrm{D};f^2) = 3/10\,W(d^2\ ^3\mathrm{P}) + 7/10\,W(d^2\ ^3\mathrm{F}). \quad (26)$$

Alternately, (26) could have been obtained directly from (20) (with $r=2$) by first calculating the coefficients of fractional parentage $(d^2(S_1L_1)d^2(S_2L_2), {}^5\mathrm{D}\|d^4\ {}^5D)$ with (32) of III. The step-by-step procedure used above is simpler because the quantum numbers $\alpha_2 S_2 L_2$ do not enter the calculation explicitly. The values (23) and (26) are now inserted into (18) and the sums over P replaced by factors $\binom{n}{r}$ to obtain the desired formula,

$$W_2(d^4\ ^5\mathrm{D}) = 6/5\,W(d^3\ ^4\mathrm{P}) + 14/5\,W(d^3\ ^4\mathrm{F}) - 9/5\,W(d^2\ ^3\mathrm{P}) - 21/5\,W(d^2\ ^3\mathrm{F}) + 4\,W(d). \quad (27)$$

Formula (27) is a good one to use in testing the Bacher and Goudsmit theory. All term values used in the formula should be unperturbed, and they are likely to be known experimentally. The following two formulas, obtained in a similar fashion, are not so generally useful: the terms that are most likely to be perturbed by configuration interaction are starred:

$$W_2(d^4\ ^1\mathrm{I}) = 6/5\,W(d^3\ ^2\mathrm{G})^* + 14/5\,W(d^3\ ^2\mathrm{H}) - 3/7\,W(d^2\ ^1\mathrm{D})^* - 3\,W(d^2\ ^3\mathrm{F}) - 18/7\,W(d^2\ ^1\mathrm{G}) + 4\,W(d) \quad (28)$$

$$W_2(d^4\ ^3\mathrm{H})^* = 1/3\,W(d^3\ ^2\mathrm{F})^* + 4/3\,W(d^3\ ^4\mathrm{F}) + 3/5\,W(d^3\ ^2\mathrm{G})^* + 26/15\,W(d^3\ ^2\mathrm{H}) - 3/5\,W(d^2\ ^3\mathrm{P}) - 2/7\,W(d^2\ ^1\mathrm{D})^* - 17/5\,W(d^2\ ^3\mathrm{F})^* - 12/7\,W(d^2\ ^1\mathrm{G}) + 4\,W(d). \quad (29)$$

Formulas for all other terms would require an addition to the theory of Bacher and Goudsmit. The parentages of duplicated terms in d^4 and/or d^3 would depend on the particular spectrum under consideration, whereas in the formulas for the terms given above the coefficients were defined by purely mathematical considerations.

3.2. The $l^{n-1}l'$ Configuration

The evaluation of $W(\gamma;P_r)$ when the specification γ contains the $l^{n-1}l'$ configuration, can be carried out similarly if tables of coefficients of fractional parentage for nonequivalent electrons are available.[18] In general, such tables are not available, and the coefficients must be calculated from tables for equivalent electrons with the help of transformations between different coupling schemes given in section 2 of III. Again a step-by-step procedure is simplest, so that only selections P with $n-1$ electrons need be considered. The parent term in the l^{n-1} configuration again is assumed, for simplicity, to be in an exactly specified state. The single selection containing the equivalent electrons has an average energy $\overline{W}((l^{n-1}\gamma SL)l'S'L';l^{n-1})$, which is the same as the observed energy in the ion $W(l^{n-1}\gamma SL)$. The only new feature is the selection specified by the $l^{n-2}l'$ configuration. The coefficients of fractional parentage will have the form

$$(l^{n-2}(\alpha S_1 L_1)l'(S''L''), lS'L'\|l^{n-1}(\gamma SL)l'S'L') = (l^{n-2}(\alpha S_1 L_1)lSL\|l^{n-1}\gamma SL)(S_1L_1l(SL)l'S'L'|S_1L_1l'(S''L'')lS'L'). \quad (30)$$

On the right, the first factor is the coefficient of fractional parentage for equivalent electrons; the

[17] Formula (33a) of III. To get the expressions to agree exactly, the following generalization of formula (29) of III is used:

$$(l^n(\alpha_1 S_1 L_1)l^{n-r}(\alpha_2 S_2 L_2)SL\|l^n\gamma SL) = (-1)^{S+L+L_2-S_2-S_1-L_1+\frac{1}{2}n}\delta_S(l^{n-r}(\alpha_2 S_2 L_2)l^r(\alpha_1 S_1 L_1), SL\|l^n\gamma SL)$$

[18] Tables for p^2 s, p^2 s, and d^2 p have been given by S. Meshkov in Phys. Rev. **91**, 871 (1953). With his convention for the normalization of the coefficients, the sums over P required in the formulas given here would be replaced by factors $\binom{n}{r}$; the different selections P are then accounted for during the calculation of the tables. To allow what seems to be the most direct use of Racah's tables, the coefficients of fractional parentage have been normalized to unity for each selection in the present paper.

second factor is a transformation coefficient evaluated in (5) of III,

$$(S_1L_1l(SL)l'S'L'|S_1L_1l'(S''L'')lS'L')$$
$$=[(2S+1)(2S''+1)(2L+1)(2L''+1)]^{\frac{1}{2}}$$
$$W(S_1^{\frac{1}{2}}\,\tfrac{1}{2}S'';S'S_1)\,W(Ll'lL'';L'L_1). \quad (31)$$

The W-functions in this expression are calculated from (36) of II; some values of the W-function have also been tabulated.[19]

The particular case where l' is an s-electron is the only one we consider in detail. In this case, the result of applying (30) and (31) reduces to a fairly simple formulation. To evaluate the average energies for a term $l^{n-1}(\gamma SL)sS'L$:

(a) Evaluate $\overline{W}(l^{n-1}\gamma SL;l^{n-2})$ in terms of the observed energies $W(l^{n-2}\,\alpha S_1L_1)$, as already described.

(b) If the spin S_1 of the ion term in l^{n-2} does not have the same value S' as the original term under consideration in $l^{n-1}s$, then add an s-electron to this ion term, making the resultant spin S'' equal to S, the spin of the parent term in l^{n-1}; i. e., change $W(l^{n-2}\,\alpha S_1L_1)$ to $W(l^{n-2}\,(\alpha S_1L_1)sSL_1)$.

(c) If the spin S_1 has the value S', then add the s-electron to the ion, and split the latter into two terms, each having one of the two spins that are allowed, i. e., give S'' the two values S and $(2S'-S)$. The part having the resultant spin S is given a coefficient $(2S'+1)^{-2}$, whereas the other part has a coefficient of unity minus this; i. e., change $W(l^{n-2}\,\alpha S_1L_1)$ into $[(2S'+1)^{-2}\;W(l^{n-2}(\alpha S'L_1)sSL_1)+[1-(2S'+1)^{-2}]W(l^{n-2}(\alpha S'L_1)s(2S'-S)L_1)]$.

This formulation could also be used when $l'\neq 0$ to take care of the spin. Another subdivision would then be made among the L-values, using only that part of (31) that depends on the orbital momentum.

As an example, the second approximation (18) will be evaluated for a $d^2(^4\mathrm{F})s\ ^5\mathrm{F}$ term. Step (a) is already carried out in (25), so that according to step (b)

$$\overline{W}(d^2\ (^4\mathrm{F})s\ ^5\mathrm{F};d^2s)$$
$$=1/5W(d^2(^3\mathrm{P})s\ ^4\mathrm{P})+4/5W(d^2(^3\mathrm{F})s\ ^4\mathrm{F}). \quad (32)$$

The procedure is repeated for the terms on the right, and the results obtained are substituted back in (32) to get the average energy for the ds selection:

$$\overline{W}(d^2(^4\mathrm{F})s\ ^5\mathrm{F};ds)=W(ds\ ^3\mathrm{D}). \quad (33)$$

This result could also be written by inspection. The average energies (32), (33), and (25) are inserted into (18), together with the trivial values for $\overline{W}(\gamma;d^2)$, $\overline{W}(\gamma;d)$, and $\overline{W}(\gamma;s)$; the sums over P introduce factors $\binom{n-1}{r}$ when P_r is the l^r configuration and $\binom{n-1}{r-1}$ when P_r is the $l^{r-1}s$ configuration:

$$W_2(d^2(^4\mathrm{F})s\ ^5\mathrm{F})=W(d^3\ ^4\mathrm{F})+3/5W(d^2s\ ^4\mathrm{P})$$
$$+12/5W(d^2s\ ^4\mathrm{F})-3/5W(d^2\ ^2\mathrm{P})$$
$$-12/5W(d^2\ ^2\mathrm{F})-3W(ds\ ^3\mathrm{D})+3W(d)+W(s). \quad (34)$$

The following formulas are obtained similarly:

$$W_2(d^2(^4\mathrm{P})s\ ^5\mathrm{P})=W(d^3\ ^4\mathrm{P})+8/5W(d^2s\ ^4\mathrm{P})$$
$$+7/5W(d^2s\ ^4\mathrm{F})-8/5W(d^2\ ^2\mathrm{P})-7/5W(d^2\ ^2\mathrm{F})$$
$$-3W(ds\ ^3\mathrm{D})+3W(d)+W(s), \quad (35)$$

$$W_2(d^2(^2\mathrm{H})s\ ^1\mathrm{H})=W(d^3\ ^2\mathrm{H})+3/2W(d^2s\ ^2\mathrm{F})^*$$
$$+3/2W(d^2s\ ^2\mathrm{G})^*-3/2W(d^2\ ^2\mathrm{F})-3/2W(d^2\ ^1\mathrm{G})$$
$$-3/2W(ds\ ^3\mathrm{D})-3/2W(ds\ ^1\mathrm{D})^*,$$
$$+3W(d)+W(s), \quad (36)$$

$$W_2(d^2(^2\mathrm{H})s\ ^3\mathrm{H})^*=W(d^3\ ^2\mathrm{H})+1/6W(d^2s\ ^2\mathrm{F})^*$$
$$+4/3W(d^2s\ ^4\mathrm{F})+3/2W(d^2s\ ^2\mathrm{G})^*-3/2W(d^2\ ^2\mathrm{F})$$
$$-3/2W(d^2\ ^1\mathrm{G})-1/2W(ds\ ^1\mathrm{D})^*-5/2W(ds\ ^3\mathrm{D})$$
$$+3W(d)+W(s), \quad (37)$$

Formulas (34) and (35) are valid even when configuration interaction is present.

3.3. The $l^{n-2}\,l'^2$ Configuration

The final configuration considered is $l^{n-2}l'^2$. Both the l^{n-2} and the l'^2 configuration are assumed to have SL-values that are exactly specified. For the selection P_{n-1} that contains only one of the l'-electrons, the coefficient of fractional parentage is simply a transformation coefficient given by (6) of III:

$$(l^{n-2}(\gamma SL)l'S_1L_1,l'S''L''][l^{n-2}(\gamma SL)l'^2(S'L')S''L'')$$
$$=(SL,l'^2(S'L')S''L''|SLl'(S_1L_1)l'S''L'')$$
$$=[(2S'+1)(2S_1+1)(2L'+1)(2L_1+1)]^{\frac{1}{2}}$$
$$W(S_1^{\frac{1}{2}}\,S''\tfrac{1}{2};S_1S')\,W(Ll'L''l';L_1L'). \quad (38)$$

This leads to a simple formulation for the $l^{n-2}s^2$ configuration: (d) The parentage of an s-electron in a term $l^{n-2}s^2\gamma SL$ is divided in the ratio of the multiplicities between the possible parent terms, generally two.

[19] L. C. Biedenharn, Oak Ridge National Laboratory Report ORNL-1098 (unpublished).

For the selection P_{n-1} that contains both l' electrons, the coefficient of fractional parentage becomes,

$$(l^{n-3}(\alpha S_1L_1)l'^2(S'L')S_2L_2|S''L'']l^{n-2}(\gamma SL)l'^2(S'L')S''L'')$$
$$=(l^{n-3}(\alpha S_1L_1)lSL]l^{n-2}\gamma SL)$$
$$(S_1L_1l(SL)S'L'(S''L'')|S_1L_1S'L'(S_2L_2)lS''L''). \quad (39)$$

The transformation coefficient is given by (5) of III and has a form similar to (31). In a term $l^{n-2}\,s^2\gamma SL$, however, the closed shell of two s-electrons can be disregarded for this selection, so that (39) reduces to the procedure already given for a configuration of equivalent electrons.

To evaluate the average energy (6) for a $d^2s^2\ ^3$F term the formulation (d) is used:

$$\overline{W}(d^2\,s^2\,{}^3\mathrm{F};d^2\,s)=2/3\,W(d^2\,s\,{}^4\mathrm{F})+1/3\,W(d^2\,s\,{}^2\mathrm{F}), \quad (40)$$

$$\overline{W}(d^2\,s^2\,{}^3\mathrm{F};ds^2)=W(ds^2\,{}^2\mathrm{D}). \quad (41)$$

Relation (41) is obtained by inspection; using (d) again with (41) leads to the average energy for a choice ds,

$$\overline{W}(d^2\,s^2\,{}^3\mathrm{F};ds)=3/4\,W(ds\,{}^3\mathrm{D})+1/4\,W(ds\,{}^1\mathrm{D}). \quad (42)$$

The result (42) could be obtained also from (40) by use of formulations (b) and (c),

$$\overline{W}(d^2\,s\,{}^4\mathrm{F};ds)=W(ds\,{}^3\mathrm{D}),$$

$$\overline{W}(d^2\,s\,{}^2\mathrm{F};ds)=1/4\,W(ds\,{}^3\mathrm{D})+3/4\,W(ds\,{}^1\mathrm{D}). \quad (43)$$

When these values are substituted for the observed energies W on the right of (40) the result (42) is obtained; this checks the consistency of the procedures and illustrates the use of (c). The values (40), (41), and (42), together with trivial values for $\overline{W}(\gamma;d^2)$, $\overline{W}(\gamma;s^2)$, $\overline{W}(\gamma;d)$, and $\overline{W}(\gamma;s)$ are then inserted into (18). The number of selections P_γ of type l^r is $\binom{n-2}{r}$; $l^{r-1}\,s$ can be selected in $2\binom{n-2}{r-1}$ ways and $l^{r-2}\,s^2$ in $\binom{n-2}{r-2}$ ways:

$$W_z(d^2\,s^2\,{}^3\mathrm{F})^*=4/3\,W(d^2\,s\,{}^4\mathrm{F})+2/3\,W(d^2\,s\,{}^2\mathrm{F})^*$$
$$+2\,W(ds^2\,{}^2\mathrm{D})^*-3\,W(ds\,{}^3\mathrm{D})$$
$$-W(ds\,{}^1\mathrm{D})^*-W(d^2\,{}^3\mathrm{F})$$
$$-W(s^2\,{}^1\mathrm{S})^*+2\,W(d)+2\,W(s). \quad (44)$$

The following formula is obtained in the same way:

$$W_z(d^2\,s^2\,{}^3\mathrm{P})^*=4/3\,W(d^2\,s\,{}^4\mathrm{P})+2/3\,W(d^2\,s\,{}^2\mathrm{P})^*$$
$$+2\,W(ds^2\,{}^2\mathrm{D})^*-3\,W(ds\,{}^3\mathrm{D})$$
$$-W(ds\,{}^1\mathrm{D})^*-W(d^2\,{}^1\mathrm{G})$$
$$-W(s^2\,{}^1\mathrm{S})^*+2\,W(d)+2\,W(s). \quad (45)$$

The formulas for the $d^2\,s^2$ configuration always contain terms that are likely to be perturbed by configuration interaction. The $s^2\ ^1$S term is usually unknown, and the applicability of the formulas is limited by this also.

4. Comparison With Experiment

In all the formulas derived above, the observed energies, W, are referred to the core with all four electrons removed. Because ionization potentials are often not accurate, these absolute energies may not be well known. To check the theory of Bacher and Goudsmit only differences between terms have been calculated. Ionization potentials cancel in the differences, and energies W can then be taken as the relative-energy levels with respect to the lowest term as zero; these are given in a Bureau Circular.[20] In particular, the following two differences would be unaffected by configuration interaction:

$$D_1\equiv W_2(d^3\,s\,{}^5\mathrm{P})-W_2(d^3\,s\,{}^5\mathrm{F})=W(d^3\,{}^4\mathrm{P})-W(d^3\,{}^4\mathrm{F})$$
$$+W(d^2\,s\,{}^4\mathrm{P})-W(d^2\,s\,{}^4\mathrm{F})-W(d^2\,{}^3\mathrm{P})+W(d^2\,{}^3\mathrm{F}) \quad (46)$$

$$D_2\equiv W_2(d^4\,{}^5\mathrm{D})-W_2(d^3\,s\,{}^5\mathrm{F})=6/5\,W(d^3\,{}^4\mathrm{P})$$
$$+9/5\,W(d^3\,{}^4\mathrm{F})-3/5\,W(d^2\,s\,{}^4\mathrm{P})-12/5\,W(d^2\,s\,{}^4\mathrm{F})$$
$$-6/5\,W(d^2\,{}^3\mathrm{P})-9/5\,W(d^2\,{}^3\mathrm{F})+3\,W(ds\,{}^3\mathrm{D})$$
$$+W(d)-W(s). \quad (47)$$

In table 1 the calculated and observed values of D_1 and D_2 are compared. In the spectra of titanium and zirconium sufficient data are available to compare the D_1-values. The calculated and observed values are in close agreement, the calculated value exceeding the observed value by 357 K in titanium and by 293 K in zirconium. Separations of terms in the same configuration are thus given closely by the theory. By assuming that D_1 will be given with the same error in more highly ionized spectra, it is possible to calculate positions for some terms that are not known experimentally, and use the values obtained to calculate D_2 in these spectra.[21] According to table 1 the difference between the two terms in different configurations is predicted very badly by (47) for titanium, the error in D_2 being 6068 K. However, the error is much less for the spectra of the higher ionization of vanadium (error 1841 K), and it is still less in chromium (error 635 K). The error is also less in the homologous sequences of zirconium (error 2296 K), where the nuclear charge is much greater (Z=40) than in titanium (Z=22), but the degree of ionization is the same. The

[20] C. E. Moore, Atomic energy levels, NBS Circular 467, vol. I (1949), vol. II (1952).

[21] The $d^2(^3\mathrm{P})s\ ^4$P term is unknown in V III and Cr IV; the calculated positions of these terms are given in table 1. If the errors in D_1 were to decrease rapidly as the errors in D_2 do, then these calculated positions would be about 357 K too high, and the calculated values of D_2 would be too small by about three-fifths of this error, or 220 K. This is a small error compared to the total errors found in the calculated values of D_2. However, it is noted later that the errors in D_1 probably will not decrease.

TABLE 1. *Term separations in spectra with d- and s-electrons*

$D_1 \equiv W(d^3\,s\,{}^5\mathrm{P}) - W(d^3\,s\,{}^5\mathrm{F})$

$D_2 \equiv W(d^4\,{}^5\mathrm{D}) - W(d^4\,s\,{}^5\mathrm{F})$

Term	Ti	V	Cr	Zr
	Observed values			
$d^4\,{}^5D$	28881	206	350	22138
$d^3s\,{}^5\mathrm{F}$	6721	2926	50020	5460
$d^3s\,{}^5\mathrm{P}$	14055	13647	63261	11103
D_1	7334	10721	13241	5643
D_2	22160	−2720	−49670	16678
$d^3\,{}^3\mathrm{P}$	9452	11668	14324	9824
$d^3\,{}^3\mathrm{F}$	1085	336	554	3273
$d^3s\,{}^4\mathrm{P}$	9968	(57014)	(119671)	7860
$d^3s\,{}^4\mathrm{F}$	225	44343	104637	758
$d^3\,{}^1\mathrm{P}$	10661	13344	15868	8581
$d^2\,{}^1\mathrm{F}$	242	419	662	864
$ds\,{}^1\mathrm{D}$	38277	96547	167715	19063
$d\,{}^3\mathrm{D}$	230	372	574	750
$s\,{}^2\mathrm{S}$	80379	148100	227775	38258
	Calculated differences			
D_1	7691	(11078)	(13598)	5936
D_2	28228	−879	−49335	18974
	Errors			
D_1(calc) − D_1(obs)	357	[a](357)	[a](357)	293
D_2(calc) − D_2(obs)	6068	1841	635	2296

[a] Values in parentheses are calculated to make the error in D_1 the same for all spectra with 3*d*- and 4*s*-electrons.

improvement from titanium to vanadium to chromium is especially remarkable in view of the fact that the errors in D_2 form a rapidly decreasing geometric sequence, whereas D_2 itself starts at a large positive value and decreases to a twice as large negative value.

Racah [22] has pointed out that the energies would be expected to vary more smoothly if the degree of ionization (rather than the atomic number) were the same in the different spectra. The results obtained by use of this empirical modification of the Bacher and Goudsmit theory are given in table 2. Except for the first spectra, the errors in calculated values of D_2 are on the order of 100 K; part of the good agreement must be fortuitous, however.

A partial explanation of the poor agreement obtained in the first spectra may be that the $d^3\,{}^4\mathrm{P}$ (of Sc I and Y I) is perturbed by interaction with the term $dsd'f\,{}^4\mathrm{P}$ (in the spectra with 4*d*- and 5*s*-electrons, this has the added effect of making the calculated position for the $d^2\,{}^3\mathrm{F}$ too high, as seen from the small separation of the $d^2\,{}^3\mathrm{P}$ and $d^2\,{}^3\mathrm{F}$ in Sr I). This effect can be estimated in the spectra containing 3*d*- and 4*s*-electrons by calculating the position of $d^3\,{}^4\mathrm{P}$ so that the error in D_1 will be 170 K as it is in the second spectra. When this calculated position (40048 K) is used, the error in D_2 is still very large (−5769 K). Racah has noted that the observed position of d^2 D in K I is about 5117 K lower than expected from the behavior of the difference between baricenters of the

[22] G. Racah, Bul. Research Council Israel **III,** 200 (1954). I am indebted to Professor Racah for making a preliminary copy of this manuscript available and for discussing the relationship of his results to those of this paper. See also M. A. Catalan, F. Rohrlich, and A. G. Shenstone, Proc. Roy. Soc. [A] **221,** 421 (1954).

TABLE 2. *Term separations in spectra with d- and s-electrons*

Term	Spectrum					
	I	II	III	IV	I	II
	Observed values					
$d^4\,{}^5\mathrm{D}$	(Ti) 28881	(V) 206	(Cr) 350	(Mn) 537	(Zr) 22138	(Nb) 772
$d^3\,s\,{}^5\mathrm{F}$	6721	2926	50020	112295	5460	3397
$d^3\,s\,{}^5\mathrm{P}$	14055	13647	63261	.....	11103	11034
D_1	7334	10721	13241	.....	5643	7637
D_2	222160	−2720	−49670	−111759	16678	−2625
$d^3\,{}^3\mathrm{P}$	(Sc) 36540	(Ti) 9452	(V) 11668	(Cr) 14324	(Y) 32210	(Zr) 9824
$d^3\,{}^3\mathrm{F}$	33846	1085	336	554	29035	3273
$d^3\,s\,{}^4\mathrm{P}$	17969	9968	(56841)	[a] 119671	15385	7860
$d^3\,s\,{}^4\mathrm{F}$	11610	225	44343	104637	11277	758
$d^3\,{}^1\mathrm{P}$	(Ca) 48551	(Sc) 12128	(Ti) 10661	(V) 13344	(Sr) 44052	(Y) 14048
$d^2\,{}^1\mathrm{F}$	43494	4909	242	419	(43989)	8429
$ds\,{}^1\mathrm{D}$	20357	105	38277	96547	18254	1193
$d\,{}^3\mathrm{D}$	(K) 21535	(Ca) 13987	(Sc) 118	(Ti) 230	(Rb) 19355	(Sr) 14724
$s\,{}^2\mathrm{S}$	0	0	25537	80379	0	0
	Calculated differences					
D_1	3996	10891	(13411)	.....	(6040)	8034
D_2	12181	−2613	−49738	−112020	−3012	−2582
	Errors					
D_1(calc) − D_1(obs)	−3338	170	[b] (170)	.....	[b] (397)	397
D_2(calc) − D_2(obs)	−9979	107	−68	−261	−19690	43

[a] From table 1 calculation.
[b] Values in parentheses calculated to make error in D_1 have the indicated value.

$d^{n-1}\,s$ and d^n configurations in Ca I, Sc I, Ti I, and V I, and this may explain the poor agreement obtained in first spectra.

5. Relations Between Radial Parameters

All formulas of the Bacher and Goudsmit theory can be used also to calculate the matrix elements of scalar operators; this has been noted in specific cases in the discussions of formulas (21) and (22), and it was also pointed out in BG. If the term values could be expressed in terms of such matrix elements, and if the zero-order functions were the same for all configurations, then the formulas derived from (16) to (19) (such as (46) and (47)) would be identities if the W's were replaced by matrix elements of these operators.

The matrix elements of the operators are linear combinations of a limited number of radial integrals. For the Slater theory, these combinations are well known (most of the formulas necessary for the present paper are contained in II). The observed separations of terms in the same configuration are predicted well by the Slater theory (i. e., with an accuracy equal to that obtainable with the Bacher and Goudsmit theory) if an empirical correction proportional to $L(L+1)$[23] is added to account for the polarization energy (see footnotes 8 and 9). Radial integrals defined by zero-order one-electron functions having the same n- and l-values must be considered independent of each other when in different configurations to get this good agreement, however; if the Bacher and Goudsmit theory were directly applicable, all such integrals would have to have the same value. The derivation of the theory, given in section 2, shows how much of the observed variation of these radial integrals will be accounted for by the Bacher and Goudsmit theory in any given approximation.

To illustrate, formulas for the W's that enter into (46) are given here according to the notation used in section 2:

$$W(d^3\,s\ ^5\mathrm{P}) = A(d^3\,s) - 3C_2(d^3\,s) - 16\alpha(d^3\,s)$$

$$W(d^3\,s\ ^5\mathrm{F}) = A(d^3\,s) - 15B(d^3\,s) - 3C_2(d^3\,s) - 6\alpha(d^3\,s)$$

$$W(d^3\ \ ^4\mathrm{P}) = A(d^3) - 16\alpha(d^3)$$

$$W(d^3\ \ ^4F) = A(d^3) - 15B(d^3) - 6\alpha(d^3)$$

$$W(d^2\,s\ ^4\mathrm{P}) = A(d^2\,s) + 7B(d^2\,s) - 2G_2(d^2\,s) - 10\alpha(d^2\,s)$$

$$W(d^2\,s\ ^4\mathrm{F}) = A(d^2\,s) - 8B(d^2\,s) - 2G_2(d^2\,s)$$

$$W(d^2\ \ ^2\mathrm{P}) = A(d^2) + 7B(d^2) - 10\alpha(d^2)$$

$$W(d^2\ \ ^2\mathrm{F}) = A(d^2) - 8B(d^2) \qquad (48)$$

[23] The $L(L+1)$ correction is represented as the matrix element of the scalar operator $2\alpha\sum_{i>j=1}^{n} l_i \cdot l_j$. The value of this for a term in the $l^n s^1$ configuration is $\alpha[L(L+1) - nl(l+1)]$. In the present work, this, rather, than simply $\alpha L(L+1)$, is added to each term; this change in the form of the correction is compensated by a change in the value of the constant parameter A. The modification has been made so that the relationships obtained later between the A-values in different configurations will have a simpler form.

If these values are substituted in (46), then the latter is an identity if the F's and α's in different configurations are assumed equal. Relation (46) will still be satisfied if the following two less restrictive conditions hold:

$$B(d^3\,s) = B(d^3) + B(d^2\,s) - B(d^2),$$

$$\alpha(d^3\,s) = \alpha(d^3) + \alpha(d^2\,s) - \alpha(d^2). \qquad (49)$$

It is sufficient for $B = 2/3\alpha$ to satisfy a relation of similar form for (46) to be satisfied, but if separations of all pairs of terms in the $d^3\,s$ configuration are to be correct, then both relations must hold and in addition the following two:

$$C(d^3\,s) = C(d^3) + C(d^2\,s) - C(d^2),$$

$$G_2(d^3\,s) = 2G_2(d^2\,s) - G_2(ds). \qquad (50)$$

Formulas of this type can be derived easily by inspection, and there is no need to consider fractional parentage. To obtain the second equation in (50), for instance, note that in (18) the combination of a d- and an s-electron (needed to define G_2) occurs three ways in $W_2(d^3\,s)$; it occurs two ways in each of three possible selections F^2 that contain the s-electron (in the $d^2\,s$ configuration); it occurs only once in each of the three possible selections P_2 that contain the s-electron (in the ds configuration). As far as the relation for the parameter G_2 is concerned, this direct interpretation of (18) leads immediately to (50) (multiplied by a factor of three). As F, C, and α are all defined by the combination of two d-electrons, a similar derivation leads to the same form of equation for all three of these parameters, and this equation is the one represented by (49) and the first equation of (50). In this way it can be shown that the Bacher and Goudsmit second approximation (relation (18) with $n=4$) will predict correctly the separations of terms in the same configuration if the following relations hold between the parameters:

$$B(d^4) = 2B(d^3) - B(d^2) \qquad (51)$$

$$B(d^3\,s) = B(d^3) + B(d^2\,s) - B(d^2) \qquad (52)$$

$$B(d^2\,s^2) = 2B(d^2\,s) - B(d^2). \qquad (53)$$

Three similar relations must be satisfied by the C's and three more by the α's. Also, it is necessary that

$$G_2(d^3\,s) = 2G_2(d^2\,s) - G_2(ds). \qquad (54)$$

The derivation from (18) fails to bring out the fact that the two-electron parameters must have a linear variation if the formulas are to be valid. In general, a two-electron parameter defined between electrons with orbital angular momentum l and l' in the configuration γ will be specified by $(\gamma)G(ll')$. According to the derivation with the second series of (9), only a first-power variation with the number of

electrons in γ can be accounted for by the Bacher and Goudsmit second approximation. In particular then, any one of the parameters B, C, or α must satisfy a relation of the form

$$(d^{r-k}\,s^k)G(dd)=A+rB+kC. \qquad (55)$$

It is easy to verify that (51) to (53) are satisfied when a formula of this kind is applicable.

It is possible to generalize (55) to include all similar spectra rather than just those of the ions of the same atom, in two-, three- and four-electron spectra. If q is the degree of ionization, this generalization will have the form $(d^{r-k}s^k)G(dd)=A+rB+kC+qD$. The difference D_1 defined by (46) (and equal to $15B-10\alpha$ according to the linear theory) should also be expressible by a formula of this type. Racah [22] has fitted 34 experimentally observed P-F differences in spectra with $3d$- and $4s$-electrons with a mean error of 340 K by use of the formula

$$D_1=2679+853r+1334k+3158q-111q^2. \qquad (56)$$

This formula is adjusted to spectra with eight different ionizations, and without a quadratic term the mean error would be increased to about 520 K. According to this formula, the differences D_1 calculated from (46) will be too great on the average by about 220 K. Modifying the theory so that spectra with the same ionization are utilized tends to eliminate this systematic error. This could also be accomplished by using the W_3 approximation.

The original series (9) will often have to be satisfied, for a given γ, by more than one value of α, and this leads to the conclusion that the ratios of similarly defined radial parameters in different spectra of a given element should be equal. In particular, the following ratio must be constant in configurations with d- and s-electrons:

$$\frac{B(d^r\,s^k)}{C(d^r\,s^k)}=\text{constant}. \qquad (57)$$

This is not really a necessary consequence of the theory developed in section 2, however, as the series (9) can be reinterpreted in terms of radial parameters that independently satisfy relations such as (55). When irrational roots are considered, it is shown in section 7 that (57) is a necessary condition for consistency of this interpretation, in terms of a linear theory, with a direct application of the method of BG.

In the same way that the differences such as (46) were replaced by the formulas (51) to (54), the differences similar to (47) can be replaced by relationships between the A values. The Bacher and Goudsmit second approximation will give the separations of terms in different configurations correctly if the following two relationships between the A's are satisfied:

$$A(d^4)-A(d^3\,s)=3A(d^3)-3A(d^2\,s)-3A(d^2)+3A(ds)+A(d)-A(s) \qquad (58)$$

$$A(d^3\,s)-A(d^2\,s^2)=A(d^3)+A(d^2\,s)-2A(ds^2)-2A(d^2)+A(ds)+A(s^2)+A(d)-A(s)+2G_2(d^2\,s)-2G_2(ds) \qquad (59)$$

By redefining the A-values suitably,[24] the dependence on G_2 may be omitted from (59); equations (58) and (59) may therefore be regarded as two relations between the differences $A(d^{r-k}\,s^k)-A(d^{r-k-1}\,s^{k+1})$. In the second approximation, the parameter A must satisfy a cubic relation, and these differences then satisfy quadratic equations having the general form

$$A(d^{r-k}\,s^k)-A(d^{r-k-1}\,s^{k+1})=D+Ek+Fr+Gkr+Hr^2. \qquad (60)$$

The k^2 dependence is omitted because it adds nothing extra when k has only the two values 0 and 1. It is easy to verify that (58) and (59) are satisfied when a formula like this is applicable. This formula can be generalized to apply to all similar spectra in a manner similar to that used for (55) if the "A" is suitably defined in the spectra with more than four electrons. If third (or fourth) power terms were important, a constant (or linear) error would result. The errors of D_2 in table 1 change too rapidly to be explained in this way, however.

In the one-electron, two-electron, and three-electron spectra considered in section 4, there are five experimentally determinable differences between A-values, and the five unknown constants in (60) can be evaluated from these observed values. Similarly, the three constants in (55) can be evaluated from observed separations of terms in the two-electron and three-electron spectra. The Bacher and Goudsmit second approximation is then equivalent to using the formulas obtained in this way to extrapolate values in the four-electron system.

This equivalence has been verified by using all available experimental data in titanium and zirconium to evaluate the radial parameters for all spectra with least squares.[25] The results confirmed

[24] The parameter G_2 appears in (59) because an s^2 subshell is neglected in defining the A-values; thus the formula for a $d^2\,s^2\,{}^1F$ term would have the same form as the last relation in (48). If the effects of the s-electrons in the s^2 subshell were explicitly expressed, as done when only a single s-electron is present, then $2G_2(d^2\,s^2)$ would be subtracted from the formulas for all terms in the $d^2\,s^2$ configuration. This has not been done since the effect would be included in $A(d^2\,s^2)$ if the parameters were evaluated by least squares and $G_2(d^2\,s^2)$ could not be evaluated. This applies also to $G_2(ds^2)$. The G's that cannot be evaluated satisfy the relation $G_2(d^2\,s^2)-G_2(ds^2)=G_2(d^2\,s)-G_2(ds^2)=G_2(d^2\,s)-G_2(d^2\,s)$.

[25] The $a\,{}^1F$ term of Ti II and the $a\,{}^1S$ and $c\,{}^1F$ terms of Zr I were excluded. The $a\,{}^1F$ term is probably not real. It was predicted 2000 K lower than observed when it was not included in the least-squares calculation. As long as it was included, it and several other terms were in error by 500 to 600 K, regardless of uncertainties in effects of configuration interaction. It is not well-established experimentally, as only three weak lines were observed; one strong line used to identify it is a blend (H. N. Russell, Astrophys. J. **66**, 283 (1927)). The $a\,{}^1S$ term was calculated 8000 K higher than observed; as ${}^1S$ terms are always hard to establish, it is fairly certain that this term is also unreal. The $c\,{}^1F$ term was calculated 5000 K higher than observed; although highly unlikely, it is not certain that consideration of of configuration interaction could not explain the result. However only one strong transition has been observed from each level of this triplet; five other confirming transitions are all weak (C. C. Kiess and H. K. Kiess, BS J. Research *6*, 621 (1931) RP296). The $a\,{}^3D$, $b\,{}^3G$, and $d\,{}^3P$ terms in the d^4 configuration of Ti I are observed much closer together than called for by the theory; this may be because of configuration interaction, or it may represent a failure of the W_3 approximation. In addition to the experimental values listed in Atomic Energy Levels, the recently located terms $d\,{}^3D$ of Zr II and the $a\,{}^1S$ and $b\,{}^1S$ terms of Zr III (C. C. Kiess, J. Opt. Soc. Am. **43**, 1024 (1953))were also available. I am indebted to Dr. Kiess for furnishing these data before publication.

the conclusion already obtained from the limited amount of data utilized in table 1. In all spectra of both elements, the terms could be fitted with absolute errors less than 400 K. The parameters obtained could be adjusted to fit the relations contained in (51) to (57) without significantly changing the original agreement. This verifies the conclusion that the separations of terms in the same configuration are given by the Bacher and Goudsmit method with an absolute error less than 400 K in titanium and zirconium. The discrepancy in calculating $A(d^4)-A(d^3\,s)$ from relation (58) was found to be 6560 K in titanium and 2086 K in zirconium. These values are approximately the same as the errors found for D_2 in table 1, which verifies the conclusion that calculated separations of terms in different configurations may be considerably in error.

If the ionization potentials are accuratley known the aboslute values of the A's can be calculated (rather than just the differences (58) and (59)),

$$A(d^4)=4A(d^3)-6A(d^2)+4A(d)+\delta \tag{61}$$

$$A(d^3\,s)=A(d^3)+3A(d^2\,s)-3A(d^2)$$
$$-3A(ds)+A(s)+3A(d)+\delta \tag{62}$$

$$A(d^2\,s^2)=2A(d^2\,s)+2A(ds^2)-A(d^2)-4A(ds)-A(s^2)$$
$$+2A(d)+2A(s)-2G_2(d^2s)+2G_2(ds)+\delta, \tag{63}$$

where

$$\delta=I_1-3I_2+3I_3-I_4.$$

The ionization potentials appear only in the combination δ; I_1 is the principal ionization potention of the four-electron spectrum (*Ti* I, for instance); I_2 is that for the three-electron spectrum (as *Ti* II), etc. If (61) to (63) are utilized, errors in the theory will not cancel as they may in the differences (58) and (59). In titanium the error of (61) in calculating $A(d^4)$ is found to be 24130 K, and the error of (62) in $A(d^3\,s)$ is 1757 K; on the other hand, the corresponding errors in zirconium are −2100 K and −4186 K. The inconsistent behavior of the errors in these two calculations probably arises from the well-known need for better ionization potentials, particularly in the one- and two-electron spectra.

6. Weak Configuration Interaction

The proof of the method of Bacher and Goudsmit is established with second-order perturbation theory, so that the theory is not directly applicable if configuration interaction is too strong to be evaluated with perturbation theory. However, it may not be directly applicable even if the spectrum has weak configuration interaction that can be evaluated with perturbation theory.

For example, consider interaction between terms of d^n and those of $d^{n-1}\,s$ and assume that second-order perturbation theory can be used. The perturbation of, say, a d^3 ^{2}G term by a $d^2\,s$ ^{2}G term is evaluated in terms of a characteristic interaction parameter associated with the d^3 and $d^2\,s$ configurations; this is designated $H_2(d^3-d^2\,s)$ in agreement with the notation in (80) of III. For arbitrary n, there is a similar parameter defined between d^n and $d^{n-1}\,s$. Particularly with the help of table XX of III the following two perturbations are evaluated:

$$\Delta(d^3\,^2\mathrm{G})=\frac{50[H_2(d^3-d^2\,s)]^2}{W(d^3\,^2\mathrm{G})-W(d^2\,s\,^2\mathrm{G})} \tag{64}$$

$$\Delta(d^2\,^1\mathrm{D})=\frac{140[H_2(d^2-ds)]^2}{W(d^2\,^1\mathrm{D})-W(ds\,^1\mathrm{D})}. \tag{65}$$

By considering terms marked with asterisks in (28), it follows that configuration interaction between d^n and $d^{n-1}\,s$ will be correctly accounted for by the Bacher and Goudsmit theory if the following relation exists between the two perturbations (64) and (65):

$$6/5\Delta(d^3\,^2\mathrm{G})-3/7\Delta(d^2\,^1\mathrm{D})=0. \tag{66}$$

According to the perturbation calculation used by Bacher and Goudsmit, the energy difference $W(d^3\,^2\mathrm{G})-W(d^2\,s\,^2\mathrm{G})$ would equal the difference $W(d^2\,^1\mathrm{D})-W(ds\,^1\mathrm{D})$ and the parameter $H_2(d^3-d^2\,s)$ would equal $H_2(d^2-ds)$. If these two conditions held, then (66) would clearly be satisfied. Relations similar to (66) can be found from other formulas (such as (29), (36), and (37)). By assuming that all energy differences $W(d^n\,\alpha SL)-W(d^{n-1}\,s\alpha' SL)$ are equal, and all parameters $H_2(d^n-d^{n-1}\,s)$ are identical, matrix elements of configuration interaction can be calculated with the Bacher and Goudsmit theory by solving a set of simultaneous equations, although such a procedure would not be the most practical. Similar considerations would apply to any pair of configurations; in particular, the interaction between $d^n\,s$ and $d^{n-1}\,s^2$ is interesting because the parameter defined between these two configurations would be equal to the parameter defined between d^n and $d^{n-1}\,s$ according to this direct application of the Bacher and Goudsmit theory.

Alternatively, (66) could be satisfied if the parameters $H_2(d^3-d^2\,s)$ and $H_2(d^2-ds)$ accidentally had the same ratio as the square roots of the energy denominators in (64) and (65). To get consistency for all formulas similar to (66) that could be derived, it is necessary that a representative average energy difference exist that approximates separations of terms with the same S- and L-values in the two configurations (in many cases no average value will adequately represent the data). An easily defined value for this average is the difference in the A-values of the two configurations. In table 3 calculated H_2-values and differences between A-values have been collected. In a given atom, the differences between A-values in this table are greater the greater the ionization; H_2 is also larger in the spectra of higher ionization, according to the results obtained for vanadium.

An extension of this argument indicates that the polarization energy arising from interactions with configurations in which only one electron is excited may be partially included in the second approxima-

TABLE 3. *Average term separations and interaction parameters*

	Titanium		Vanadium		Chromium		Zirconium	
	$A(\alpha)-A(\beta)$	H_2	$A(\alpha)-A(\beta)$	H_2	$A(\alpha)-A(\beta)$	H_2	$A(\alpha)-A(\beta)$	H_2
$A(s)-A(d)$	80150		147730		227200		37508	
$A(ds)-A(d^2)$	34470		92460		162720		16700	
$A(s^2)-A(ds)$							20304	
$A(d^3\,s)-A(d^3)$	[a] −896		[a] 42102		103100		[b] −1260	
H_2		[a] 172						[b] 387
$A(ds^2)-A(d^2\,s)$	[a] 16980						[b] 3600	
$A(d^3\,s)-A(d^4)$	−17140		[a] 6332		52424		−13230	
H_2				[a] 153				
$A(d^2\,s^2)-A(d^2\,s)$	[a] −13103						−11700	
$A(d^4\,s)-A(d^5)$			[c] −21335		[c] 11875			
H_2						[c] 150		
$A(d^3\,s^2)-A(d^4\,s)$			[c] −8759		30400			
H_2				[c] 106				

[a] A. Many, Phys. Rev. **72**, 511 (1946).
[b] C. W. Ufford, Phys. Rev. **44**, 732 (1933).
[c] A. Schweizer, Phys. Rev. **80**, 1080 (1950).

tion of BG. However, it is unlikely that the interaction parameters would behave exactly as required so that it might not be well accounted for.

It is clear from table 3 that in the titanium spectra of moderate ionization, the Bacher and Goudsmit method would not account for the configuration interaction. Even though the interaction is weak enough to be evaluated with second-order perturbation theory, the calculations discussed in section 5 show that errors of 300 to 700 K would be introduced into formulas (28), (29), (36), and (37). Whenever the average term separation is small or negative, which is the case in Ti I and Ti II, no set of values for the interaction parameters can produce agreement. When the configuration interaction is so strong that perturbation theory cannot be used, the errors are even larger. For zirconium, errors in excess of 1000 K result when the formulas are applied directly. The differences in A-values are all large and positive in chromium, so that the configuration interaction would probably be well accounted for in the second approximation; in this case, however, the interaction is weak and could be neglected in the linear theory.

7. Irrational Roots

This section deals with one of the simplest examples in which irrationality of the energy levels plays a part. As a preliminary, the two ^{2}D terms of the d^3 configuration are discussed.

The determination of the energy levels of the two ^{2}D terms of d^3 was first carried out by Ufford and Shortley.[26] They chose two mutually orthogonal ^{2}D eigenfunctions, which they characterized as a ^{2}D and b ^{2}D; in the more recent notation of III these same two eigenfunctions are designated as $^2_1$D and $^2_3$D, respectively.[27] In terms of this choice of eigenfunctions, the electrostatic energy matrix was evaluated and found to have the form

$$M \equiv \begin{matrix} {}^2_1\mathrm{D} \\ {}^2_3\mathrm{D} \end{matrix} \begin{pmatrix} A+7B+7C & 3\sqrt{21}B \\ 3\sqrt{21}B & A+3B+3C \end{pmatrix}. \quad (67)$$

The energy eigenvalues of the two ^{2}D states of d^3 are the characteristic values of this matrix; these values (as well as the observed energies for the ^{2}D terms) are specified by $W(^2\mathrm{D}^+)$ and $W(^2\mathrm{D}^-)$.

The matrix S that diagonalizes (67) will have the form

$$S = \begin{pmatrix} C_1 & C_2 \\ -C_2 & C_1 \end{pmatrix} (C_1^2 + C_2^2 = 1), \quad (68)$$

$$SMS^{-1} = \begin{pmatrix} W(^2D^+) & 0 \\ 0 & W(^2D^-) \end{pmatrix}. \quad (69)$$

The elements of S can be specified by the condition for the vanishing of the nondiagonal elements of $S\,M\,S^{-1}$,

$$[4B(d^3)+4C(d^3)]C_1C_2-(C_1^2-C_2^2)3\sqrt{21}B(d^3)=0. \quad (70)$$

Although $W(^2_1\mathrm{D})$ and $W(^2_3\mathrm{D})$ have no physical reality, they will be used subsequently to indicate the energies that would be associated with the diagonal elements of the matrix (67). The following formulas are obtained from (69):

$$W(^2_3\mathrm{D}) = C_1^2\,W(^2\mathrm{D}^-) + C_2^2\,W(^2\mathrm{D}^+), \quad (71)$$

$$W(^2_1\mathrm{D}) = C_1^2\,W(^2\mathrm{D}^+) + C_2^2\,W(^2\mathrm{D}^-). \quad (72)$$

If the polarization energy can be accounted for with the $L(L+1)$ correction, then all the preceding discussion will still apply even when polarization energy is considered if the constant A in (67) is suitably redefined.

By direct application of the methods in section 3, the energy for, say, a d^4 ^{2}G term, can be expressed in

[26] C. W. Ufford and G. H. Shortley, Phys. Rev. **42**, 167 (1932). See also, E. U. Condon and G. H. Shortley Theory of atomic spectra, p. 233 (Cambridge, 1951).
[27] In III the classification of terms in d^n is carried out by introducing the seniority number; this is given as the prefixed subscript in the notation above.

the form

$$W_2(d^4\,{}^3\mathrm{G})^* = 10/21\,W(d^3\,{}^2_3\mathrm{D})^* + 3/4\,W(d^3\,{}^2\mathrm{F})^* + 4/3\,W(d^3\,{}^4\mathrm{F}) + 99/140\,W(d^3\,{}^2\mathrm{G})^* + 11/15\,W(d^3\,{}^2\mathrm{H}) - 11/10\,W(d^2\,{}^3\mathrm{P}) - 9/14\,W(d^2\,{}^1\mathrm{D})^* - 29/10\,W(d^2\,{}^3\mathrm{F}) - 19/14\,W(d^2\,{}^1\mathrm{G}) + 4\,W(d). \quad (73)$$

If the linear theory is valid, $W(^2_3\mathrm{D})$ in (73) can be replaced by the value (71); the approximation obtained in this way will be specified by a prime. In the exact application of the Bacher and Goudsmit theory, (71) can still be used to replace $W(d^3\ {}^2_3\mathrm{D})$, but C_1 and C_2 are not necessarily specified by (70). Also, instead of evaluating $W(d^3\ {}^2_3\mathrm{D};d^2)$ which was done in deriving (73), it is necessary to evaluate $\overline{W}(d^3[\mathrm{C}_1\ {}^2\mathrm{D}^- + C_2\ {}^2\mathrm{D}^+];d^2)$. The following is the correct formula which is obtained in this way:

$$W_2(d^4\,{}^3\mathrm{G}) = W_2'(d^4\,{}^3\mathrm{G}) - \epsilon(d^4\,{}^3\mathrm{G}) \quad (74)$$

$$\epsilon(d^4\,{}^3\mathrm{G}) = C_1^2\,C_2^2[8/21\,W(d^2\,{}^1\mathrm{S}) - 2/7\,W(d^2\,{}^3\mathrm{P}) - 50/147\,W(d^2\,{}^1\mathrm{D}) + 2/7\,W(d^2\,{}^3\mathrm{F}) - 2/49\,W(d^2\,{}^1\mathrm{G})] - \frac{C_1C_2(C_1^2 - C_2^2)}{14\sqrt{21}}[21W(d^2\,{}^3\mathrm{P}) - 15W(d^2\,{}^1\mathrm{D}) - 21\,W(d^2\,{}^3\mathrm{F}) + 15\,W(d^2\,{}^1\mathrm{G})]. \quad (75)$$

Replacing the d^2 energies by their Slater formulas (including the $L(L+1)$ correction) leads to the following approximate form for (75):

$$\epsilon(d^4\,{}^3\mathrm{G}) = 10/21\,C_1C_2\{[4B(d^2) + 4C(d^2)]C_1C_2 - (C_1^2 - C_2^2)3\sqrt{21}B(d^2)\} \quad (76)$$

It follows that when C_1 and C_2 are determined from (70) then (74) will be equivalent to (73) if the ratio of B to C is the same in d^2 as it is in d^3. To establish the general correctness of the method of applying the Bacher and Goudsmit theory which was developed in section 5, it is necessary that in general the ratios of similarly defined radial parameters be the same in all spectra of a given atom.

It is well known that the ratio of B to C is very nearly constant. Values of this ratio, obtained mainly from the calculations discussed in section 5, are given in table 4. Because of the large errors that may be present in the theory (± 400 K), the values of r_2, obtained by fitting the observed data exactly, are not well defined; to a lesser extent the d^3 and $d^3\,s$ configurations also have too few terms to define r_2 precisely. The data as a whole (giving strong weight to the two well determined r_3-values) support the conclusion that r_n is a slowly decreasing function of n. The exception apparent in titanium is less noticeable if the irrational roots are omitted from the least-squares calculations for $3d^3$ and $3d^3\,4s$ parameters (the error in fitting the irrational terms is then excessive, however).

To estimate roughly the effect that could result from inequality of this ratio, (76) can be put in the following form with the help of (70), and by use of an approximate value of r equal to 0.29:

$$\epsilon(d^4\,{}^3\mathrm{G}) = 40/21\left(\frac{r_3 - r_2}{r_3}\right)C_1^2\,C_2^2\,C(d^2) = 1.16(r_3 - r_2)C(d^2). \quad (77)$$

In Ti III, $C(d^2) = 2505$ so that if $r_3 - r_2 = 0.05$ then $\epsilon = 145$ K. This is likely to overestimate the maximum error that can result, yet within the accuracy of the theory it probably could be neglected. However, the same treatment for the $d^4\ {}^1\mathrm{F}$ term shows that ϵ will have exactly 3 times the value (75), and for the $d^4\ {}^3\mathrm{D}$ term the error will be 2.4 times this value, so it is not certain that this effect will always be negligible. The ratio G_2/C need not be constant (it varies considerably, from 0.4 to 0.8 usually).

TABLE 4. *B/C ratios*

r_n is the ratio of $F^2(d^n)$ to $C(d^n)$, $F^2(d^n\,s)$ to $C(d^n\,s)$, or $F^2(d^n\,s^2)$ to $C(d^n\,s^2)$, according to whichever definition has meaning for the spectrum specified.

	r_2	r_3	r_5
Ti I	0.289	[c] 0.343 (0.319)	
Ti II	.290	.317 (0.290)	
Ti III	.291		
Fe III [a]			0.271
Zr I	.304	.279	
Zr II	.289	.287	
Zr III	.297		
Mo I [b]			.257

[a] See footnote 8, page 33. [b] See footnote 3, page 35.
[c] Values in parentheses are calculated with irrational roots omitted.

Though the method of BG introduces new nonlinear effects if the parameter ratios are not equal, these effects would probably represent errors in the method. Because of this, and because the ratios are so nearly equal, it is not expected that a correction with this variation will produce improved agreement when added to the linear theory. However, irrational terms often cannot be fitted by the linear theory with the accuracy that is obtainable for rational terms [28] and some additional correction of this form may be needed. This correction would not change the agreement obtainable for the rational terms of d^4, but it would introduce corrections into the irrational terms. These considerations may be less academic for spectra with p- and d-electrons where there are more parameter ratios that may differ, and where most of the terms are irrational.[29]

I am indebted to C. C. Kiess for suggesting the problem on which this work is based, and I thank also G. Racah and C. W. Ufford for their comments on the original manuscript of this paper.

[28] R. E. Trees, Phys. Rev. 85, 382 (1952).
[29] Meshkov has introduced a method which combines the Slater theory with a Bacher and Goudsmit first approximation, and has obtained improved agreement for the $3d^2\,4p$ configuration of Ti II (footnote 18). A simple extension of the linear theory to include correlations between p- and d-electrons may explain this improvement, but the possibility that new types of crorrections are needed to explain it, cannot yet be excluded. His theory also leads to better agreement than is obtainable with the Slater theory alone, in the d^5 configuration of V III and the d^4 configuration of V II (Phys. Rev. **93**, 270 (1954)). In the d^4 configuration his final mean deviation of ± 663 K is still rather large; this may be because there are a large number of irrational terms present in this configuration or because configuration interaction was neglected. See also S. Meshkov and C. W. Ufford, Phys. Rev. **94**, 75 (1954).

WASHINGTON, January 8, 1954.

Journal of Research of the National Bureau of Standards Vol. 53, No. 1, July 1954 Research Paper 2516

Self-Ignition Temperatures of Combustible Liquids

Nicholas P. Setchkin*

The methods previously used for determination of the ignition temperatures of liquids are briefly reviewed, and the large discrepancies in reported values noted. Various factors which affect the determined values of ignition temperature are discussed. A practical ignition apparatus consisting in part of an insulated spherical flask, designed to provide conditions favorable to low ignition temperature values, is described, and data obtained with this apparatus on a considerable number of combustible liquids are presented. The usefulness of time-temperature curves of a thermocouple junction placed in mixtures of combustible liquid and air, as a means of studying the preignition reactions in such mixtures is illustrated.

1. Introduction

The fire hazards associated with the use, storage, and shipment of combustible liquids are so familiar as to need no discussion, and the tremendous and varied consumption of such liquids carries the problem of protection against these hazards into every element of modern economy. For the development of effective protective measures, as well as for efficient use of these liquids, extensive and accurate knowledge of their ignition characteristics is highly important.

Although standard definitions and methods of determination have been established for many of the physical and chemical properties of materials, such as density, viscosity, solubility, etc., there has been no general agreement on the definition or determination of ignition temperature. Consequently, determinations of this quantity by different investigators have varied widely both in numerical value and significance, with much resultant confusion and difficulty in the interpretation and practical application of the information.

Preparatory to the experimental work reported in this paper a study was made of the various methods previously employed for the determination of ignition temperature. It appeared that, although the ignition characteristics of a material were doubtless a function of some actual property of the material, the measurement of that property by any means readily available would be greatly affected by the ambient conditions. Hence, any practical definition of ignition temperature which might be adopted must continue to be based on a careful definition and standardization of the test apparatus and procedure. It was further concluded that a criterion that indicated the lowest temperature producing self-ignition of the material under conditions as favorable as might normally occur, would be the most useful in the practical analysis and elimination of hazards, and would also provide a suitable basis for data of research interest.

Accordingly, the apparatus and test procedure described in this paper were designed to determine values in the lower temperature range in which ignition may be possible. The method developed appears well suited to the purpose, and in tests of a large number and variety of materials it has given results of satisfactory reproducibility. The present paper covers the work carried out over a period of about 15 years on a considerable number of commonly used combustible liquids.

*Present address, Library of Congress, Washington 25, D. C.

2. General Considerations

2.1. Previous Determinations of Ignition Temperature

Most of the methods that have been used in the determination of ignition temperature may be grouped into two general types, the "rising-temperature" method, and the "constant-temperature" method. In the former, a combustible mixture is introduced into the ignition apparatus, and its temperature is then continuously increased until positive evidence of ignition is observed. The self-ignition temperature is usually taken as the point at which the time-temperature curve for the material shows a definite increase in slope or as the point of intersection between the time-temperature curve for the material and that for the heating medium [1].[1] In the constant-temperature method of determination, the ignition apparatus is preheated to a selected initial constant temperature before the specimen is introduced, and no adjustment of heat input to the apparatus is made after introduction of the specimen. The test is repeated with fresh specimens at different initial temperatures until the lowest temperature at which ignition is produced has been established. It has been determined as the temperature of the heating bath surrounding the reaction chamber, as the temperature of the combustion chamber wall, or as the temperature of the air within the chamber.

Within these two general approaches to the problem, numerous and diverse methods of determination have been developed (C. R. Brown [2] gives references to 16 different methods of the rising temperature type alone). Following are brief outlines of a number of procedures that have been used, and the data in tables 1 and 2 illustrate the wide variation in values obtained by different investigators.

Oil-drop method. Early determinations of ignition temperature with the so-called "oil-drop method" were made by Holm [3] in 1913 with a heated

[1] Figures in brackets indicate the literature references at the end of this paper.

TABLE 1. *Ignition temperature (in degrees centigrade) of various combustible liquids determined with oil-drop meth[od]* [7]

Material	Investigators							
	Holm	Moore	Tausz and Shulle	Masson and Hamilton	Thompson	Edgerton and Gates	Sortman and Beatty	Jentzsch and Von Zerbe
n-Heptane	.....	451	.....	.....	.....	430	259	560
n-Hexane	.....	.....	.....	520	248	.....	.....	560
n-Pentane	.....	579	487	579	308	515	418	580
Benzene	520	566; 656	740	656	580	700	625	720
Toluene	.....	516; 633	810	633	553	780	630	730
Carbon disulfide	.....	.....	.....	343	125	120	.....	.....
Ethyl ether	410	347	343	487	193	440	.....	500
Ethyl alcohol	510	518	558	568	420	515	.....	575

TABLE 2. *Ignition temperature (in degrees centigrade) of liquids determined with different methods* [15]

Material	Temperature initial oxidation			Cold flame	Minimum ignition temperature				
	T. I. C. (A)[1]	C. I. T. (B)	T. T. R. (C)	T. C. F. (D)	(D)	(B)	(E)	(F)	(G)
	Tube method					Evacuated vessel		Bomb	Adiabatic compression
n-Pentane	295	255	.....	225; 243	254; 263	255; 259	510; 548	225; 237	336
n-Hexane	265	230	330	220; 230	253	232	285; 570	222; 232	330; 306
n-Heptane	.....	209	300	220	236	219	.....	225	283
n-Octane	.....	197	.....	210	248	203	.....	320	278
n-Nonane	205	193	.....	.....	.....	.....	.....	.....	.....
Isooctane	.....	.....	500	.....	.....	.....	.....	.....	.....
Cyclohexane	.....	.....	345	235; 260	262	.....	.....	324	.....
Benzene	670	.....	650	570	695	.....	.....	.....	.....
Toluene	550	.....	.....	600	585	.....	.....	.....	.....

[1] Investigators: (A) Callendar; (B) Lewis; (C) Estradere; (D) Prettre; (E) Townend and Cohen; (F) Dumanois and others; (G) Tizard and Pye.

porcelain surface. Moore [4] used a platinum crucible submerged in molten metal or embedded in a steel block. Sortman and Beatty [5] made a small cylindrical cavity of 43-ml capacity in a stainless-steel block and provided for the circulation of preheated air. Jentzsch and Von Zerbe [6] also used a steel block with four cylinders (7.1 ml) and circulation of oxygen or air. A modified type of the Moore apparatus, heated electrically, has been widely used by many investigators [7]. The initial temperature of the bath, or wall of the ignition vessel, leading to ignition is usually considered as the self-ignition temperature. The values given in table 1 are reproduced from reference [7].

Dynamic tube method. In this method, a Pyrex tube is heated in a conventional electric furnace to the desired temperature indicated by a thermocouple in contact with the outside surface of the tube. A combustible substance, being preheated separately or together with air or oxygen, is allowed to pass through the tube. The tests are repeated at different temperatures of the tube until evidence of ignition is observed. Apparatus of this type was used by Dixon and Coward in 1909 and 1934 [8, 9], by Mason and Wheeler [10], and by many others. Dixon and Coward limited their test to 15 seconds. Callendar [11] and Moureu [12] made a study of slow combustion and determined the "Temperature of Initial Combustion" (T. I. C.) in an improved apparatus. This temperature was defined as the tube temperature necessary to provide the first appearance of products of combustion (steam, carbon dioxide, aldehyde, etc.) and was determined by chemical analysis of samples taken periodically during various phases of the reaction.

This temperature has some relation to the "Temperature of Thermal Reaction" (T. T. R.) introduced by Estradére [13], and the "Critical Inflection Temperature" (C. I. T.) introduced by Lewis [14]. All these temperatures are related to the "Temperature of Initial Oxidation" [15] or, in other words, to the temperature of incipient self-heating. Prettre defined the ignition temperature by means of two criteria, the appearance of "cold flame" (T. C. F.) and the appearance of normal flame at "Minimum Ignition Temperature" (M. I. T.). A tabulation of ignition temperatures measured by this method is included in table 2, which is reproduced from reference [15].

Evacuated-vessel method. In this method a combustible mixture is suddenly admitted into an evacuated vessel preheated to the desired temperature. This method was originated by Mallard and Le Chatelier in 1880 and was used subsequently by Mason and Wheeler [10] and Townend [16]. Ignition was indicated by rapid rise in pressure. Lewis and also Pidgeon and Egerton [17] modified this method by admission of the cold combustible mixture into an evacuated vessel heated at a steady rate (rising-temperature method).

Bomb method. The bomb method was used by Neumann [18] and other investigators for determination of the ignition temperatures of combustible mixtures at high pressures.

Adiabatic compression method. Heating of a combustible mixture to the ignition point by adiabatic compression was used by Tizard and Pye [19] and Pignot [20]. It is hardly likely that ignition temperatures measured by this method, which involves the use of rising temperature and pressure, are directly comparable to those measured at constant pressure.

ASTM standard method. Committee D–2 on Petroleum Products and Lubricants of ASTM in 1930 adopted a standard method and apparatus (D286–30) [21] for the determination of the "Autogeneous Ignition Temperature." The standard apparatus consists of a conical Pyrex flask of 160-ml capacity, submerged in molten solder heated by a gas burner. A few drops of the liquid to be tested are allowed to fall into the flask, previously heated to different initial temperatures. The ignition temperature is defined as the lowest temperature of the solder bath, indicated by a thermocouple placed in a silica protection tube submerged in the bath near the flask, necessary to cause ignition of the specimen.

2.2. Selection of Method and Definition of Self-Ignition Temperature

With the rising-temperature procedure of determination, the ignition temperatures vary with the rate of temperature rise and with the criterion of ignition. Elaborate control equipment is necessary to obtain reproducible results either on the basis of a fixed rate of heating or on that of maintaining a fixed temperature difference between any part of the specimen and its surroundings. Furthermore, the comparatively slow heating of the specimen in this method is not generally well suited to the study of liquids, many of which apparently produce vapors that form relatively stable compounds with oxygen at low temperatures. If the system has time in a low-temperature range to permit the formation of such compounds in appreciable amount, the observed ignition temperature may be well above that which might have been obtained with the constant-temperature method. In this latter method, on the other hand, precise control of the initial temperature may be accomplished with relatively simple equipment, and the rapid heating of the specimen limits the time in which low-temperature reactions may take place. The constant-temperature method of determination was selected for the present work, and the liquid charge was sprayed into the heated chamber as a fine dispersion, so that it rapidly became vaporized and mixed throughout the air in the chamber.

The characteristic thermal effects when a combustible liquid is thus introduced into the chamber at different initial temperatures are illustrated by the time-temperature curves of figure 1. After injection of the dispersed charge, the temperature within the chamber first falls below the initial temperature because heat is absorbed in vaporizing and heating the sample. In a short time, heat supplied mainly from the walls of the chamber reestablishes the initial

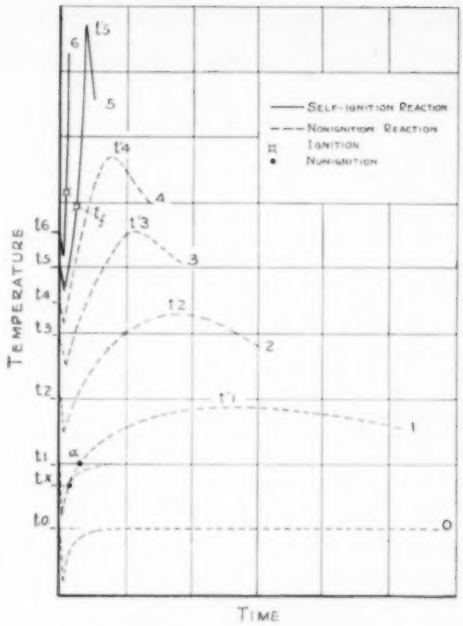

FIGURE 1. *Idealized time-temperature curves for self-ignition and nonignition reactions of combustible liquids.*

temperature. At relatively low initial temperatures, there may be no further thermal effects, and the temperature of the sample-air mixture may remain constant at the initial value, as at t_0. At higher initial temperatures, exothermic reactions within the sample-air mixture may be induced and the temperature of the reaction mixture raised above the initial value. The extent of this temperature rise depends upon the difference between the rate of heat generation within the mixture and the rate of heat loss to the chamber walls. At initial temperatures that produce relatively mild reaction within the mixture, the heat generated is eventually lost through the chamber walls without visible effect on the mixture, and the temperature returns to the initial value after a period of time dependent on the intensity of the exothermic reaction. This situation is illustrated by initial temperatures t_1, t_2, t_3, and t_4 in figure 1. However, at some temperature, characteristic of the material under study and of the particular test chamber employed, the reaction within the mixture will become sufficiently intense to raise the temperature to the ignition point, as evidenced by flame or explosion. The initial temperatures t_5 and t_6 represent such ignition reactions and further illustrate the reduction in ignition lag, which usually results as the initial temperature is increased.

For the present study, the following definition of self-ignition temperature was adopted:

> The self-ignition temperature (SIT) of a liquid is the minimum temperature from which a combustible mixture with air will pass into a condition of observable combustion in the experimental apparatus employed.

2.3. Factors Affecting the Observed Values of SIT

a. Thermal Characteristics of the Apparatus

Inasmuch as ignition depends upon the temperature reached by the reacting mixture, the governing factor in its development is the amount of heat retained within the mixture and available for increasing the temperature. Hence, ignition will result only when the reaction is intense enough to generate heat more rapidly than it is lost from the reaction mixture to its surroundings, and the initial temperature of the chamber must be high enough to induce such a reaction. Therefore, the higher the rate of heat loss, the higher will be the initial temperature required to accelerate the reaction to ignition, that is, the higher will be the determined values of the SIT.

Thus, the design and construction of the reaction chamber affect the SIT values that will be obtained. In order for the determinations to approach the lowest temperatures from which there may be danger of ignition, the chamber walls should be constructed with as low heat capacity and heat conductivity as may be practicable. The size and shape of the chamber, as well as the structural materials, must also be considered.

b. Pressure and Uniformity of Temperature

The relation between the pressure within the ignition chamber and the observed value of the SIT has not been determined. However, for the development of a practical test method, it is reasonable to assume that atmospheric-pressure variations will have little effect on the determined values of the SIT.

It is probable that the ignition reaction between the combustible substance and the oxidizing agent initiates with the most highly energized molecules of the mixture, and supplies the heat necessary to raise the energy level of adjacent molecules to the ignition point, thus propagating itself throughout the mixture [22]. If all of the molecules present are very close to the required energy level at the same instant, the spread of ignition through the mass will be extremely rapid. Hence, the maintenance of uniform temperature throughout the reaction chamber will favor rapid propagation of the ignition reaction.

c. Reaction Mixture Ratio

The ratio of the combustible substance to air in the reaction mixture has an appreciable effect upon the SIT. Mixtures that are excessively rich or excessively lean usually ignite at higher temperatures than those close to some intermediate composition characteristic of the material. Carbon and soot, which may have been deposited from previous determinations with over-rich mixtures, may also influence the SIT value obtained.

d. Method of Temperature Measurement

Temperature measurements are usually made by means of one or more thermocouples either embedded in the heating bath or medium outside the chamber walls or installed directly inside the reaction chamber. Reproducible results may be obtained with any of these methods, but because heat loss from the chamber cannot be conveniently eliminated, lower values of SIT are usually observed with the last arrangement. Furthermore, a thermocouple placed inside the chamber may also be used to indicate temperature changes during the reaction.

e. Criteria of Ignition

The intensity of the visual evidence of ignition varies decidedly with the initial temperature from which the reaction proceeds. At high initial temperatures, self-ignition usually occurs in more or less violent form, such as a bright flash of flame and audible expulsion of gases (explosion). At somewhat lower initial temperatures the flaming becomes relatively mild, whereas at the lowest temperature from which ignition is detected, the flame may be very dull violet or blue, often visible only under darkroom conditions. The latter may be confused with cool flame reaction, which is not generally recognized as evidence of ignition even when, occasionally, it is accompanied by a rapid rise in the temperature of the reaction mixture.

The time lag before the development of ignition is also affected by the initial temperature of the reaction. It is an inverse function of the initial temperature and may be only a fraction of a second at high initial temperatures and may amount to a number of minutes at the lowest temperature from which ignition occurs. For example, methyl cyclohexane showed an ignition lag of 30 seconds at 275° C, and, using the same test equipment, the lag was 20 min 10 sec at 248° C. By limiting the tests to 10 or 15 seconds, as some investigators have done, the self-ignition temperature would have been determined as well above 275° C.

In addition to the visual evidence of ignition, the time-temperature curves for many liquids provide supporting indication of its occurrence. The curves at t_3 and t_4 in figure 1 illustrate typical differences in the curves for ignition and nonignition reactions proceeding from only slightly differing initial temperatures. Although the rate of temperature rise was at first about the same in the two cases, it soon became much more rapid and pronounced in the ignition reaction and was followed by a sharper drop from the peak temperature. This decided difference in the time-temperature curves for ignition and nonignition reactions is often helpful in the final determination of the SIT, particularly when the detection of flame becomes difficult and somewhat uncertain.

f. Extraneous Stimuli of Ignition

The ignition reaction may be induced by a number of means extraneous to the reaction mixture itself, and devices used by various investigators have included pilot flames, sparks, detonators, overheated surfaces, and catalytic agents. The introduction of such stimuli is often accompanied by complex effects

other characteristics of the equipment, and in general it tends to complicate the problem of accurate interpretation and evaluation of the results. Until more extensive research has been carried out on problems related to their use, it would appear advisable to carefully avoid their introduction, either intended or incidental.

3. Test Apparatus and Procedure

3.1. Development of Apparatus

Preliminary experiments were conducted with the ASTM standard ignition apparatus [21] with solder bath and gas burner. Because of difficulties in controlling the temperatures and poor reproducibility in the results, this apparatus was modified to include electric heating elements, a 0.2-liter spherical Pyrex flask, a stirring arrangement in the bath, and direct measurement of temperature in the flask. In order to reduce the heat loss from the reacting mixture to the surroundings and improve uniformity of temperature control in the flask, the solder bath was later replaced with two sets of heating elements made of nichrome wire, in asbestos sleeving, wound around the upper and lower halves of the spherical flask and protected with a refractory cement. The final design of the ignition apparatus consisted of a 1-liter spherical Pyrex flask, as shown in figure 2, placed concentrically inside a refractory casing so that a ½-in. air space was provided between the flask and the casing for further reduction of heat loss. The heating wires were wound around the upper and lower halves of the casing and the neck, with independent temperature controls. Temperatures of the three heaters were indicated by three thermocouples made of chromel-alumel (26 B&S gage) wire placed behind each group of heating coils. Two additional thermocouples were placed in contact with the upper and lower surfaces of the flask. The sixth thermocouple, insulated by glass sleeving

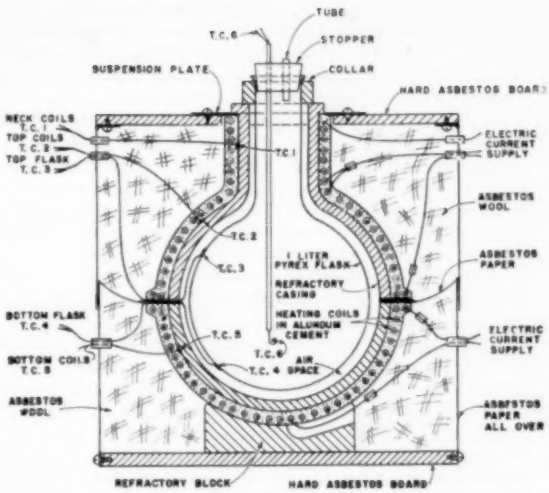

FIGURE 2. *One liter spherical pyrex flask ignition apparatus for liquids with air space and refractory casing.*

and also of 26 (B&S gage) wire, was placed in the lower part of the flask for indicating the temperature inside the flask. The flask neck was closed with a cement-asbestos stopper having two passages, one for the thermocouple wires and the other for injection of the charge.

The effect of chamber size on the observed self-ignition temperature was studied by means of additional test units of the following capacities: 0.008, 0.035, 0.2, 12, and 15 liters. These units were constructed in substantially the same manner as shown in figure 2, with the exception of the 15-liter apparatus, the chamber walls of which were made of opaque silica about ⅜ in. thick, with no air space between the walls and the heating coils. From the results shown in table 3 and figure 5 it is evident that, over

TABLE 3. *Effect of flask size on ignition characteristics*

Material	Flask size											
	0.008 liter		0.035 liter		0.2 liter		1 liter		12 liters		15 liters	
	SIT	Lag	SIT	Lag	SIT	Lag	SIT	Lag	SIT	Lag	SIT	Lag
	°C	min:sec	°C	min:sec	°C	min:sec	°C	min:sec	°C	min:sec	°C	min:sec
Carbon disulfide	151	------	127	------	120	0:08	110	0:14	90	0:20	96	0:20
Ethyl ether	212	------	197	------	180	0:20	170	0:25	160	1:40	162	1:08
Gasoline (65 octane)	------	------	283	------	248	2:30	248	4:30	224	10:50	240	8:15
Gasoline (73 octane)	------	------	------	------	----	------	258	5:00	----	------	252	3:35
Varsol	------	------	------	------	237	1:52	235	3:00	215	6:48	----	------
Kerosine	283	------	248	1:00	233	1:30	227	2:55	210	7:25	215	5:55
Cleaner's solvent	------	------	------	------	----	------	243	2:44	224	9:42	235	4:25
Furnace oil No. 2	------	------	------	------	242	0:55	233	2:40	226	2:55	230	2:30
Motor oil	------	------	------	------	357	0:05	351	0:04	313	0:35	320	0:48
Benzene	668	------	619	------	579	1:05	559	0:48	----	------	----	------
Toluene	649	------	584	------	538	0:45	519	0:55	482	3:40	----	------
Acetone	676	------	570	------	519	0:26	491	0:40	467	1:25	----	------
Acetic acid	611	------	544	------	505	0:08	488	0:13	464	1:30	----	------
Ethyl alcohol	495	0:05	445	------	402	0:28	391	0:40	363	2:40	----	------
Methyl alcohol	498	------	473	0:23	441	1:10	428	1:30	386	3:00	----	------
Glycerine	------	------	------	------	----	------	389	0:31	----	------	371	0:36
Ethylene glycol	505	------	447	0:20	----	------	398	0:23	----	------	----	------
n-Pentane	295	------	273	0:25	----	------	258	1:00	----	------	----	------
n-Heptane	255	------	248	0:20	----	------	223	0:45	----	------	----	------

the size range studied, the observed self-ignition temperature becomes lower with increasing chamber size in units of similar construction. This effect should not be unexpected as the rate of heat loss per unit volume from the reacting mixture will be smaller with the larger chambers because of the smaller ratio of surface to volume. The higher values of SIT obtained with the 15-liter unit than with the 12-liter unit indicate a greater heat loss to the thicker opaque silica walls. Although slightly lower SIT values were obtained with the 12-liter Pyrex unit, it was unwieldy and fragile. Consequently, the standard, easily replaceable 1-liter flask was used as the more practical test apparatus, in making most of the determinations.

An investigation was also made of the comparative SIT values obtained with different types of casing around the 1-liter flask. In addition to the refractory casing separated from the flask by a ½-in. air space shown in figure 2, two other units were constructed. In one of these a ⅛-in.-thick copper casing was fitted as closely as possible around the flask, and in the other, a refractory casing with mirrored inner surface was separated from the flask by a ¼-in. air space. The results obtained with several different liquids tested in these three units are shown in table 4. In each case the highest value of SIT was obtained when using the metal-encased flask, whereas the lowest value was obtained with the mirrored refractory casing. However, it appeared that the mirror coating on the refractory casing would not hold up well at high temperatures and would be subject to variable deterioration with repeated use. As it is important that the thermal characteristics of the apparatus remain as constant as possible, the simple refractory casing was selected for the major portion of the work.

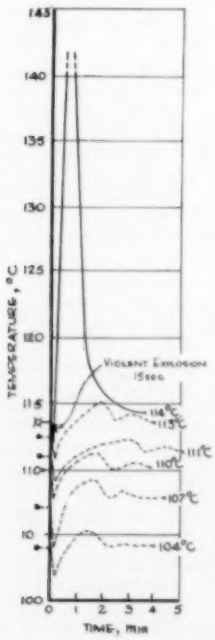

FIGURE 3. *Time-temperature curves for carbon disulfide.*
1-liter flask, charge equals 0.5 ml

TABLE 4. *Effect of chamber wall construction on self-ignition temperature with the 1-liter flask*

Liquids	Type of casing		
	Metal	Refractory	Mirror surface
	°C	°C	°C
Acetic acid	501	488	474
Acetone	505	491	...
Ethyl alcohol	405	391	385
Gasoline (motor)	249	243	238
Isooctane	431	420	409
Toluene	529	519	...
Varsol	237	235	234
Ethyl ether	172	170	...

The possibility that the thermocouple wires might exert some catalytic effect on the reaction was seriously considered. A test apparatus was carefully prepared so that heat losses by conduction were practically eliminated. Comparative tests were conducted, with the thermocouple remaining in its usual position in the chamber throughout the reaction, and with the thermocouple removed from the chamber just before injection of the liquid charge. The self-ignition temperature was a little higher with the thermocouple present than without it, and increased slightly as the length of the wire in the chamber was increased, but no evidence of catalytic action was detected.

Callendar [23] conducted experiments on the possible catalytic influence of a variety of metals placed in a test tube and, of those studied, only platinum black showed catalytic action. Thompson [24], and Matson and Dufour [25], used different metals for construction of the entire wall of the reaction chamber. Definite variation of the self-ignition temperature with the metal used was found, but the effects were evidently related to the heat losses to and through the container walls.

3.2. Test Procedure

The procedure followed in establishing the self-ignition temperature of a combustible material consisted of a series of experiments at different temperatures and with different proportions of combustible material and air. In conducting an experiment, the power supplied to the individual heating elements of the ignition apparatus was adjusted until the temperature inside the flask was uniform to 2 deg C and constant at some value estimated to be near the SIT. A charge of 0.2 ml of the combustible liquid per liter of flask volume was injected into the flask by means of a hypodermic syringe fitted with a fine needle. This provided the dispersion necessary for rapid evaporation and nearly simultaneous initiation of the reaction throughout the flask. The

tion was permitted to proceed without any variations of the power supplied to the apparatus. In order to follow the nature of the reaction, observations of the electromotive force of the thermocouple inside the flask, at intervals of 15 to 20 seconds, were plotted against time as the reaction proceeded. The temperatures of the heating coils and flask surface were checked at intervals of 3 to 5 minutes.

The experiment was repeated at different initial temperatures until the lowest temperature from which ignition occurred was determined for the charge of 0.2 ml of combustible material per liter of air. Additional experiments were then made with different charges to establish the lowest temperature from which the optimum ratio of combustible material to air would proceed to ignition.

Generally, ignition was clearly indicated by audible or visible evidences (explosion, puff, flame), and it was also shown by characteristic changes in the time-temperature curves, which served as dependable criteria when the visible evidence became uncertain or obscured. As an aid to visual detection in the final determinations, the interior of the reaction flask was viewed under dark room conditions by means of a mirror placed above the flask opening. Under these conditions, even very weak flames were distinctly visible, and flames obscured by the production of dense smoke and fumes could be detected from the illumination of the fumes.

Materials such as gums, waxes, and tars, which were too viscous at room temperature to be handled by syringe injection, were tested by placing them in a small crucible suspended in the lower part of the flask by a thin wire. This crucible arrangement was also used for at least the preliminary tests on certain oils, lacquers, and paints, which produced especially sooty residues, because it helped to prevent an excessive accumulation of soot on the walls of the flask. It was necessary, however, to make a correction for the cooling effect of the crucible, on any SIT values obtained in this way.

After each test, the products of decomposition were blown out of the flask by a jet of air in order to reduce the amount of carbon or soot deposited on the walls. The interior flask surface was cleaned at regular intervals during the preliminary tests for approximate determinations of the SIT, and before each test in the final determinations.

4. Test Results

The following ignition characteristics were determined under the specified test conditions for a number of combustible liquids:

1. Self-ignition temperature.
2. Character and intensity of the evidence of ignition.
3. Favorable fuel-air mixture ratio for minimum ignition temperature.
4. Time-temperature curves and ignition lags for different initial temperatures.

Values for the SIT given in tables 3 to 9 are the minimum values obtained under the most favorable conditions for ignition of the particular material. Representative characteristics and time-temperature curves for the materials under study are shown in figures 3 to 22, but they do not in all cases include the determination that gave the lowest SIT value. Some minor discrepancies will therefore be observed between the SIT values in the tables and those shown by the curves.

For convenience, the combustible materials studied in this investigation have been grouped as follows:

1. Liquids of low ignition temperature.
2. Common petroleum products.
3. Petroleum compounds.
4. Reference fuels.
5. Miscellaneous compounds.
6. Miscellaneous commercial materials.

4.1. Liquids of Low Ignition Temperature

The ignition characteristics of two liquids, carbon disulfide and ethyl ether, ignitible at comparatively low temperatures are given in table 3.

a. Carbon Disulfide

The self-ignition of carbon disulfide was usually indicated by a violent explosion accompanied by flame and a very rapid rise in temperature (see fig. 3). The preignition reaction, however, was of a very mild form, indicated by a gradual rise in tempera-

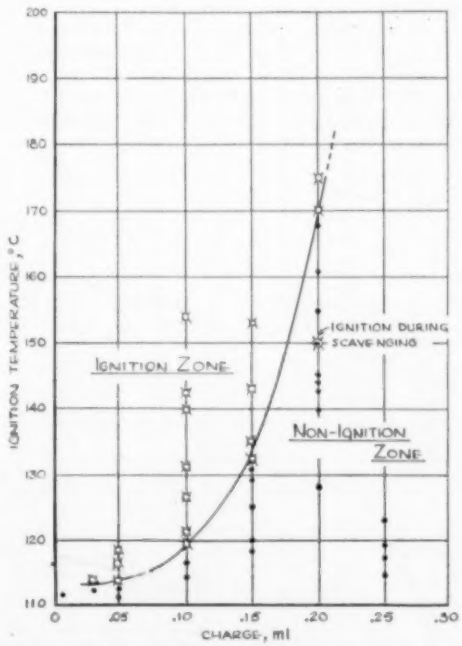

FIGURE 4. *Effect of charge on ignition temperature of carbon disulfide.*
1-liter flask

ture, even for temperatures just below the ignition region. Minor fluctuations in the time-temperature curves sometimes resulted from secondary reactions caused by rich mixtures or by gases evolved from deposits on the flask surface if not cleaned before each test. Both of these factors may have a retarding effect on the ignition reaction. Normally the lowest self-ignition temperatures for combustible liquids were observed when using charges of 0.2 to 0.25 ml per liter of air. However, self-ignition temperatures of carbon disulfide showed a rapid drop as the fuel charge was reduced from 0.2 to 0.05 ml/liter of air and remained almost constant for charges below 0.03 ml, as shown in figure 4.

The carbon disulfide-air mixture had one critical ratio for each initial temperature, above which the mixture remained nonignitible. For example, the critical charge for the initial temperature of 150° C was about 0.18 ml. With a charge of 0.25 ml, the reaction was not accelerated to ignition during the 2½-min test period. If a fresh charge of air was admitted at the end of this nonignition reaction, a violent ignition occurred. This ignition probably resulted from reducing the concentration of the mixture below the critical value of 0.18 ml per liter.

b. Ethyl Ether

Self-ignition of ethyl ether was characteristically indicated by a violent explosion accompanied by a large flame and rapid rise in temperature. Typical time-temperature curves are shown in figure 5 for different sizes of ignition chambers.

The nonignition reaction of this liquid was characterized by a slow rise of temperature for a considerable time after injection of the charge. During the first period of the exothermic reaction, extending from 5 to 10 seconds, the pressure inside the flask increased slightly and gases were expelled from the neck with a barely audible sound. The temperature of the mixture continued to rise and, in about 10 or 15 min, reached its maximum (25 deg C above the initial temperature). However, at slightly higher initial temperatures ignition occurred at a time when the thermocouple indicated a lower temperature of the mixture than the maximum observed in the preceding test. This fact seemed to indicate that either the development of ignition is not a simple function of gas temperature or the thermocouple and temperature-indicating system could not accurately follow the rapid temperature changes at the point within the gas where ignition actually took place.

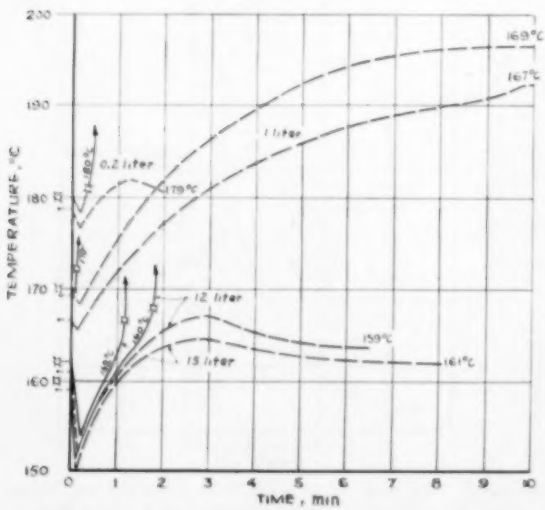

FIGURE 5. *Effect of chamber size on SIT of ethyl ether.*

4.2. Common Petroleum Products

The ignition characteristics of 18 common petroleum products were determined, and the final SIT values obtained are given in table 5.

TABLE 5. *Ignition characteristics of common petroleum products determined in the 1-liter flask*

Product	SIT	Lag
	°C	min sec
Gasoline (65 octane)	248	4 30
Gasoline (73 octane)	258	5 00
Gasoline (87 octane)	415	0 06
Varsol	235	3 00
Kerosine	227	2 55
Cleaners' solvent	243	2 44
Crude oil	262	0 35
Diesel fuels:		
41 cetane	233	3 00
55 cetane	230	2 30
60 cetane	225	2 40
68 cetane	226	1 45
Furnace oil No. 2	233	2 40
Lubricating oils:		
USN No. 2075	241	2 15
USN No. 8190	271	0 15
Chlorinated paraffin oil	414	0 03
Motor oil	351	0 04
Benzene	559	0 48
Toluene	519	0 55

a. Motor Gasoline

The time-temperature curves for motor gasolines were characteristic of a number of refined petroleum products and differed from those of combustible liquids of nonpetroleum origin. The exothermic reaction appeared to proceed in two stages. It was characterized by a consistently reproducible temporary drop in temperature as the reaction progressed, probably caused by an interruption of the exothermic reaction or the occurrence of some endothermic process. The time-temperature curves of figure 6 show this two-stage reaction, the characteristics of which were not appreciably altered by varying the charge or the size of the flask. Ignition of gasoline usually occurred during the last stage of the reaction, whereas that of kerosine and cleaner's solvent occurred in the first stage.

A comparison of adjacent ignition and nonignition curves suggests that the rate of formation of stable compounds was highly sensitive to slight variations in temperature. Not only did the temperature in

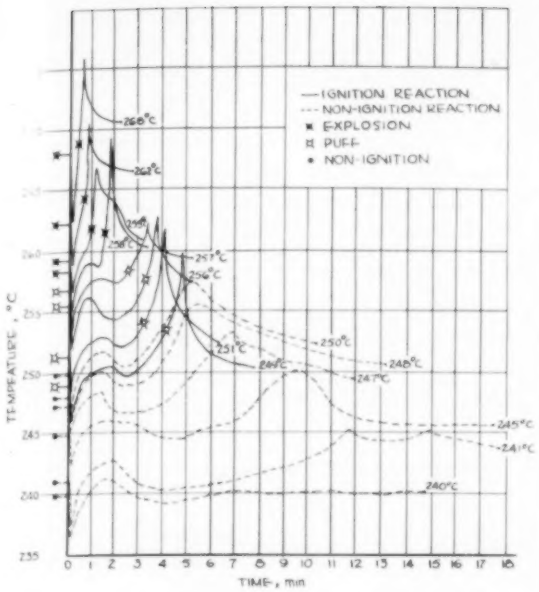

FIGURE 6. *Time-temperature curves for 65 octane motor gasoline.*

1-liter flask, charge equals 0.2 ml.

the nonignition reaction rise well above the SIT, but the reaction mixture had become so stable that it was not ignitible either by spark or flame, or by additional heating up to 400° C, unless diluted with fresh air.

The intensity of the evidence of ignition varied with the initial temperature. From initial temperatures close to the SIT, gasolines of high octane number tended to ignite with a dull blue flame observable under dark-room conditions, and gasolines of low octane number generally ignited with a mild orange flame accompanied by audible expulsion of gases ("puff"). Ignition at higher initial temperatures was usually indicated by a more violent flash of flame or by audible expulsion of gases. It was noted also that ignition from high initial temperatures left the surface of the flask more heavily coated with soot and combustion products than did ignition from lower initial temperatures.

Ignition lag was found to be closely correlated with the ignition temperature, as shown in figure 7. The lowest self-ignition temperature was usually determined from tests conducted with different charges, as shown in figure 8.

b. Other Gasolines and Varsol

The ignition characteristics of other gasolines and Varsol were substantially the same as those of motor and aviation gasolines (supply of 1937), with a two-stage reaction and with ignition occurring in the second stage of reaction.

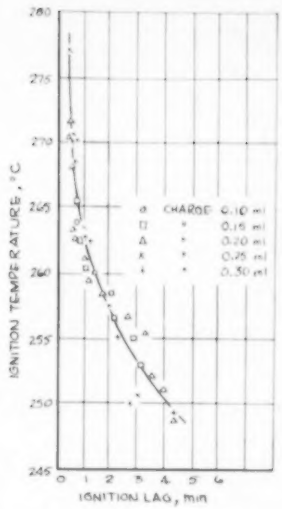

FIGURE 7. *Relation between ignition lag and ignition temperature for motor gasoline.*

1 liter flask.

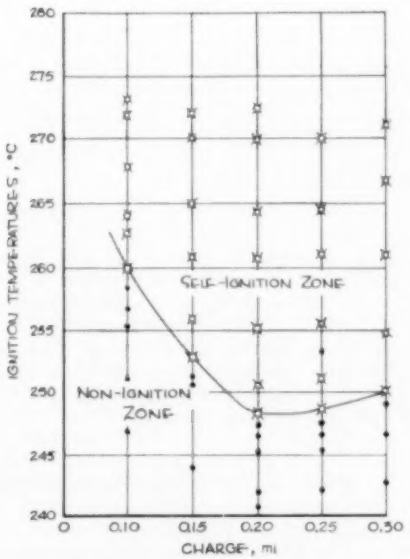

FIGURE 8. *Effect of charge on ignition temperature of motor gasoline.*

1-liter flask.

c. Kerosine and Cleaner's Solvent

Kerosine and cleaner's solvent belong to another group of petroleum products, the ignition of which seemed to occur during the first stage of reaction in spite of the fact that the nonignition reaction pro-

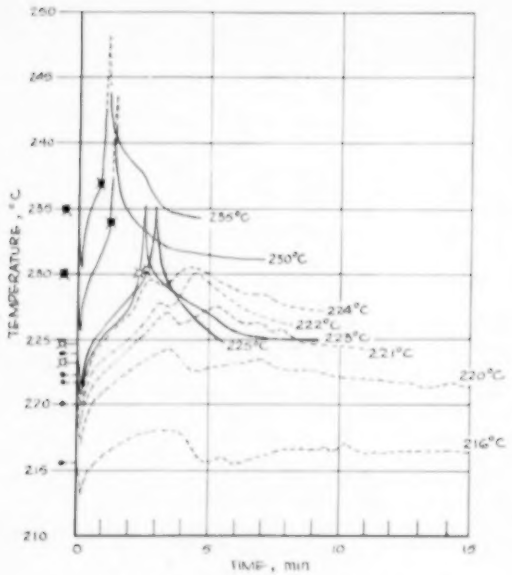

FIGURE 9. *Time-temperature curves for kerosine.*
1-flask, charge equals 0.25 ml.

ceeded with a two-stage reaction. Typical time-temperature curves are shown in figures 9 and 10. "After-burning" of cleaner's solvent in the region of high ignition temperatures was more pronounced than with other fuels, and ignition at all temperatures was indicated by mild flame and a barely audible expulsion of gases.

d. Crude Oil

Lagunillas crude oil of gravity 17 API, flashpoint 15° C, and sulfur content 1.91 percent, was tested in connection with a study of the explosion of an oil tanker. The SIT of this oil was found to be 262° C, with an ignition lag of 35 seconds. The ignition and nonignition reactions proceeded in a one-stage pattern, in contrast with the two-stage reactions of the gasoline and kerosine groups.

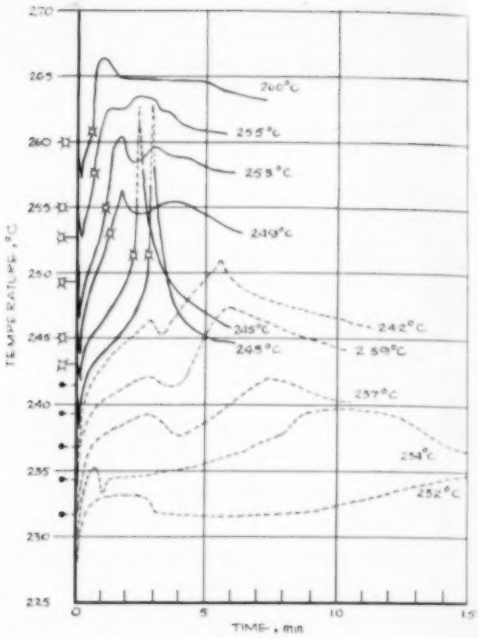

FIGURE 10. *Time-temperature curves for cleaner's solvent.*
1-liter flask, charge equals 0.25 ml.

e. Diesel Fuels

The physical properties of four Diesel fuels, and their ignition characteristics determined in the 1-liter flask, are given in table 6.

The time-temperature curves of figure 11 are representative for these fuels. The two upper curves were obtained for a straight-run fuel (55 cetane); the two lower curves were obtained with the same fuel, to which 1 percent of ethyl nitrate had been added. A small addition of the accelerator reduced the ignition temperature from 230° to 226° C, and the ignition lag from 2½ min to 1¾ min, and the intensity of ignition changed from explosion to normal flame.

TABLE 6. *Physical properties and ignition characteristics of Diesel fuels*

Property		Fuel—			
Cetane number		41	55	60	68.
Production method		Cracked distillate	Straight run	Straight run	55 cetane with combustion accelerator.
Specific gravity	API	33.7	32.8	38.3	38.2.
Viscosity, Saybolt	sec	34.7	50.4	43.0	36.2.
Flash point	° F	185	213	151	130.
Boiling point	° F	405	415	323	221.
Sulphur content	%	0.29	0.25	0.10	0.14.
SIT	° C	233	230	225	226.
Ignition lag	min-sec	3:00	2:30	2:30	1:45.
Evidence[a]		1	5	4	3.

[a] Key for evidence of ignition: 1, Mild flame; 3, flame; 4, mild explosion; 5, explosion.

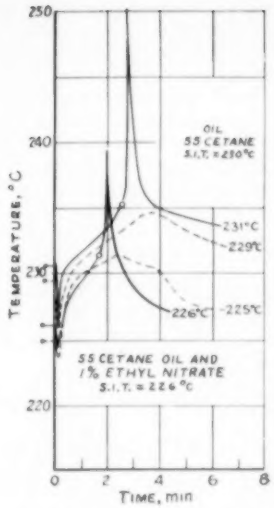

FIGURE 11. *Effect of ethyl nitrate on the SIT of diesel oil.*
1-liter flask, charge equals 0.2 ml.

f. Furnace Oil No. 2

The general ignition characteristics of furnace oil No. 2 were substantially the same as those of Diesel fuels of 41 and 55 cetane number, i. e., single-stage reaction with medium self-heating before ignition, which occurred at 233° C, with mild flame after 2 min 40 sec.

g. Lubricating Oils

Lubricating oils generally represent a complex mixture of different hydrocarbon components having different affinity for oxygen. Because of this, the self-ignition of oil vapor does not always proceed in a definite order, or as consistently as in the case of other combustible liquids. Oils having a comparatively low ignition temperature, such as U. S. Navy Nos. 2075 and 8190, ignited in a more or less definite and reproducible manner. However, chlorinated paraffin oils and motor lubricating oils used for internal-combustion engines usually showed irregular ignition in the zone of minimum ignition temperatures. Above this zone, ignition was observed regularly, and below it the oil vapors were definitely not ignitible. For chlorinated paraffin oil this doubtful zone covered a range of about 10 deg C, but for motor oil it amounted to about 35 deg C, as indicated in figure 12.

The reasons for this irregularity of ignition were not established. However, from observation of the reacting mixture under a strong light directed through the pyrex cover over the neck of the flask, it appeared that poor distribution of the charge may have been largely responsible. As these oils were sprayed into the reaction chamber, they formed dense clouds that required an appreciable time to become well mixed with the air throughout the

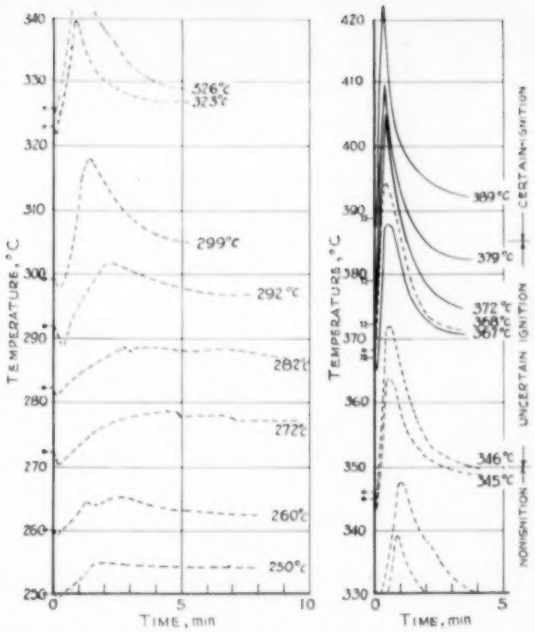

FIGURE 12. *Time-temperature curves for motor lubricating oil.*
1-liter flask, charge equals 0.2 ml.

chamber. In this nonuniform mixture there was a tendency for ignition to take place in small local areas. At relatively high initial temperatures, such local ignition was commonly followed by multiple ignitions in other parts of the chamber, but at lower initial temperatures, a partial ignition frequently occurred without sufficient violence to affect the remainder of the mixture. Moreover, the dense clouds of unburned oil tended to obscure the evidence of a mild ignition, even when viewed under darkroom conditions, and detection was sometimes uncertain. These variable conditions could be expected to produce irregular ignition results in the temperature range near the SIT. It was noted, furthermore, that the irregularities became more pronounced as richer reaction mixtures or larger flasks were used, a situation particularly susceptible to nonuniform distribution of the charge.

h. Benzene

The time-temperature curves obtained for pure benzene (C_6H_6) are shown in figure 13. Appreciable self-heating of the reacting mixture was observed 50 deg C below the self-ignition temperature. At the initial temperature of 557° C, the mixture self-heated to 690° C. However, at the initial temperature of 565° C, actual ignition was observed at 603° C, or about 87 deg C below the maximum temperature of the preceding test. Here, again, evidence is presented of the fact that the initial temperature from which the exothermic reaction proceeds to ignition is more significant than the

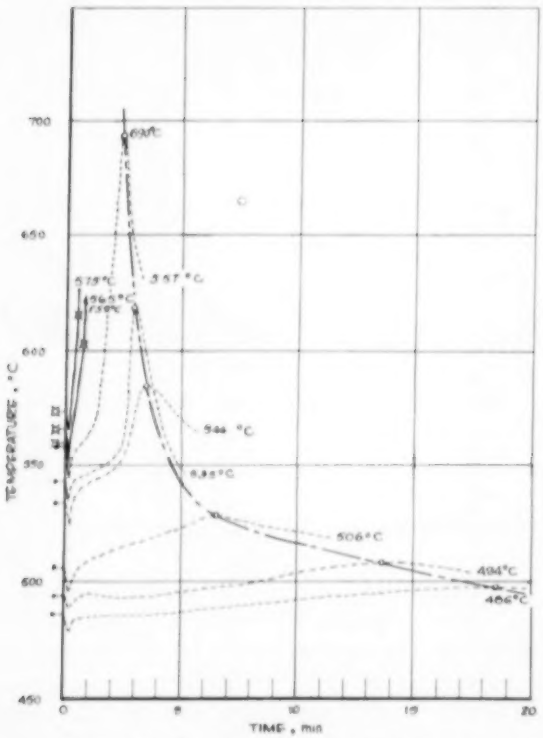

FIGURE 13. *Time-temperature curves for benzene.*
1-liter flask, charge equals 0.2 ml.

temperature of the reacting mixture at the instant of ignition. It is interesting to note that the maximum temperatures for each reaction fall on a smooth curve. The shape of the nonignition reaction time-temperature curve is similar to, but not identical with, that of single-stage reactions of other materials. Although both the ignition and nonignition reactions were characterized by rapid increases in temperature, ignition was indicated by a barely audible expulsion of dense smoke and mild flame.

i. Toluene

The self-heating and ignition characteristics of toluene were similar to those of benzene, and time-temperature curves of substantially the same type were obtained.

4.3. Petroleum Compounds

Three groups of hydrocarbon compounds derived from petroleum, were supplied by the division of thermochemistry. The ignition characteristics of these hydrocarbons were determined in the 1-liter apparatus, and are given in table 7.

a. Normal Paraffins

Figure 14 gives representative time-temperature curves for fractions of the chain type, which showed substantially the same behavior, with the exception of dodecane and cetane, the nonignition reactions of which had a retarding portion similar to a two-stage reaction. The rate of the inducing reaction preceding ignition gradually decreased, and the ignition lag increased with the carbon content.

TABLE 7. *Physical properties and ignition characteristics of petroleum compounds*

Compound [a]	Formula	Ratio H/C	Boiling point	Ignition characteristics (1-liter flask)			
				SIT	Lag		Evidence [b]
(a) Normal paraffins							
			°C	°C	min	sec	
n-Pentane	C_5H_{12}	3.60	36.1	258	1	00	1
n-Hexane	C_6H_{14}	2.33	68.7	240	1	30	1
n-Heptane	C_7H_{16}	2.28	98.4	223	0	45	5
n-Nonane	C_9H_{20}	2.22	150.7	211	1	25	3
n-Decane	$C_{10}H_{22}$	2.20	174.0	206	2	10	1
n-Dodecane	$C_{12}H_{26}$	2.17	216.5	203	2	17	5
n-Cetane	$C_{16}H_{34}$	2.12	287.5	202	2	35	5
(b) Cycloparaffins							
Cyclohexane	C_6H_{12}	2.0	81.4	249	17	15	1
Methylcyclohexane	C_7H_{14}	2.0	163.0	248	20	10	1
(c) Branched-chain paraffins							
Trimethylbutane	C_7H_{16}	2.28	80.9	421	1	26	2
Isooctane	C_8H_{18}	2.25	99.3	420	1	20	2

[a] The time-temperature curves for the above liquids are given in figures 23 to 29.
[b] Key for evidence of ignition: 1, mild flame; 2, blue flame; 3, flame; 5, explosion.

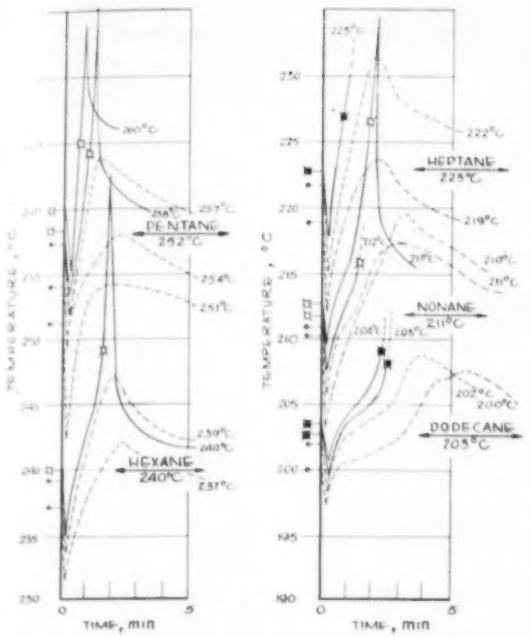

FIGURE 14. *Time-temperature curves for some normal paraffins.*
1-liter flask.

The self-ignition temperature of liquids of the chain type consistently diminished with an increasing number of carbon atoms up to 16 ($C_{16}H_{34}$), as shown in figure 15. The curve for fractions of larger carbon content was not determined because of limited quantities of rare fractions. However, tests of very small amounts of dotriacontane ($C_{32}H_{66}$) indicated the self-ignition temperature to be somewhere above 300° C. In other words, it would appear that the curve must turn upward after carbon 16. Additional tests will be necessary to confirm the shape of this curve.

b. Cycloparaffins

The time-temperature curves for cyclohexane and methylcyclohexane, the two ring type fractions tested, were similar. Curves for methylcyclohexane are shown in figure 16. It will be noted that the reaction appeared to be of a two-stage type, with an extended period of constant temperature before the rapid heating of the second stage began. Ignition took place during the second stage, and, as the initial temperature was raised, the delay between stages was gradually eliminated. The two-stage pattern of reaction for cyclohexane is nearly identical with the patterns obtained for motor and aviation gasolines in the same region of initial temperatures.

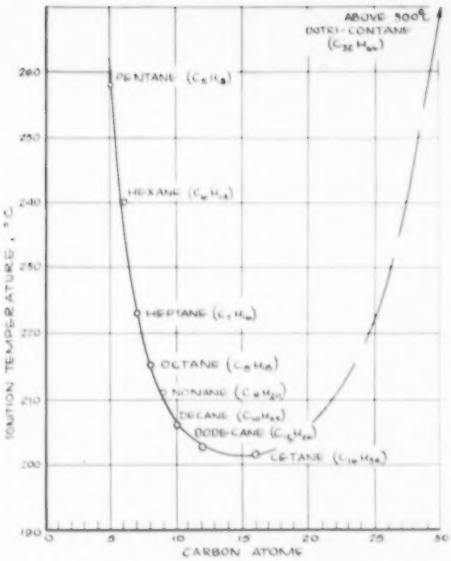

FIGURE 15. *Relation between SIT and carbon content of normal paraffins.*
1-liter flask.

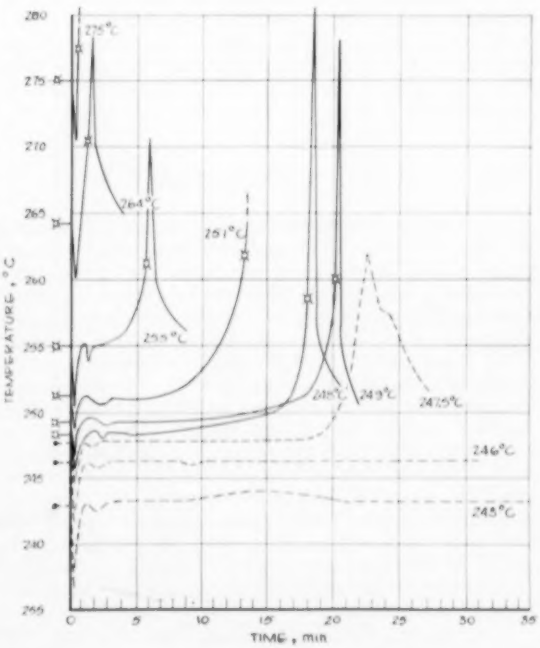

FIGURE 16. *Time-temperature curves for methylcyclohexane* (C_7H_{14}).
1-liter flask, charge equals 0.2 ml

c. Branched-Chain Paraffins

Trimethylbutane (*Triptane*). As the minimum self-ignition temperature of this compound was approached, the visible and audible evidences of ignition became weak, and precise determination of the SIT was difficult. Furthermore, the time-temperature curves for ignition and nonignition reactions had substantially the same shape. However, at an initial temperature of 421° C the reaction definitely proceeded to ignition with a blue-violet flame. At lower temperatures light produced by the reacting mixture appeared to be that of a cool flame reaction.

Isooctane (*2,2,4-Trimethylpentane*). The ignition characteristics of isooctane (and difficulties of ignition-temperature determination) were similar to those for trimethylbutane. The observed reproducibility of blue flame, or cool flame, was very poor and was affected by deposits on the flask wall, by direction of the charge stream, and by relative humidity of the air. Injection of the charge along the side of the neck wall usually stimulated ignition at slightly lower temperatures than injection directly to the bottom of the flask. Self-ignition temperatures obtained at different times ranged from 408° to 425° C. The value of 420° C (with corresponding ignition lag of 1 min 20 sec) recorded in table 7 was fairly reproducible.

Although these difficulties were encountered with all sizes of flasks used, reproducibility of the determinations was slightly better in the 0.2 and 12-liter flasks than in the 1-liter flask. The band of uncertainty in the 0.2-liter flask was no more than 12 deg C, and in the 12-liter flask it was reduced to 4 deg C.

4.4. Reference Fuels

The reference fuels commonly used in determining the knock ratings of motor fuels comprise variously proportioned mixtures of isooctane and *n*–heptane. Essentially the rating procedure consists in determining what mixture most closely matches the performance of the fuel under study, using a standard CFR (Cooperative Fuel Research Committee) engine operated under specified conditions. The percentage of isooctane in this mixture is taken as the octane number of the fuel being tested. Details of the procedure differ with the purpose of the fuel, and the ASTM has established four different methods (motor, research, aviation, and supercharged) for gasolines, and one for Diesel fuels. The rating of a particular fuel may vary appreciably with the method used, and it is therefore necessary to consider the method of determination when knock ratings are used as a basis of comparison.

The ignition characteristics of these primary reference-fuel mixtures were studied in the regular 1-liter test apparatus, and time-temperature curves for a number of them are shown in figure 17. In addition two other types of mixtures, formerly used as secondary reference fuels were also tested. These secondary reference fuels were prepared from three specific fuels, and consisted of (1) mixtures of fuel A_6 with fuel C_{12}, and (2) mixtures of fuel C_{12} with fuel F_3. Although improved methods of manufacture and reduced cost of the primary reference fuels have now eliminated the need for intermediate standards, investigation of the well-defined secondary reference fuels were of interest at the time the tests were performed.

In figures 18 and 19 the data obtained for primary and secondary reference-fuel mixtures, respectively, have been plotted to show the effect of change in composition on different ignition characteristics. With increasing isooctane content, up to about 70 percent, the SIT of the primary reference-fuel mixtures increased gradually and continuously, and the ignition was marked by the characteristic red flame of *n*-heptane. The intensity of ignition changed gradually from explosion to mild flame as the isooctane content increased. With isooctane concentrations of 50 percent and higher an audible expulsion of gases without flame was observed at temperatures below ignition, and this "puff" also diminished in intensity as the concentration of isooctane increased. At 70 percent isooctane, the SIT-composition curve showed a break; mixtures containing more than 70 percent of isooctane igniting only at decidedly higher temperatures, and generally with the blue flame and considerable variability noted previously for pure isooctane. Ignition was somewhat erratic also in mixtures of slightly less than 70 percent isooctane content, forming a so-called "secondary nonignition zone" similar to those observed by Prettre [15] with pentane and hexane by Townend [16] with hexane, by Sortman and Beatty [5] with heptane and cetane, and by many other investigators. The fact that nonignition zones with these latter liquids were not observed in the present investigation suggests that the appearance of such zones may be a function of the test apparatus and conditions rather than of the material under study.

The series of secondary reference-fuel mixtures prepared from fuels A_6 and C_{12} showed a continuous linear increase in ignition temperature with increasing C_{12} content as indicated in curve II of figure 19. The series of mixtures of fuels C_{12} and F_3, however, gave a pattern of ignition behavior (curve III) similar to that obtained for the primary reference-fuel mixtures, including a secondary nonignition zone and the "puff" without flame at temperatures below ignition for mixtures rich in the component having the higher ignition temperature.

In order to indicate the degree of correlation between self-ignition temperature and motor-method octane number, SIT—octane-number curves were plotted for both the primary and secondary reference-fuel mixtures. In addition, self-ignition temperature determinations were made on three other gasolines of known octane number. Of the secondary reference fuels, only the end fuels A_6 and F_3 showed substantially the same SIT values as the primary reference fuels of corresponding octane

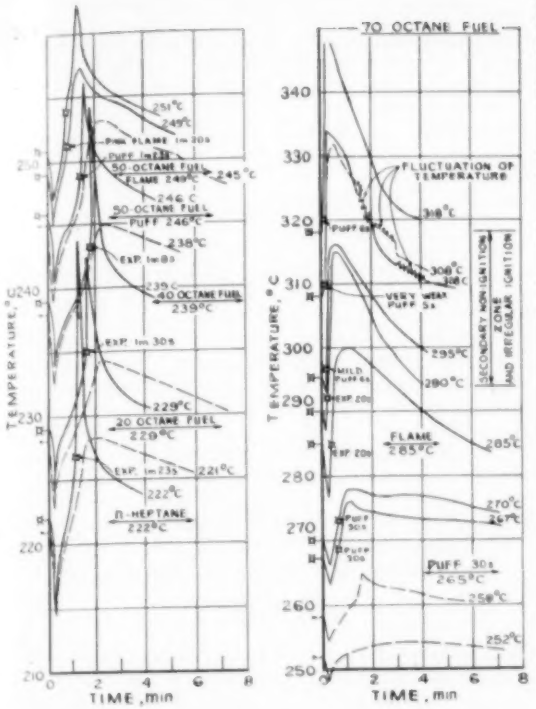

FIGURE 17. *Time-temperature curves for primary reference fuels.*
1-liter flask.

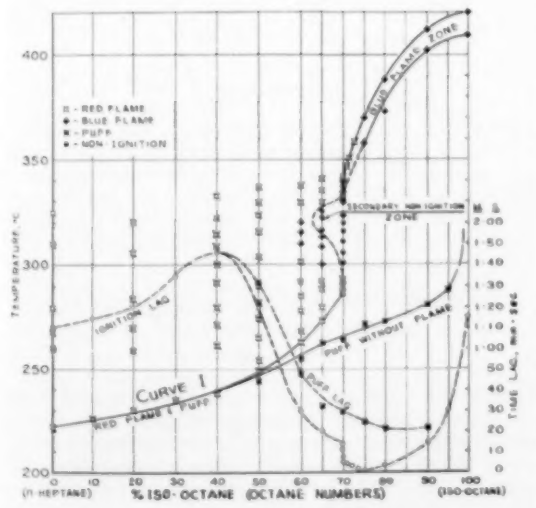

FIGURE 18. *Relation between SIT and composition of primary reference fuels.*
1-liter flask.

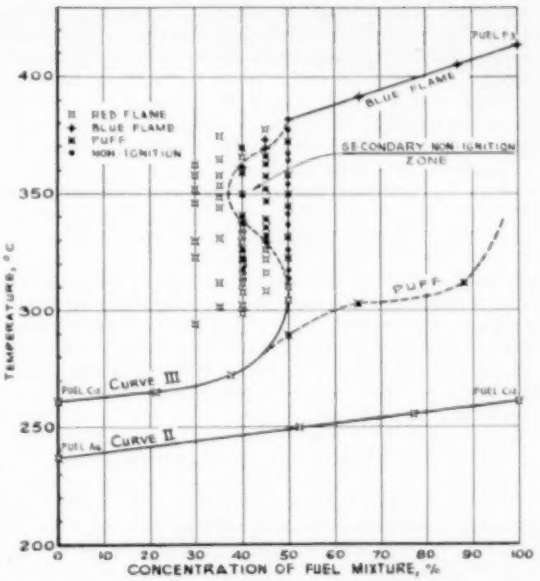

FIGURE 19. *Relation between SIT and composition of secondary reference fuels.*
1-liter flask.

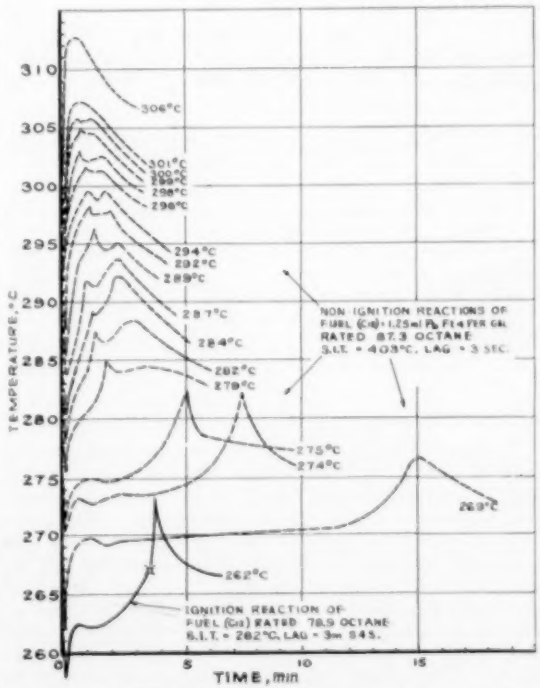

FIGURE 20. *Effect of a combustion accelerator on the time-temperature curves of fuel* C_{12}.
1-liter flask, charge equals 0.2 ml.

numbers. Only one of the three additional gasolines tested gave an SIT value approximately the same as that of the primary reference fuel of corresponding octane number. Similar poor correlation between ignition characteristics and octane-number ratings have been noted by other investigators with other test apparatus (Jentzsch Eckert Zerbe and Carhart).

The effects of a small amount of ethyl fluid additive on the ignition characteristics of a fuel were also studied. A typical time-temperature curve for the ignition of fuel C_{12} (78.9 octane number) is shown in the lower part of figure 20. The broken-line curves in the upper part of the figure are time-temperature curves for nonignition reactions, at increasing initial temperatures, of the same fuel with 1.25 ml of tetraethyl lead added per gallon. The shape of these curves changed entirely, and many additional stages of reaction developed before the reaction finally accelerated to ignition.

4.5. Miscellaneous Compounds

The SIT values obtained in the 1-liter flask for seven miscellaneous liquids are given in table 8. The effect of varying the flask size is shown for several of them in table 3.

For all except methyl alcohol, both the ignition and nonignition reactions were characterized by an immediate rapid acceleration, as illustrated by the curves for acetone shown in figure 21. With methyl alcohol (fig. 22), the acceleration was somewhat delayed, and the curves for ignition and nonignition reactions differed distinctly in shape. Additional comments on the reaction characteristics of the individual liquids follow.

TABLE 8. *Ignition characteristics of miscellaneous compounds determined in the 1-liter flask*

Compound	SIT	Lag	
	°C	min	sec
Acetone	491	0	40
Acetic acid	488	0	13
Ethyl alcohol	391	0	40
Ethylene glycol	398	0	23
Methyl formate	467	0	25
Methyl alcohol	428	1	30
Glycerine	389	0	31

a. Acetone

At the minimum self-ignition temperature, acetone ignited with a blue-violet light, often initiated at and spreading from a small, red, glowing center of carbonized deposit of acetone on the flask wall. The light usually appeared without audible manifestation and continued to be visible for about 20 seconds at 491° C and about 15 seconds at 505° C. The nature of this light gradually changed from dull blue-violet at 491° C to blue-pink at 515° C and to a pink-violet flash with an audible explosion at higher temperatures. The initial blue-violet light was similar to

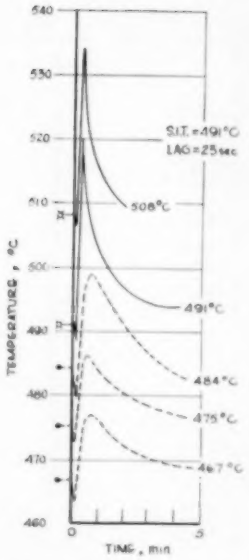

FIGURE 21. *Time-temperature curves for acetone.*
1-liter flask, charge equals 0.2 ml.

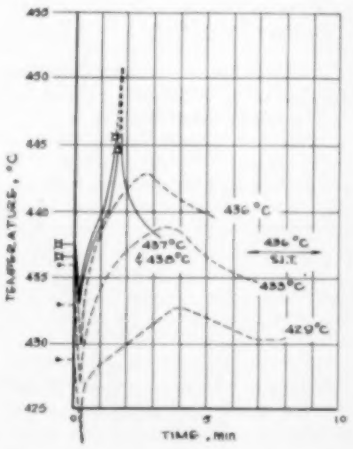

FIGURE 22. *Time-temperature curves for methyl alcohol.*
1-liter flask, charge equals 0.2 ml.

that of a cool flame, and when first observed it was questioned whether this could be taken as an indication of ignition. However, in consideration of the very sharp increase in the time-temperature curve (fig. 21) at 491° C, this temperature was taken as the self-ignition temperature.

b. Acetic Acid

Ignition of acetic acid occurred so irregularly that it was difficult to define the lowest self-ignition temperature. One possible explanation of such irregularity may lie in the ability of acetic acid to exist in two interchangeable states, "dimer" and "monomer", expressed by the relationship

$$(CH_3COOH)_2 \rightleftarrows 2CH_3COOH.$$

The two forms may have different ignition temperatures, and uncontrolled variables might have caused a shift from one form to the other.

Ignition of acetic acid, in spite of the irregularity of occurrence, was distinctly defined by audible and visible evidence, and usually occurred about 8 seconds after injection of the charge. Ignition was initiated with a blue flame, which, at the end of the ignition period, changed to a pink color. This pink color, however, might have been due to reflection of the dull-red furnace walls from fog formed within the chamber. Although the mixture remained clear and transparent throughout most of the reaction, there was some evidence of the development of fog toward the end of the exothermic reaction.

c. Ethyl Alcohol

Due to the rapid increase of pressure at the time of evaporation, an audible expulsion of gases was observed before ignition. The actual ignition, at 391° C after 40 seconds, was accompanied by blue flame with a second expulsion of gases.

Ethyl alcohol-water mixtures were also found to be readily ignitible. The self-ignition temperature increased from 391° to 444° C as the water content of the mixture approached 70 percent. Very weak flame was observed at 467° C even with 80 percent water.

d. Ethylene Glycol

The ignition of ethylene glycol in the 1-liter flask was indicated at 398° C by orange-blue flame and a hardly audible expulsion of gases. However, the same liquid containing 3 percent of an antirusting ingredient (triethanolamine phosphate) ignited at 395° C with a violent explosion. Tests on ethylene glycol-water solutions showed ignition of mixtures containing up to 90 percent of water (for which an ignition temperature of 460° C was obtained), although with more than 40 percent of water the flame became very weak.

Two other antifreeze liquids, R–19 and R–19d, were tested, and the results indicated that these liquids were highly ignitible. Both liquids were petroleum distillates (kerosine type), liquid R–19 being the product without additive and R–19d being a mixture of the product with an ingredient reported to prevent the softening of rubber hose in engine installations. The self-ignition temperature of R–19 was 211° C, with an ignition lag of 3 min 50 sec; R–19d ignited at 223° C after 1 min 30 sec. Ignition of both liquids occurred suddenly with a violent explosion when the thermocouple indicated a temperature only 3 deg C above the initial temperature.

e. Methyl Formate

Ignition of methyl formate was indicated regularly by a mild explosion and rapid rise in temperature similar to that for acetone (fig. 21).

f. Glycerine

Glycerine ignited with a violent explosion accompanied by long flame and smoke expelled from the neck of the ignition apparatus. The rise in temperature of the gas mixture immediately after injection of the charge was particularly extreme for both ignition and nonignition reactions.

Observation of the flask interior showed that, immediately after injection of the charge, viscous glycerine droplets accumulated on the bottom surface of the flask and rapidly produced a dense white fog. After about 20 seconds, this fog became clear either due to superheating or partial oxidation. This was followed, usually in about 5 seconds, by the appearance of a small blue flame with a pink center. Due to rapid propagation of flame, gases were expelled from the neck of the flask with considerable force.

g. Methyl Alcohol

Methyl alcohol showed a mild form of ignition characterized by a dull blue flame and a weak expulsion of clear gas, but the difference in shape of the time-temperature curves for ignition and nonignition reactions (fig. 22) provided supplemental evidence of the definite location of the SIT.

4.6. Miscellaneous Commercial Materials

A number of commercially produced combustible materials were tested in the 1-liter ignition apparatus and their ignition characteristics are given in table 9. The time-temperature curves typical of many of these materials were similar to those for acetone (fig. 21).

TABLE 9. *Ignition characteristics of miscellaneous commercial materials*

Material	Grade	SIT	Lag		Evidence [a]
		°C	min	sec	
Black enamel	Synthetic (001)	478	0	06	4
Pine tar	Commercial	439	0	10	3
Pine oil	do	316	0	07	4
Linseed oil (raw)	do	425	0	04	3
Castor oil	do	409	0	24	3
Varnish (interior)	TT-V-71	359	0	02	6
Varnish (spar)	TT-V-121a	359	0	03	3
Lacquer (red)	Nitrocellulose	349	0	25	3
Lacquer (clear)	do	342	0	14	3
Lacquer (thinner)	Commercial	258	0	12	5
Turpentine	do	230	0	40	3

[a] Key for evidence of ignition: 3, Flame; 4, mild explosion; 5, explosion; 6 violent explosion.

a. Black Enamel

Noticeable decomposition of synthetic black automobile enamel (601) was indicated at 270° C by the appearance of smoke. At a temperature of about 445° C, carbonized residue of the charge self-heated to the glow state. However, self-ignition occurred at 478° C with a large flame and audible expulsion of gas and smoke. As a result of ignition, all the carbon residue was burned out and the flask surface became clear.

b. Pine Tar

Pine tar of commerical grade, due to its low "fluidity", was preheated in boiling water before injection with a hypodermic syringe. The exothermic reaction began far below the ignition temperature and ignition was indicated by flame and a mild expulsion of smoke. The flask surface, after ignition, was usually covered by a brownish coating and tar residue, baked to a hard carbon deposit removable only with a scraper. However, with pine oil the residue after ignition was soft and easily removable from the surface.

c. Linseed Oil

The ignition characteristics of linseed oil were similar to those of lubricating oils, and appreciable self-heating of the vapor-air mixture was observed at temperatures far below the ignition temperature.

d. Varnish and Lacquer

The reaction characteristics of varnish and lacquers were substantially the same, particularly in the nonignition region. Self-heating of the vapor-air mixture was initiated far below the self-ignition temperature, and often amounted to 20 to 25 deg C in nonignition reactions near the self-ignition temperature. Ignition of these liquids, with the exception of interior varnish and lacquer thinner, was very mild; both the lacquer thinner and interior varnish ignited with an audible explosion.

e. Turpentine

The time-temperature curves for turpentine were similar to those for kerosine, having the same two-stage nonignition reaction with ignition definitely in the first stage.

5. Summary

The apparatus and method described for the determination of self-ignition temperatures is practical and readily adaptable to combustible liquids of widely different physical and chemical properties. Data on a considerable number of liquids are presented.

Time-temperature curves of a thermocouple junction in mixtures of combustible liquid and air, offer a convenient means of studying the preignition reactions in such mixtures. Typical time-temperature curves are given.

The importance of careful standardization of equipment and procedure in obtaining reproducible results has been demonstrated. Thus, for reaction vessels of similar construction, the self-ignition temperature was found to decrease with increase in size of the chamber, over the capacity range studied, with differences as high as 200 deg C being obtained in vessels of 0.008-and 12-liter capacity. With Pyrex reaction chambers of the same size but with different exterior casings, variations up to nearly 30 deg C were observed in the determined self-ignition temperature. In view of the effects produced by these modifications of equipment within a single method, the large discrepancies in ignition temperatures reported by different investigators using various methods are not surprising.

The ignition temperatures measured with the apparatus described are lower than those reported by most other workers.

The author is indebted to M. Sandholzer for assistance in the preparation of this paper.

6. References

[1] T. T. S. Sebastian and M. A. Mayers, Ind. Eng. Chem. **29,** 1118 (1937).
[2] C. R. Brown, The determination of the ignition temperature of solid materials (Doctoral Thesis, Catholic Univ. of America 1934).
[3] H. Holm, Z. Angew. Chem. **26,** 273 (1913).
[4] H. Moore, J. S. C. I. **36,** 109 (1917); J. I. P. T. **6,** 186 (1920).
[5] C. W. Sortman and H. A. Beatty, Ind. Eng. Chem. **33,** 357 (1941).
[6] H. Jentzsch, Z. Ver. deut. Ing. **68,** 1150 (1924); **69,** 1353 (1925).
[7] D. M. Newitt and D. T. A. Townend, The Science of Petroleum, vol. IV, p. 2958 (1938).
[8] H. B. Dixon and H. F. Coward, J. Chem. Soc. **98,** 514 (1909).
[9] H. B. Dixon and H. F. Coward, J. Chem. Soc. P. 1382 (1934).
[10] W. Mason and R. V. Wheeler, J. Chem. Soc. **121,** 2079 (1922); **125,** 1869 (1924).
[11] H. L. Callendar, Engineering **123,** 147 (1927).
[12] C. Moureu, Chim. et Ind. **18,** 3 (1927); Compt. rend. **185,** 1545 (1927).
[13] S. M. Estradére, Pub. Tech. of Ministry of Air (Paris), No. 49 (1934).
14] S. J. Lewis, J. Chem. Soc. p. 1555 (1927); p. 58 and 2241 (1930).
[15] M. Prettre, The Science of Petroleum, vol. IV, p. 2951 (1938).
[16] D. T. A. Townend, Proc. Roy. Soc. **141A,** 484 (1933); **143A,** 168 (1933); **146A,** 113 (1934).
[17] L. M. Pidgeon and A. C. Egerton, J. Chem. Soc. p. 661, 676 (1932).
[18] Neumann, Z. Ver. deut. Ing. **70,** 1071 (1926); NACA Tech. Mem. 391 (Dec. 1926).
[19] H. T. Tizard and D. R. Pye, Auto. Eng. **13,** 136 (1923).
[20] A. Pignot, Compt. rend. **182,** 376 (1926).
[21] ASTM Standard Method, ASTM Standards, pt. 5, 147 (1952).
[22] L. F. Mareck and D. A. Hahn, Catalytic oxidation of organic compounds in vapour phase, Chem. Soc. Monograph Series (Chemical Catalog Co., N. Y., 1932), p. 311.
[23] H. L. Callendar, Engineering **125,** 183 (1927).
[24] N. J. Thompson, Ind. Eng. Chem. **21,** 134 (1929).
[25] A. F. Matson and R. E. Dufour, Underwriters' Laboratories, Inc., Bul. of Research No. 43 (1950).

WASHINGTON, March 5, 1954.